



UNIVERSITY OF BEIRA INTERIOR  
Engineering

# **Computer-Aided Detection and Diagnosis of Breast Cancer in 2D and 3D Medical Imaging Through Multifractal Analysis**

**Filipe Cruz Gomes Soares**

Thesis for obtaining the degree of Doctor of Philosophy in  
**Computer Science and Engineering**  
(3rd Cycle Studies)

Advisor: Prof. Doctor Mário Marques Freire (University of Beira Interior)  
Co-advisor: Eng. João Seabra Ferreira Pinto (Siemens S.A. Healthcare Sector)

**Covilhã, October 2013**



Thesis prepared at Siemens S.A. Healthcare Sector, at *Instituto de Telecomunicações*, within Multimedia Signal Processing - Covilhã Group and at University of Beira Interior, and submitted to University of Beira Interior for defense in a public examination session.

Work financed by the Portuguese *Fundação para a Ciência e a Tecnologia* through the grant identified by SFRH/BDE/15624/2006 under the program QREN - POPH - Type 4.1 – Advanced Training, co-funded by the European Social Fund and by national funds from the Portuguese *Ministério da Educação e Ciência*.

## **FCT** Fundação para a Ciência e a Tecnologia

MINISTÉRIO DA EDUCAÇÃO E CIÊNCIA



UNIÃO EUROPEIA  
Fundo Social Europeu



# Dedicatory

*À minha avó Celeste.*

*Computer-Aided Detection and Diagnosis of Breast Cancer in 2D and 3D Medical Imaging Through Multifractal Analysis*

# Acknowledgments

I would like to acknowledge Siemens S.A. Healthcare Sector for giving me the opportunity to develop this challenging research project in industry, where I could understand how to excel at innovation.

I am thankful to Fundação para a Ciência e Tecnologia for partially funding together with Siemens these research years under the PhD studentship in industry SFRH/BDE/15624/2006. I also thank Instituto de Telecomunicações for providing me extra resources and supporting my publications in international conferences and specialized training.

I am also grateful to Clínica João Carlos Costa from Viana do Castelo for providing me all the breast magnetic resonance data used in this Thesis.

I have to acknowledge the following people:

My main advisor Professor Mário Marques Freire for the strong motivation and enthusiasm, always pushing me to go further in pursuing the PhD, and for following my work even on distance. Prof. Manuela Pereira for all the valuable teaching and research work shared.

Eng. João Seabra and Eng. Filipe Janela from Siemens S.A. Healthcare Sector for co-supervising my work. I expressly thank Filipe for all the guidance, trust and support, for letting me take responsibility on the project, and also for the professional lessons that he gave me.

My Siemens colleagues Inês Sousa, Celina Lourenço, Pawel Andruszkiewicz, Liliana Caldeira, José Ferrão, Linda Gomes, Catarina Duarte, David Afonso, Catarina Runa, Teresa Mendes, Pedro Almeida, Paulo Cruz and António Martins. Especially, I would like to thank you Inês for the most mind blowing ideas and permanent intellectual stimulus. You were one of the greatest assets from Siemens.

Pawel, Alessia Pagotto and Manuel Stadlbauer for being the coolest roommates in Porto. João, Rui, Marta, Ricardo, Nery, David, Liliana, Guida and Celina Lourenço for their faithful friendship. In particular, I must express my deep gratitude to Celina for her patience, generosity, presence, care, and also for the happiness moments and experiences shared during these years.

Finally, I have to thank in Portuguese:

À minha família por todo o amor, ajuda e atenção, durante estes largos anos de grande desafio. À minha irmã por toda a força e alegria. Em especial à minha Mãe pelo inesgotável carinho, preocupação e admiração incondicional que me fez acreditar sempre num futuro brilhante.

Inês, obrigado por seres a minha maior fonte de inspiração e energia, por me fazeres sonhar e ser cada vez melhor. Obrigado pelo teu amor desmedido, pela tua ajuda constante e por estares sempre a meu lado em todos os momentos. Obrigado por me mostrares o lado bom e feliz da vida.



# Foreword

This Thesis describes the research work performed in the scope of a doctoral research program and presents its conclusions and contributions. The research activities were carried on in the industry with Siemens S.A. Healthcare Sector, in integration with a research team.

Siemens S.A. Healthcare Sector is one of the world biggest suppliers of products, services and complete solutions in the medical sector. The company offers a wide selection of diagnostic and therapeutic equipment and information systems. Siemens products for medical imaging and in vivo diagnostics include: ultrasound, computer tomography, mammography, digital breast tomosynthesis, magnetic resonance, equipment to angiography and coronary angiography, nuclear imaging, and many others.

Siemens has a vast experience in Healthcare and at the beginning of this project it was strategically interested in solutions to improve the detection of Breast Cancer, to increase its competitiveness in the sector.

The company owns several patents related with self-similarity analysis, which formed the background of this Thesis. Furthermore, Siemens intended to explore commercially the computer-aided automatic detection and diagnosis field for portfolio integration. Therefore, with the high knowledge acquired by University of Beira Interior in this area together with this Thesis, will allow Siemens to apply the most recent scientific progress in the detection of the breast cancer, and it is foreseeable that together we can develop a new technology with high potential.

The project resulted in the submission of two invention disclosures for evaluation in Siemens A.G., two articles published in peer-reviewed journals indexed in ISI Science Citation Index, two other articles submitted in peer-reviewed journals, and several international conference papers. This work on computer-aided-diagnosis in breast led to innovative software and novel processes of research and development, for which the project received the Siemens Innovation Award in 2012.

It was very rewarding to carry on such technological and innovative project in a socially sensitive area as Breast Cancer.

*Computer-Aided Detection and Diagnosis of Breast Cancer in 2D and 3D Medical Imaging Through Multifractal Analysis*

# List of Publications

## Articles included in the thesis resulting from the doctoral research program

- 1. 3D Lacunarity in Multifractal Analysis of Breast Tumor Lesions in Dynamic Contrast-Enhanced Magnetic Resonance Imaging**  
Filipe Soares, Filipe Janela, Manuela Pereira, João Seabra and Mário M. Freire  
*IEEE Transactions on Image Processing*, Volume 22, Issue 11, pp. 4422-4435, 2013.  
DOI: 10.1109/TIP.2013.2273669
- 2. Classification of Breast Masses on Contrast-Enhanced Magnetic Resonance Images Through Log Detrended Fluctuation Cumulant-Based Multifractal Analysis**  
Filipe Soares, Filipe Janela, Manuela Pereira, João Seabra and Mário M. Freire  
*IEEE Systems Journal*, accepted for publication, 2013.  
DOI: 10.1109/JSYST.2013.2284101
- 3. Review and Performance Evaluation of Multifractal Approaches for Computer-aided Detection of Microcalcification Clusters in Mammograms**  
Filipe Soares, Filipe Janela, Manuela Pereira, João Seabra and Mário M. Freire  
Submitted for publication in an international journal, 2013.
- 4. Computer-Aided Detection and Diagnosis of Breast Cancer: Overview on Typical Systems and Methods in Mammography and Breast Magnetic Resonance Imaging**  
Filipe Soares, Filipe Janela, Manuela Pereira, João Seabra and Mário M. Freire  
Submitted for publication in an international journal, 2013.

## Other publications resulting from the doctoral research program not included in the thesis

- 1. The Role of Self-Similarity for Computer Aided Detection Based on Mammogram Analysis**  
Filipe Soares, Mário M. Freire, Manuela Pereira, Filipe Janela, João Seabra  
Chapter 6: *Biomedical Diagnostics and Clinical Technologies: Applying High-Performance Cluster and Grid Computing*  
IGI Global, 2011, ISBN13: 9781605662800, pp. 181-199.  
DOI: 10.4018/978-1-60566-280-0.ch006
- 2. Self-similarity classification of breast tumour lesions on dynamic contrast-enhanced magnetic resonance images - Special Session on Breast CAD**  
Filipe Soares, Filipe Janela, João Seabra, Manuela Pereira, and Mário Marques Freire  
*International Journal of Computer Assisted Radiology and Surgery*  
Springer-Verlag, Volume 5, Supplement 1, pp. S203-S205, 2010.  
DOI: 10.1007/s11548-010-0459-y

**3. Multifractal Analysis of Arterial Spin Labeling Functional Magnetic Resonance Imaging of the Brain**

Filipe Soares, Inês Sousa, Filipe Janela, João Seabra, Manuela Pereira, and Mário Marques Freire

*Proceedings of the IEEE International Workshop on Medical Measurements and Applications*

IEEE Press, 2010, pp. 161-164.

DOI: 10.1109/MEMEA.2010.5480209

**4. A New Computer-Aided Approach for Breast Cancer Diagnosis**

Filipe Soares

*Proceedings of the 3rd World Cancer Congress - Breast Cancer Conference*

BIT Life Sciences, 2010, pp. 273

**5. Towards the detection of microcalcifications on mammograms through Multifractal Detrended Fluctuation Analysis**

Filipe Soares, Mário Marques Freire, Manuela Pereira, Filipe Janela, and João Seabra

*Proceedings of the IEEE Pacific Rim Conference on Communications, Computers and Signal Processing*

IEEE Computer Society Press, 2009, pp. 677-681.

DOI: 10.1109/PACRIM.2009.5291288

**6. Self-Similarity Analysis Applied to 2D Breast Cancer Imaging**

Filipe Soares, Pawel Andruszkiewicz, Mário Marques Freire, Paulo Cruz, Manuela Pereira

*Proceedings of the International Conference on Systems and Networks Communications, on the First International Workshop on High Performance Computing Applied to Medical Data and Bioinformatics*

IEEE Computer Society Press, 2007, pp. 77-83.

DOI: 10.1109/ICSNC.2007.76

# Resumo

No cancro da mama a deteção precoce e o diagnóstico correto são de extrema importância na prescrição terapêutica eficaz e eficiente, que potencie o aumento da taxa de sobrevivência à doença. A teoria multifractal foi inicialmente introduzida no contexto da análise de sinal e a sua utilidade foi demonstrada na descrição de comportamentos fisiológicos de bio-sinais e até na deteção e predição de patologias. Nesta Tese, três métodos multifractais foram estendidos para imagens bi-dimensionais (2D) e comparados na deteção de microcalcificações em mamogramas. Um destes métodos foi também adaptado para a classificação de massas da mama, em cortes transversais 2D obtidos por ressonância magnética (RM) de mama, em grupos de massas provavelmente benignas e com suspeição de malignidade. Um novo método de análise multifractal usando a lacunaridade tri-dimensional (3D) foi proposto para classificação de massas da mama em imagens volumétricas 3D de RM de mama. A análise multifractal revelou diferenças na complexidade subjacente às localizações das microcalcificações em relação aos tecidos normais, permitindo uma boa exatidão da sua deteção em mamogramas. Adicionalmente, foram extraídas por análise multifractal características dos tecidos que permitiram identificar os casos tipicamente recomendados para biópsia em imagens 2D de RM de mama. A análise multifractal 3D foi eficaz na classificação de lesões mamárias benignas e malignas em imagens 3D de RM de mama. Este método foi mais exato para esta classificação do que o método 2D ou o método padrão de análise de contraste cinético tumoral. Em conclusão, a análise multifractal fornece informação útil para deteção auxiliada por computador em mamografia e diagnóstico auxiliado por computador em imagens 2D e 3D de RM de mama, tendo o potencial de complementar a interpretação dos radiologistas.

## Palavras-chave

Deteção auxiliada por computador (CADe), Diagnóstico auxiliado por computador (CADx), Mamografia, Ressonância magnética de mama, Extração de características, Classificação, Análise multifractal, Multi-escala, Wavelets, Cancro da mama.

*Computer-Aided Detection and Diagnosis of Breast Cancer in 2D and 3D Medical Imaging Through Multifractal Analysis*

# Resumo Alargado

## Introdução

Neste capítulo é apresentado um resumo alargado do trabalho de investigação conducente à Tese de Doutoramento intitulada *Computer-Aided Detection and Diagnosis of Breast Cancer in 2D and 3D Medical Imaging Through Multifractal Analysis*. O enquadramento da Tese é descrito numa fase inicial, definindo-se depois o problema abordado, os objetivos do trabalho de investigação e o argumento da Tese. De seguida, são abordados os principais temas objeto de investigação nesta Tese: a deteção de microcalcificações em mamogramas e a classificação de lesões em imagens de ressonância magnética de mama. As metodologias são brevemente discutidas bem como as contribuições resultantes do trabalho desenvolvido. Por último, apresentam-se as principais conclusões.

## Enquadramento da Tese

O cancro da mama é curável se detetado precocemente e mediante um tratamento apropriado. Além de salvar vidas, espera-se dos médicos que encontrem a forma menos invasiva e dolorosa para verificar o estado em que se encontra a doença. Com respeito ao desconforto que os exames de Mamografia e Biopsia Mamária podem causar, reduzir o número de deteções falso-positivas torna-se um problema igualmente importante como a redução de falso-negativas. A anatomia complexa da mama é uma inevitável fonte da estrutura altamente irregular dos mamogramas, que constitui uma informação delicada de analisar pelos radiologistas, a quem se espera que distingam anomalias muito subtis de uma massa de ambiguidade global. Além disso, a variabilidade entre dois casos acresce a dificuldade na decisão humana, que enfatiza a necessidade de ferramentas de processamento de imagem confiáveis que possam assistir o processo de deteção de anomalias e diagnóstico em imagens da mama. A finalidade do trabalho enquadra-se no desenvolvimento de novos métodos não lineares de estimação de auto-semelhança, aplicável à imagiologia, que possam auxiliar a deteção da patologia do cancro da mama, segmentando regiões mamárias de risco para otimizar o processo de diagnóstico. Pretende-se apurar histologicamente o estado e evolução do cancro da mama, descrevendo a natureza fractal e multifractal dos objetos presentes nas imagens recolhidas determinando o grau de auto-semelhança. A metodologia a desenvolver de sistemas de apoio à decisão auxiliada por computador deverá permitir não só a deteção ou diagnóstico automático a partir de imagens de Mamografia como de Ressonância Magnética (RM). Trata-se de um projeto de investigação inovador, com uma iminente aplicação prática, conseguindo conjugar num único trabalho de Doutoramento os aspetos do desenvolvimento científico e a sua implementação em ambiente industrial, numa área onde a empresa Siemens S.A. tem vindo a apostar fortemente. Com prestadores de cuidados de saúde e outros parceiros de negócio interessados nos resultados do projeto, perspectiva-se a oportunidade de concretização de um protótipo e respetivo produto. Contudo, o projeto de investigação envolve ainda restrições de confidencialidade dos

casos clínicos utilizados para validação, e tem como principal risco a concorrência industrial neste mercado e o forte crescimento da investigação e desenvolvimento nesta área.

## **Descrição do Problema e Objetivos de Investigação**

O objetivo do trabalho descrito nesta Tese é a melhoria da deteção e diagnóstico precoce do cancro da mama, através do desenvolvimento de sistemas de apoio à decisão auxiliada por computador, baseados nas propriedades de auto-semelhança dos tecidos mamários. Sistemas de deteção auxiliada por computador (CADE) são desenvolvidos para extração de sinais precoces de anormalidade, em particular microcalcificações, das imagens mamográficas. Sistemas de diagnóstico auxiliado por computador (CADx) são implementados para classificação da malignidade de lesões mamárias em imagens 2D e 3D obtidas por RM de mama. O trabalho de investigação desenvolvido pode ser dividido em três objetivos principais, correspondentes aos três principais capítulos da Tese, conforme se descreve a seguir.

**Aplicação de métodos de análise de imagem multifractal a mamogramas para extração automática de microcalcificações, que constituem sinais precoces de anormalidade no tecido mamário**

- a) Generalização para 2D dos três principais métodos multifractais: Multifractal Detrended Fluctuation Analysis (MF-DFA), Modulus Maxima Wavelet Transform (MMWT) e Wavelet Leaders Multifractal Formalism (WLMF).
- b) Desenvolvimento de uma estrutura comum que inclua os três métodos, MF-DFA, MMWT and WLMF, para análise de imagens mamográficas.
- c) Comparação dos três métodos, MF-DFA, MMWT and WLMF, em termos da sua capacidade de extração de microcalcificações e eficiência computacional.
- d) Redução da deteção de falsos positivos usando a auto-semelhança para criar um mapa de potenciais estruturas a remover, por exemplo: estruturas lineares como os vasos sanguíneos.

**Extração de características das lesões mamárias relacionadas com a sua morfologia e textura, por análise multifractal de imagens 2D de RM de mama**

- a) Aplicação do método MF-DFA a imagens 2D de RM de mama correspondentes a cortes de tumores ou lesões mamárias.
- b) Identificação dos descritores matemáticos dos espectros multifractais relevantes para a discriminação de lesões mamárias em imagens de RM de mama.

- c) Extração de propriedades de auto-semelhança por análise multifractal baseada nos cumulantes logarítmicos da flutuação destendenciada dos cortes de lesões mamárias em imagens RM de mama.
- d) Avaliação dos descritores e propriedades multifractais num esquema de classificação supervisionada para distinção de lesões suspeitas de malignidade das potencialmente benignas em imagens RM de mama.

Desenvolvimento de um novo método de análise multifractal usando a lacunaridade 3D como uma medida para obter propriedades multifractais de imagens volumétricas de RM de mama

- a) Estimação do expoente de escala multifractal usando a lacunaridade como a medida multifractal.
- b) Investigação do uso da teoria multifractal condicionada pela medida lacunaridade 3D para classificação de lesões mamárias em imagens volumétricas de RM de mama.
- c) Extração de características dos novos espectros multifractais para classificação automática de lesões benignas e malignas em imagens volumétricas de RM de mama.
- d) Comparação da capacidade de discriminação entre lesões benignas e malignas com os métodos MF-DFA 2D e 3D e 3TP (standard clínico para análise da cinética do tumor) num esquema de classificação supervisionada.

## **Argumento da Tese**

Esta tese propõe uma nova abordagem para a deteção e classificação de características do cancro da mama. Especificamente, o argumento de tese é o seguinte:

*O tecido mamário apresenta alto grau de complexidade, revelando propriedades de auto-semelhança passíveis de serem descritas matematicamente por análise multifractal. O tecido mamário normal e regiões com potencial tumoral mostram comportamento multifractal distinto, o que pode ser usado para a deteção precoce de cancro da mama assistida por computador em mamografias. Características multifractais são bem correlacionadas com o estado de evolução de um tumor e fornecem uma indicação da probabilidade de malignidade através de diagnóstico assistido por computador em imagens 2D e 3D de RM de mama.*

## **Principais Contribuições**

### **Abordagens multifractais para detecção auxiliada por computador de clusters de microcalcificações em mamogramas**

Os métodos multifractais generalizados para 2D e aplicados a um conjunto de mamogramas de duas bases de dados públicas foram eficazes na detecção de microcalcificações. O método 2D MF-DFA resultou numa melhor performance de detecção do que os outros dois métodos baseados em wavelets (MMWT and WLMF), independentemente da resolução espacial das imagens na base de dados. O método WLMF demonstrou a melhor eficiência computacional, no entanto a performance de detecção é apenas mediana. A análise multifractal permite obter características dos tecidos mamários que estão correlacionadas com a caracterização da complexidade subjacente às lesões mamárias, que constituem sinais precoces de cancro da mama. Estas características mostraram-se úteis na identificação de microcalcificações e na eliminação de falsos positivos, como estruturas lineares que evidenciam características distintas. A análise multifractal de mamogramas permite, assim, obter informação útil para sistemas de detecção precoce de cancro da mama auxiliados por computador.

### **Classificação de massas mamárias em imagens de ressonância magnética de mama com contraste dinâmico através de cumulantes logarítmicos obtidos da análise baseada em flutuações destendenciadas**

Foi desenvolvido um sistema de apoio à decisão que permite identificar casos de massas mamárias tipicamente recomendadas para biópsia a partir de imagens RM de mama 2D. Este sistema utiliza descritores matemáticos dos espectros multifractais e cumulantes logarítmicos num esquema de classificação supervisionada que proporciona uma recomendação de biópsia. A eficácia do sistema de apoio à decisão é elevada na distinção de lesões com suspeita de malignidade, principalmente com uma das oito características estudadas.

### **Análise multifractal com lacunaridade 3D de lesões tumorais da mama em imagens volumétricas de ressonância magnética com contraste dinâmico**

A presença de características multifractais nas imagens volumétricas de RM de mama foi confirmada através da observação de prevalência de múltiplos graus de auto-semelhança a múltiplas escalas. Uma combinação de características multifractais foi obtida da análise multifractal usando a lacunaridade 3D como medida e demonstrou-se eficaz na classificação de lesões benignas e malignas. Este método foi mais exato na determinação da probabilidade de malignidade do que o 2D MF-DFA ou o standard clínico para análise da cinética tumoral, 3TP. Desta forma, o método proposto para extração de características multifractais e classificação tem o potencial de complementar a interpretação dos radiologistas e vir a ser usado num sistema de diagnóstico

assistido por computador (CADx).

## **Discussão da Metodologia**

### **Abordagens multifractais para detecção auxiliada por computador de clusters de microcalcificações em mamogramas**

A detecção auxiliada por computador de padrões mamográficos é frequentemente baseada na caracterização de texturas. A análise multifractal pode ser usada para caracterizar texturas de imagens, no entanto, esta abordagem é raramente aplicada no contexto da detecção de cancro da mama em imagens de mamografia. Este capítulo revê e investiga a generalização dos três principais métodos multifractais recentemente propostos: Multifractal Detrended Fluctuation Analysis (MF-DFA), Modulus Maxima Wavelet Transform (MMWT) and Wavelet Leaders Multifractal Formalism (WLMF). Pretende-se avaliar se as generalizações 2D destes métodos podem ser usadas na extração de elementos de importância clínica para a detecção do cancro da mama. Os métodos foram implementados numa plataforma comum e aplicados à detecção de microcalcificações em mamogramas. A avaliação foi feita sobre duas bases de dados públicas com diferente resolução espacial de imagem, relacionando a sensibilidade com o número de falsos positivos da detecção, através de curvas FROC (Free-Response Receiver Operating Characteristic). A performance dos métodos na detecção de microcalcificações e os seus custos computacionais foram comparados. No conjunto de 290 imagens médicas, o método MF-DFA obteve um desempenho superior independentemente da resolução das imagens nas bases de dados. No entanto, em ambos os algoritmos foi verificado o impacto de uma maior resolução de imagem nos resultados superiores da detecção. É de salientar que o método baseado em wavelets MMWT foi mais sensível à alteração da base de dados. O método WLMF apresenta uma performance de detecção mediana mas melhor eficiência computacional. A inspeção de singularidades e respetivas flutuações a múltiplas escalas revelou que o estudo multifractal é muito importante para a caracterização da complexidade subjacente às potenciais localizações de microcalcificações. A análise multifractal de mamogramas permite, assim, obter informação útil para sistemas de detecção precoce de cancro da mama auxiliados por computador.

### **Classificação de massas em imagens de ressonância magnética de mama com contraste dinâmico através de cumulantes logarítmicos obtidos da análise multifractal baseada em flutuações destendenciadas**

Foi desenvolvido um sistema de apoio à decisão que permite identificar casos de massas mamárias tipicamente recomendadas para biópsia a partir de imagens RM de mama 2D com contraste dinâmico. Este sistema utiliza descritores matemáticos dos espectros multifractais e cumulantes logarítmicos num esquema de classificação supervisionada que proporciona uma recomendação de biópsia. Os outputs da classificação foram comparados com o diagnóstico do radiologista baseado no breast imaging-reporting and data system (BIRADS). Os resultados mostram que o

cumulante logarítmico  $c_2$  é o mais eficaz na identificação dos casos tipicamente recomendados para biópsia. A eficácia do sistema de apoio à decisão é cerca de 94% na distinção de lesões com suspeição de malignidade, com uma das oito características estudadas, o cumulante  $c_2$ . O método proposto de análise multifractal pode contribuir para novas técnicas de classificação que auxiliem os radiologistas na identificação mais exata de casos que necessitem biópsia.

## **Análise multifractal com lacunaridade 3D de lesões tumorais da mama em imagens volumétricas de ressonância magnética com contraste dinâmico**

A RM de mama com contraste dinâmico é especialmente robusta para diagnóstico de cancro em casos de alto risco, devido à sua elevada sensibilidade. No entanto, a especificidade pode ser comprometida uma vez que as diferenças entre as cinéticas do contraste dinâmico são subtis entre massas benignas e malignas. Nesta Tese é proposto um método multifractal 3D que permite caracterizar a complexidade (arranjo espacial de texturas) dos tumores mamários a múltiplas escalas. Propriedades de auto-semelhança são extraídas da estimação do expoente de escala multifractal de cada caso clínico, usando a lacunaridade 3D como medida multifractal. Estas propriedades incluem diversos descritores dos espectros multifractais que refletem a morfologia e estrutura espacial interna das lesões relativamente ao tecido normal. Os resultados sugerem que a combinação de várias características multifractais é eficaz na distinção entre lesões benignas e malignas, como avaliado pela performance de um método de classificação baseado em support vector machine com área da curva de receiver operating characteristics (ROC) de 0.96. Adicionalmente, a presença de multifractalidade nas imagens volumétricas de RM de mama com contraste dinâmico foi confirmada, já que múltiplos graus de auto-semelhança existem a múltiplas escalas. O método proposto de extração de características multifractais e classificação tem o potencial de complementar a interpretação do radiologista e futuros sistemas de diagnóstico assistido por computador (CADx).

## **Conclusão**

Em conclusão, a análise multifractal fornece informação útil para deteção auxiliada por computador em mamografia e diagnóstico auxiliado por computador em imagens 2D e 3D de RM de mama, tendo o potencial de complementar a interpretação dos radiologistas.

## **Abstract**

The early detection and accurate diagnosis of breast cancer is of utmost importance in providing effective and efficient treatment in order to increase survival rates. The multifractal theory was first introduced for signal analysis and has shown its utility in describing physiologic behaviors of bio-signals and even in detecting and predicting pathology. In this Thesis, three multifractal analysis methods have been extended to two-dimensional (2D) images and compared in the detection of microcalcifications in mammograms. One of these methods was adapted for classification of breast masses in 2D cross-sectional breast magnetic resonance (MR) images in suspicious malignant and probably benign groups. A novel multifractal analysis method using three-dimensional (3D) lacunarity is proposed for classification of breast masses in 3D volumetric MR images. The multifractal analysis revealed differences in the underlying complexity of the microcalcifications relatively to the normal tissue allowing a good accuracy of their detection in mammograms. Moreover, it provided meaningful features that allowed identifying the typically biopsy-recommended cases from 2D breast MR images. The 3D multifractal analysis method was also effective in the classification of malignant and benign lesions in 3D breast MR images. This method was more accurate in estimation of the likelihood of malignancy than the 2D method and the standard analysis of tumor enhancement kinetics. In conclusion, multifractal analysis provides useful information for computer-aided detection in mammography and for computer-aided diagnosis in 2D and 3D breast MR images and have the potential to complement the interpretation of the radiologists.

## **Keywords**

Computer-Aided Detection (CADe), Computer-Aided Diagnosis (CADx), Mammography, Breast Magnetic Resonance Imaging (MRI), Feature Extraction, Classification, Multifractal Analysis, Multiscale, Wavelets, Breast Cancer.



# Contents

Dedicatory	v
Acknowledgments	vii
Foreword	ix
List of Publications	xi
Resumo	xiii
Resumo Alargado	xv
Abstract	xxi
Contents	xxiii
List of Figures	xxvii
List of Tables	xxxix
Acronyms	xxxiii
<b>Chapter 1</b>	
<b>Introduction</b>	<b>1</b>
I Thesis Focus and Scope . . . . .	1
II Research Objectives . . . . .	3
III Thesis Statement . . . . .	4
IV Main Contributions . . . . .	5
V Thesis Organization . . . . .	6
References . . . . .	7
<b>Chapter 2</b>	
<b>Computer-Aided Detection and Diagnosis of Breast Cancer: Overview on Typical Systems and Methods in Mammography and Breast Magnetic Resonance Imaging</b>	<b>9</b>
Abstract . . . . .	11
I Breast Cancer Imaging . . . . .	11
II CAD in Mammography and Breast MRI . . . . .	14
III Commercial CAD for Mammography and Breast MRI . . . . .	17
IV CADE and CADx Typical Schemes . . . . .	20
V Survey on CADE and CADx Methods . . . . .	22
V.A Feature extraction for CADE detection of clustered microcalcifications in Mammography . . . . .	22

V.B	Feature extraction for CADe detection of masses in Mammography . . . . .	26
V.C	Classification for CADx diagnosis of microcalcifications and masses in Mammography . . . . .	30
V.D	CADx diagnosis of masses in DCE-MRI of the breast . . . . .	33
VI	Conclusion . . . . .	39
	References . . . . .	41

**Chapter 3**

**Review and Performance Evaluation of Multifractal Approaches for Computer-aided Detection of Microcalcification Clusters in Mammograms 53**

	Abstract . . . . .	55
I	Introduction . . . . .	55
I.A	Review of Prior Work on Detection of Mammographic Abnormalities . . . . .	56
I.B	Multifractal Image Analysis . . . . .	57
I.C	Overview of the Article . . . . .	57
II	Detection Model and Multifractal Approaches . . . . .	57
II.A	Pre-Processing and Breast Region Detection . . . . .	57
II.B	Multifractal-based Feature Extraction . . . . .	58
II.C	Selection of Findings and False Positive Reduction . . . . .	61
III	Results . . . . .	62
III.A	Experiments . . . . .	62
III.B	Detection Performance . . . . .	62
III.C	Computational Efficiency . . . . .	63
IV	Discussion . . . . .	64
V	Conclusion . . . . .	65
	References . . . . .	65

**Chapter 4**

**Classification of Breast Masses on Contrast-Enhanced Magnetic Resonance Images Through Log Detrended Fluctuation Cumulant-Based Multifractal Analysis 69**

	Abstract . . . . .	71
I	Introduction . . . . .	71
II	Materials and Methods . . . . .	72
II.A	Image Acquisition . . . . .	73
II.B	Dataset Characterization and Tumor Selection . . . . .	73
II.C	Multifractal Analysis . . . . .	74
II.D	Self-similarity Extraction . . . . .	75
III	Results . . . . .	76
IV	Discussion . . . . .	76
V	Conclusion . . . . .	79
	References . . . . .	79

**Chapter 5**

<b>3D Lacunarity in Multifractal Analysis of Breast Tumor Lesions in Dynamic Contrast-Enhanced Magnetic Resonance Imaging</b>	<b>81</b>
Abstract . . . . .	83
I Introduction . . . . .	83
II Background and Theory . . . . .	85
II.A Multifractal Analysis . . . . .	85
II.B Lacunarity Estimation . . . . .	86
III 3D Multifractal Scaling Exponent Lacunarity Analysis (MF-SELA) . . . . .	86
III.A Pre-Processing and VOI Selection . . . . .	87
III.B 3D lacunarity Estimation With Gliding Cube . . . . .	87
III.C Multifractal Analysis With 3D Lacunarity . . . . .	87
III.D Self-Similarity and Scaling Dynamics as Descriptors . . . . .	88
IV Experimental Setup and Performance Assessment . . . . .	88
IV.A Image Acquisition . . . . .	88
IV.B Tumor Collection and Diagnosis . . . . .	89
IV.C SVM-Based Classification . . . . .	90
IV.D ROC Analysis . . . . .	90
V Results . . . . .	90
VI Discussion . . . . .	92
VII Conclusion . . . . .	94
References . . . . .	94

**Chapter 6**

<b>Conclusions and Future Work</b>	<b>97</b>
------------------------------------	-----------



# List of Figures

## Chapter 2

### Computer-Aided Detection and Diagnosis of Breast Cancer: Overview on Typical Systems and Methods in Mammography and Breast Magnetic Resonance Imaging

Figure 1. CAD embedded in the clinical cycle of breast imaging. . . . .	15
Figure 2. Flowchart of a typical CADe system in breast imaging. . . . .	20
Figure 3. Flowchart of a typical CADx system in breast imaging. . . . .	21

## Chapter 3

### Review and Performance Evaluation of Multifractal Approaches for Computer-aided Detection of Microcalcification Clusters in Mammograms

Figure 1. Proposed microcalcification detection model. The first three blocks of the flow are pre-processing steps before the core feature extraction, where the method for multifractal image analysis is employed. The clustering and self-similarity analysis aim for false positive reduction. . . . .	58
Figure 2. Fragment of a mammogram and extracted microcalcifications. . . . .	61
Figure 3. Radius vectors with centroid in $C$ to create the boundary profile of a microcalcification with closed contour $L$ . . . . .	62
Figure 4. Two cropped ROI sizes from the same MiniMIAS mammogram, 128 x 128 (blue squares) and 256 x 256 (black circles), and their multifractal spectrums $f(\alpha)$ via Legendre transform with 2D MF-DFA. . . . .	62
Figure 5. (a) Detection of microcalcifications in mammogram ROIs. From top to bottom: mdb209, mdb219, mdb223 and mdb249. (b) Legendre spectrums with 2D MF-DFA. . . . .	63
Figure 6. FROC curves showing detection performance using the three multifractal methods on different datasets. 2D MF-DFA with DDSM has the best performance with bigger area under the curve. It points 85% of sensitivity for the detection of microcalcifications at 0.5 False Positives per Image. . . . .	63
Figure 7. Comparison of computational efficiency by CPU time in seconds (s) averaged per case in DDSM dataset, using the three multifractal methods. . . . .	64

## Chapter 4

### Classification of Breast Masses on Contrast-Enhanced Magnetic Resonance Images Through Log Detrended Fluctuation Cumulant-Based Multifractal Analysis

Figure 1. Flowchart of the model for Log Detrended Fluctuation Cumulant- Based Multifractal Analysis. . . . .	73
---	----

Figure 2. Morphology features: typical benign case on the left, with oval shaped mass smooth, margin and homogeneous enhancement; typical malignant case on the right with irregular shaped mass, spiculated margin and heterogeneous enhancement. . . . . 73

Figure 3. Histogram of the longest diameter of the lesions in the dataset. The longest diameter was measured where the lesion was best visualized as determined by radiologist. . . . . 74

Figure 4. Scheme of the descriptors used for the multifractal spectrum characterization. . . . . 75

Figure 5. Detrended fluctuation function  $F_q(s)$  at different scales for  $q = -2$  (left) and  $q = 2$  (right). PM cases: in black. PB cases: in green. It is shown the presence of scaling range in particular for negative moment  $q$ , with the extreme scales showing more deviation from the power law scaling (smaller scales in  $q = -2$  and larger scales in  $q = 2$ ). Bars from the group of cases represent 95% confidence interval for mean. . . . . 77

Figure 6. Estimated scaling exponent  $\tau(q)$  (left) and multifractal spectrum  $D(h)$  (right) for the lesions in the dataset. PM cases: in black. PB cases: in green. . . . 77

Figure 7. Comparison of the three *log-cumulants* estimated from  $\tau(q)$  before SVM analysis for PB (left bar) and PM (right bar) cases. The box-plots show the lower and upper quartile and median. . . . . 77

Figure 8. Comparison of the ROC curves using SVM with the self-similarity extracted features, RFE-3 feature set and the 3TP. . . . . 78

Figure 9. Comparison of computational efficiency by CPU time in seconds (s) with achieved area under the ROC curve  $A_z$  with *log-cumulant*  $c_2$ , for multiple expansions of moment  $q$  range. The CPU time presented is an average of the total time for running the complete dataset of 70 cases. . . . . 78

**Chapter 5**

**3D Lacunarity in Multifractal Analysis of Breast Tumor Lesions in Dynamic Contrast-Enhanced Magnetic Resonance Imaging**

Figure 1. Flowchart of the model for Multifractal Scaling Exponent Lacunarity Analysis (MF-SELA). . . . . 86

Figure 2. Morphology features of lesions in the dataset. Representation of tumor VOIs (top). A sliced region of interest of a typical: benign case (bottom left), with oval shaped mass smooth, margin and homogeneous enhancement; malignant case (bottom right), with irregular shaped mass, spiculated margin and heterogeneous enhancement. . . . . 89

Figure 3. BI-RADS grade of the lesions in the dataset plotted against the kinetic curve types of contrast enhancement as determined by radiologist. . . . . 89

Figure 4.	Histogram of the longest diameter of the lesions in the dataset. The longest diameter was measured where the lesion was best visualized as determined by radiologist. . . . .	89
Figure 5.	Multifractal spectra $D(h)$ of the VOIs of the cases in the dataset. Benign cases in gray. Malignant cases in black. . . . .	91
Figure 6.	Multifractal scaling exponent $\tau(q)$ of the VOIs of the cases in the dataset. Benign cases in gray. Malignant cases in black. . . . .	91
Figure 7.	Comparison of multifractal descriptors and log-cumulants as features. Top: For each feature normalized by its mean value, benign cases in gray and malignant cases in black. Bottom: Pooled features values tested for statistically significant differences with One-way ANOVA resulting in F-statistic = 588.32 and p-value < 0.05. Statistically significant differences among descriptors are identified by letters according to Post-Hoc Tukey test. . . .	91
Figure 8.	ROC curves comparing the classification performance of the multifractal features and the combined parameter ( $CP$ ) using SVM with a leave-one-out testing. . . . .	92



# List of Tables

## Chapter 2

### Computer-Aided Detection and Diagnosis of Breast Cancer: Overview on Typical Systems and Methods in Mammography and Breast Magnetic Resonance Imaging

Table I.	Representative selection of microcalcifications CADE in Mammography . . .	26
Table II.	Representative selection of mass CADE in Mammography . . . . .	31
Table III.	Area under the ROC curve $A_z$ of a representative selection of microcalcifications CADx in Mammography . . . . .	34
Table IV.	Area under the ROC curve $A_z$ of a representative selection of mass CADx in Mammography . . . . .	34
Table V.	Area under the ROC curve $A_z$ of a representative selection of mass CADx in DCE-MRI . . . . .	39

## Chapter 3

### Review and Performance Evaluation of Multifractal Approaches for Computer-aided Detection of Microcalcification Clusters in Mammograms

Table I.	Assessment of Sensitivity . . . . .	63
----------	-------------------------------------	----

## Chapter 4

### Classification of Breast Masses on Contrast-Enhanced Magnetic Resonance Images Through Log Detrended Fluctuation Cumulant-Based Multifractal Analysis

Table I.	Comparison of the area under the ROC curve $A_z$ and corresponding standard deviation (STD) using SVM . . . . .	78
----------	---	----

## Chapter 5

### 3D Lacunarity in Multifractal Analysis of Breast Tumor Lesions in Dynamic Contrast-Enhanced Magnetic Resonance Imaging

Table I.	Clinical cases in the dataset . . . . .	90
Table II.	Area under the ROC curve $A_z$ in discriminating malignant from benign lesions with multifractal-based features. $A_z$ of the SVM classifier using each feature (leave-one-out cross-validation) . . . . .	92
Table III.	ROC $A_z$ of 3TP and two multifractal methods on our dataset of 35 cases . .	93
Table IV.	ROC $A_z$ among state-of-art studies on their datasets . . . . .	93



# Acronyms

2D	Two-Dimensional
3D	Three-Dimensional
3TP	Three-Time-Points
ACO	Ant Colony Optimization
AFUM	Average Fraction Under the Minimum
ANN	Artificial Neural Network
ANOVA	Analysis of Variance
ART	Adaptive Resonance Theory
BI-RADS	Breast Imaging - Reporting and Data System
BNN	Backpropagation Neural Network
BBN	Bayesian Belief Network
BSSA	Boundary Self-Similarity Analysis
CAD	Computer-aided Medical Imaging Analysis
CADe	Computer-Aided Detection
CADx	Computer-Aided Diagnosis
CALMA	Computer Assisted Library in Mammography
CBIR	Content-Based Image Retrieval
CC	Craniocaudal
<i>CP</i>	Combined Spectral Parameter
CPU	Central Processing Unit
DBT	Digital Breast Tomosynthesis
DCE-MRI	Dynamic Contrast-Enhanced Magnetic Resonance Imaging
DDSM	Digital Database for Screening Mammography
DFA	Detrended Fluctuation Analysis
<i>Dh</i>	Hausdorff dimension
DoG	Difference-of-Gaussian
DWT	Discrete Wavelet Transform
EM	Expectation Maximization
FD	Fractal Dimension
FDA	Food and Drug Administration
FFDM	Full Field Digital Mammography
FL3D	T1-weighted FLASH 3D
FNA	Fine Needle Aspiration
FPI	False Positives per Image
FROC	Free-Response Receiver Operating Characteristic
ftp	Full-Time-Point

GA	Genetic Algorithm
Gd-DTPA	Gadopentetate dimeglumine
GDFNN	Generalized Dynamic Fuzzy Neural Networks
$H$	Hurst Parameter
$h$	Hölder Exponent
ICA	Independent Component Analysis
kNN	k-Nearest-Neighbor
LDA	Linear Discriminant Analysis
LRA	Linear Regression Analysis
LOO	Leave-One-Out
$LS$	Left Slope of the curve
MCC	Microcalcification Clusters
MCS	Multiple Classifier System
MF-DFA	Multifractal Detrended Fluctuation Analysis
MF-SELA	Multifractal Scaling Exponent Lacunarity Analysis
MI	Mutual Information
MIL	Multiple-Instance Learning
MiniMIAS	Database of Mammograms from Mammographic Image Analysis Society
MIP	Maximum Intensity Projection
MLO	Mediolateral Oblique
MMWWT	Local Maxima along the MMWT Chains
MMWT	Modulus Maxima Wavelet Transform
MR	Magnetic Resonance
MRF	Markov random field
MRI	Magnetic Resonance imaging
PACS	Picture Archiving and Communication System
PB	Probably Benign and Non-Biopsied
PBT	Probabilistic Boosting Tree
PM	Probably Malignant and Biopsied
PPV	Positive Predictive Value
RBF	Radial Basis Function
RBFNN	Radial-Based Function Neural Network
RBST	Rubber Band Straightening Transformation
RFE	Recursive Feature Elimination
ROC	Receiver Operating Characteristic
ROI	Region of Interest
RR	Round-robin
$RS$	Right Slope of the Curve
$R\alpha$	Rightmost Hölder Point

SLFFN	Single Layer Feed Forward Network
SMF	Standard Mammogram Form
SVM	Support Vector Machine
SVM-RFE	Recursive Feature Elimination-based Support Vector Machine
TE	Testing Error
UBI	University of Beira Interior
VOI	Volume of Interest
$\bar{W}$	Curve Width
WLMF	Wavelet Leaders Multifractal Formalism
WT	Wavelet Transform



# Chapter 1

## Introduction

This Thesis addresses the problem of detection and classification of breast cancer by the application of computer assisted tools for augmenting human functions, namely radiologists on their demanding job of chasing microcalcifications and tumors using data from two medical imaging modalities: Mammography and Magnetic Resonance imaging (MRI). In the form of software and applied mathematics, it is proposed to study self-similarity features found in 2D and 3D images of the breast. The focus, scope and research objectives of the Thesis are described in this chapter, followed by the Thesis statement, the main contributions and the Thesis organization.

### I Thesis Focus and Scope

Breast cancer is a malignant tumor originated in the cells of the breast. A malignant tumor is a group of cancer cells that can grow into (invade) surrounding tissues or spread (metastasize) to distant areas of the body. The disease occurs almost exclusively in women, but it can also occur in men. Breast cancer is the most common cancer among women in the western world, aside from non-melanoma skin cancer. Breast cancer is the second leading cause of cancer death in women, exceeded only by lung cancer. Death rates from breast cancer have been declining since early 90's, with larger decreases in women younger than 50. These decreases are believed to be the result of earlier detection through screening and increased awareness, as well as improved treatment [1]. This is a big argument in favor of screening programs that has been focused on traditional imaging modalities of the breast as x-ray mammography, which has been the standard imaging modality for decades [2]-[7]. Incidence rates of breast cancer have been increasing in the industrialized world, but this is expected given the higher life expectancy in those countries and the fact that many people are being screened by methods that did not exist a few decades ago. The combination of the characteristics of breast cancer: high incidence, deadly disease, asymptomatic in earlier stages, and high survival rate if detected in these stages, makes the fight against the disease, through research and development of high-end technology in breast imaging devices, worthy.

Mammographic first signs of breast cancer usually appear in the form of clusters of microcalcifications. These tiny deposits of calcium can be visible long before any palpable lesion has developed and their early detection contributes to the success of the treatment. For diagnosis,

radiologists generally rely on their shape, size, number and distribution. Malignant calcifications are typically very numerous, clustered, small, dot-like or elongated, variable in size, shape and density. Benign calcifications are generally larger, more rounded, smaller in number, more diffusely distributed, and more homogeneous in shape [8]. However, because of the small size of microcalcifications, the comparison and characterization of benign and malignant lesions represents a very complex problem even for an experienced radiologist [9].

The microcalcifications can arise in isolation or together with other areas of high density breast tissue, called masses. The term mass arises from the characteristic well-defined mammographic appearance, and they tend to be brighter than their surroundings due to the high density within their boundaries. In order to be able to characterize a mass, radiologists generally rely on its contour and different kinds can be observed in mammograms (circumscribed, spiculated, microlobulated, with dense kernel). Usually circumscribed masses are related to benign lesions while spiculated masses are related to malignant lesions.

The fractal geometry has been introduced a long time ago in image analysis through fractal dimension. Fractal compression and fractal encoding exploit the property of self-similarity of fractal objects [10]. Images of breast tissue are characterized by a high degree of self-similarity, i.e., several parts look as the whole image. In self-similar objects, irregularities are structural deviations from the global regularity. In the case of breast images these irregularities may correspond to locations of potential breast lesions and can be characterized under the light of fractal or multifractal analysis. These analyses allow a multiscale mathematical description of changes in the textural information, reflecting self-similarity. Moreover, it is possible to derive a set of mathematical quantities or features, which can be related to the type of breast lesion and malignancy level, constituting the basis of machine aid systems in the detection and diagnosis of breast cancer. The multifractal analysis provides a spectrum of fractal dimensions, characterizing multiple irregularities. This can potentially give more information about the image than the fractal analysis, which is unable to uniquely characterize a texture pattern, as different fractal sets may share the same fractal dimension values and yet have different appearances. Therefore the methods developed in the scope of this Thesis are based on multifractal analysis. Mammography and breast MRI are the gold-standard imaging techniques in the detection and diagnosis of breast cancer, respectively. Mammography is the established technique for screening tests and breast MRI is mostly used for tumor staging and treatment planning and follow-up. The usual proceeding for breast tumor detection in screening mammography is visual inspection by a radiologist. As the volumetric anatomical information is projected into a two-dimensional (2D) image plane, mammographic findings are generally hard to identify because of their superimposition on the breast parenchymal textures. In particular microcalcifications are often overlooked by the radiologist due to their small size, despite being usually an early sign of abnormality. Therefore, machine-aid based on reliable

image processing tools is valuable and it has been shown to help finding more cancers. On the other hand, in breast MRI decision-support systems are essential, since many benign and malignant tumors have similar appearances. Clinical interpretation of the images is based on visual examination of morphology features and contrast-enhancement kinetics and despite following a scoring system it still remains largely subjective. Computer assisted diagnosis may have an important impact on the accuracy, consistency and reproducibility of the diagnosis, preventing unnecessary therapies or invasive procedures, such as biopsies.

## **II Research Objectives**

The aim of the work described in this Thesis is the improvement of breast cancer early detection and diagnosis by developing computer-aided systems based on the self-similarity properties of breast tissues. Computer-aided detection (CADE) systems are developed for extraction of early signs of abnormality, specifically microcalcifications, from mammographic images. Computer-aided diagnosis (CADx) systems are implemented for malignancy classification of 2D and 3D images obtained with breast MRI. The work can be divided in three main objectives, corresponding to the three main chapters of the Thesis:

- 1) Application of multifractal image analysis methods to mammograms for automatic extraction of microcalcifications, which are early signs of abnormality in breast tissue
  - a) Generalization for 2D of the main three multifractal methods: Multifractal Detrended Fluctuation Analysis (MF-DFA), Modulus Maxima Wavelet Transform (MMWT) and Wavelet Leaders Multifractal Formalism (WLMF).
  - b) Development of a common framework including the three methods, MF-DFA, MMWT and WLMF, for mammographic image analysis.
  - c) Comparison of the three methods, MF-DFA, MMWT and WLMF, in terms of ability for microcalcification extraction and computational efficiency.
  - d) Reduction of false positive detection by using self-similarity analysis to identify and create a likelihood map of potential structures to remove, for example: normal linear structures as blood vessels.
- 2) Extraction of multifractal image analysis derived features to characterize the morphology and texture of breast tumor MR images
  - a) Application of the MF-DFA method to 2D breast MR images corresponding to tumor slices.
  - b) Identification of meaningful mathematical descriptors of the multifractal spectra for discrimination of breast lesions in MRI.

- c) Extraction of self-similarity features by log detrended fluctuation cumulant-based multifractal analysis of the tumor images.
  - d) Evaluation of the multifractal descriptors and features in a supervised classification scheme for distinguishing suspicious malignant masses in breast MR images.
- 3) Development of a novel multifractal analysis method using 3D lacunarity as a measure to derive self-similar properties from volumetric breast MR images
- a) Estimation of the multifractal scaling exponent using lacunarity as the multifractal measure.
  - b) Investigation of the use of multifractal theory conditioned by the 3D lacunarity measure, for classification of breast lesions in volumetric breast MR images.
  - c) Extraction of features from the novel multifractal spectra for automated classification of malignant and benign lesions.
  - d) Comparison of the likelihood of malignancy discrimination ability with 2D MF-DFA and Three-Time-Points (3TP) (clinical standard technique for analysis of tumor kinetics) in a supervised classification scheme.

### **III Thesis Statement**

This Thesis proposes a new approach for the detection and classification of breast cancer features. Specifically, the thesis statement is:

*Breast tissue presents high degree of complexity showing self-similarity properties mathematically described by multifractal analysis. Healthy breast tissue and potential breast tumor locations show differential multifractal behavior, which can be used for early computer-aided breast cancer detection in mammograms. Multifractal features are well correlated with tumor staging and provide an indication of the likelihood of malignancy through computer-aided diagnosis in both 2D and 3D breast MRI.*

To support this thesis statement, the following research approach was conducted. The literature on detection and diagnosis of breast cancer is reviewed in order to define the problem and research field. The various modalities for breast imaging are studied and the suitability of its application in each phase of the disease management is analyzed. The several methods of breast lesion detection in mammography and diagnosis in breast MR were reviewed and their performance was evaluated. The multifractal theory was identified as a promising area of research in computer-aided medical imaging analysis. The few works of multifractal analysis in pattern identification were studied in terms of applied mathematics and computerized performance. In the area of multifractal analysis of breast cancer images even fewer studies were

found and therefore this was an opportunity to contribute with novelty in the field. Three multifractal methods are generalized for 2D and applied in detection of microcalcifications in mammography. With the motivation of improving the distinction of benign and malignant lesions in breast MR images a new multiscale and multifractal 3D characterization of tumors is proposed. This method is compared with the most equivalent 2D method. The output of the methods developed is evaluated by free-response receiver operating characteristic (FROC) and receiver operating characteristic (ROC) curves. Additionally, their computational performance is assessed. The methods developed have the potential of being included in future CAde and CADx systems.

## **IV Main Contributions**

This section briefly describes the main scientific contributions resulting from the research work presented in this Thesis.

### **1) Review and Performance Evaluation of Multifractal Approaches for Computer-aided Detection of Microcalcification Clusters in Mammograms**

- The multifractal methods generalized for 2D and applied to a set of mammograms from two public databases were able to successfully detect microcalcifications, and their computational performance were also assessed.
- The 2D MF-DFA method has shown to outperform the other two wavelet-based variants of multifractal analysis (MMWT and WLMF), independently from the spatial resolution of the images in the database. Nevertheless, 2D WLMF is computationally more efficient having average detection performance.
- The inspection of singularities and their fluctuations at multiple resolutions revealed that the multifractal study is very important for the characterization of the underlying complexity of microcalcifications. Multifractal mammogram analysis provides, therefore, useful information for computer-aided detection.

This work was initially presented in the First International Workshop on High Performance Computing Applied to Medical Data and Bioinformatics and published in the proceedings of the conference [11]. After further developments a presentation was made in the IEEE Pacific Rim Conference on Communications, Computers and Signal Processing with a paper published in the respective proceedings [12]. Finally a journal article was prepared and has been submitted to a IEEE journal [13].

### **2) Classification of Breast Masses on Contrast-Enhanced Magnetic Resonance Images Through Log Detrended Fluctuation Cumulant-Based Multifractal Analysis**

- A decision-support system was developed to identify the typically biopsy-recommended cases from 2D breast MR images.
- This system makes use mathematical descriptors of the multifractal spectra and *log-cumulant* features in a supervised classifier scheme to effectively provide a biopsy recommendation.
- The decision-support system presents high accuracy (94%) distinguishing suspicious malignant lesions from probably benign lesions, with one of the eight features studied.

The first evidence to these findings was presented in the Special Session on Breast CAD of the conference Computer Assisted Radiology and Surgery and published in the respective proceedings. It was also published in a supplement of the International Journal of Computer Assisted Radiology and Surgery from Springer-Verlag [14]. A more complete version of the work was accepted for publication in the IEEE Systems Journal [15].

### 3) 3D Lacunarity in Multifractal Analysis of Breast Tumor Lesions in Dynamic Contrast-Enhanced Magnetic Resonance Imaging

- The presence of multifractality in breast MR volumetric images was confirmed by prevalence of multiple degrees of self-similarity at multiple scales. A combination of self-similarity characteristics retrieved from the multifractal analysis using 3D lacunarity as the measure, was effective for the classification of malignant and benign lesions.
- This method was more accurate in estimation of the likelihood of malignancy than 2D MF-DFA and the clinical standard for analysis of tumor kinetics, 3TP. Therefore, the proposed feature extraction and classification method have the potential to complement the interpretation of the radiologists and supply a computer-aided diagnosis (CADx) system.

The novel multifractal 3D method and application to breast MR images was published in IEEE Transactions on Image Processing [16].

## V Thesis Organization

The Thesis is organized as follows:

### Chapter 1: Introduction

A brief introduction to the Thesis is presented including the focus and scope, Thesis objectives, Thesis statement, and major contributions of the work carried out.

## **Chapter 2: Computer-Aided Detection and Diagnosis of Breast Cancer: Overview on Typical Systems and Methods in Mammography and Breast Magnetic Resonance Imaging**

The background concepts behind the work developed are presented and discussed including both, an overview of breast cancer imaging modalities as well as a description of typical CAD systems. Finally, a survey on methods constituting CADe and CADx is presented.

## **Chapter 3: Review and Performance Evaluation of Multifractal Approaches for Computer-aided Detection of Microcalcification Clusters in Mammograms**

This chapter presents a comparative of three multifractal methods applied in the detection of microcalcifications in mammograms.

## **Chapter 4: Classification of Breast Masses on Contrast-Enhanced Magnetic Resonance Images Through Log Detrended Fluctuation Cumulant-Based Multifractal Analysis**

MF-DFA multifractal method is applied in the classification of suspicious malignant images in 2D breast MR images.

## **Chapter 5: 3D Lacunarity in Multifractal Analysis of Breast Tumor Lesions in Dynamic Contrast-Enhanced Magnetic Resonance Imaging**

A novel multifractal method is proposed using 3D lacunarity for classification of benign and malignant breast lesions in volumetric breast MR images. This method was compared with the method of Chapter 4 in the same dataset.

## **Chapter 6: Conclusion and Future Work**

The results presented throughout the Thesis are discussed and the main achievements are summarized pointing directions for the future.

## **References**

- [1] L. Tabar, M. Yen, B. Vitak, H. Chen, R. Smith, and S. Duffy, "Mammography service screening and mortality in breast cancer patients: 20-year follow-up before and after introduction of screening," *The Lancet*, vol. 361, no. 9367, pp. 1405-1410, 2003.
- [2] M. Reddy and R. Given-Wilson, "Screening for breast cancer," *Womens Heal. Med.*, vol. 3, no. 1, pp. 22-27, Jan. 2006.
- [3] L. Wyld and C. E. Ingram, "Screening of the population for breast cancer," *Surg. Oxf.*, vol. 25, no. 6, pp. 254-256, Jun. 2007.
- [4] D. Schopper and C. de Wolf, "How effective are breast cancer screening programmes by mammography? Review of the current evidence," *Eur. J. Cancer*, vol. 45, no. 11, pp. 1916-1923, Jul. 2009.
- [5] P. Skaane, "Studies comparing screen-film mammography and full-field digital mammography in breast cancer screening: updated review," *Acta Radiol. Stockh. Swed.* 1987, vol. 50, no. 1, pp. 3-14, Jan. 2009.

***Computer-Aided Detection and Diagnosis of Breast Cancer in 2D and 3D Medical Imaging Through Multifractal Analysis***

[6] A. M. J. Bluekens, R. Holland, N. Karssemeijer, M. J. M. Broeders, and G. J. den Heeten, "Comparison of Digital Screening Mammography and Screen-Film Mammography in the Early Detection of Clinically Relevant Cancers: A Multicenter Study," *Radiology*, vol. 265, no. 3, pp. 707-714, Jan. 2012.

[7] P. Skaane, A. I. Bandos, R. Gullien, E. B. Eben, U. Ekseth, U. Haakenaasen, M. Izadi, I. N. Jebsen, G. Jahr, M. Krager, L. T. Niklason, S. Hofvind, and D. Gur, "Comparison of Digital Mammography Alone and Digital Mammography Plus Tomosynthesis in a Population-based Screening Program," *Radiology*, vol. 267, no. 1, pp. 47-56, Jan. 2013.

[8] F. van Gelderen, *Understanding X-Rays: A Synopsis of Radiology*. Springer, 2004.

[9] E. Pisano, M. Yaffe, B. Hemminger, R. Hendrick, L. Niklason, A. Maidment, C. Kimme-Smith, S. Feig, E. Sickles, and M. Braeuning, "Current status of full-field digital mammography," *Acad. Radiol.*, vol. 7, no. 4, pp. 266-280, 2000.

[10] F. Davoine, M. Antonini, J.M. Chassery, and M. Barlaud, Fractal Image Compression Based on Delaunay Triangulation and Vector Quantization, *IEEE Transactions on Image Processing*, special issue on vector quantization, vol. 5, no. 2, pp. 338-346, 1996.

[11] F. Soares, P. Andruszkiewicz, M. M. Freire, P. Cruz, M. Pereira, "Self-Similarity Analysis Applied to 2D Breast Cancer Imaging," *Proceedings of the International Conference on Systems and Networks Communications*, IEEE Computer Society Press, pp. 77-83, 2007.

[12] F. Soares, M. M. Freire, M. Pereira, F. Janela, J. Seabra, "Towards the detection of microcalcifications on mammograms through Multifractal Detrended Fluctuation Analysis," *Proceedings of the IEEE Pacific Rim Conference on Communications, Computers and Signal Processing*, IEEE Computer Society Press, 2009, pp. 677-681, 2009.

[13] F. Soares, F. Janela, M. Pereira, J. Seabra, M. M. Freire, "Review and Performance Evaluation of Multifractal Approaches for Computer-aided Detection of Microcalcification Clusters in Mammograms," Submitted for publication in an international peer-reviewed IEEE journal, 2013.

[14] F. Soares, F. Janela, J. Seabra, M. Pereira, M. M. Freire, "Self-similarity classification of breast tumour lesions on dynamic contrast-enhanced magnetic resonance images," - Special Session on Breast CAD, *International Journal of Computer Assisted Radiology and Surgery*, Springer-Verlag, Volume 5, pp. S203-S205, 2010.

[15] F. Soares, F. Janela, J. Seabra, M. Pereira, M. M. Freire, "Classification of Breast Masses on Contrast-Enhanced Magnetic Resonance Images Through Log Detrended Fluctuation Cumulant-Based Multifractal Analysis," *IEEE Systems Journal*, accepted for publication, 2013.  
DOI: 10.1109/JSYST.2013.2284101

[16] F. Soares, F. Janela, M. Pereira, J. Seabra, M. M. Freire, "3D Lacunarity in Multifractal Analysis of Breast Tumor Lesions in Dynamic Contrast-Enhanced Magnetic Resonance Imaging," *IEEE Transactions on Image Processing*, Volume 22, Issue 11, pp. 4422-4435, 2013.  
DOI: 10.1109/TIP.2013.2273669

## Chapter 2

# **Computer-Aided Detection and Diagnosis of Breast Cancer: Overview on Typical Systems and Methods in Mammography and Breast Magnetic Resonance Imaging**

This chapter consists of the following article:

Computer-Aided Detection and Diagnosis of Breast Cancer: Overview on Typical Systems and Methods in Mammography and Breast Magnetic Resonance Imaging

Filipe Soares, Filipe Janela, Manuela Pereira, João Seabra and Mário M. Freire

Submitted for publication in an international peer-reviewed Elsevier journal, 2013.



# Computer-Aided Detection and Diagnosis of Breast Cancer: Overview on Typical Systems and Methods in Mammography and Breast Magnetic Resonance Imaging

Filipe Soares<sup>1,2,\*</sup>, Filipe Janela<sup>1</sup>, Manuela Pereira<sup>2</sup>, João Seabra<sup>1</sup>  
and Mário M. Freire<sup>2</sup>

<sup>1</sup>Siemens S.A. Healthcare Sector, 4456-901 Perafita, Portugal.

<sup>2</sup>Instituto de Telecomunicações, Department of Computer Science, University of Beira Interior, 6201-001 Covilhã, Portugal.

Corresponding author. E-mail address: filipecruzsoares@gmail.com

---

**Abstract** This paper reviews computer-aided medical imaging analysis (CAD) systems in breast cancer detection and diagnosis, focused on the two complementary modalities that provide the most detailed images of the breast: Mammography and breast Magnetic Resonance Imaging (MRI). The paper presents an overview of digital image processing and pattern analysis techniques to address several areas in CAD of breast cancer, including: contrast enhancement, detection and classification of microcalcifications, detection and classification of masses. This work is organized as follows. First, the background on breast cancer imaging modalities is introduced followed by how CAD can be embedded in the clinical cycle of breast imaging. Then we proceed to the particular case of CAD in mammography and breast MRI. Finally, a survey on this research area is presented, organized by the state-of-art in detection and diagnosis, through feature extraction and classification, in mammography and breast MRI.

*Key words:* Computer-Aided Detection (CADe), Computer-Aided Diagnosis (CADx), Mammography, Magnetic Resonance Imaging (MRI), Feature Extraction, Classification, Multifractal Analysis, Multiscale, Wavelets.

---

## I Breast Cancer Imaging

Breast cancer is the second leading cause of cancer death in women, exceeded only by lung cancer [1]. The declining death rates in the last twenty years in developed countries are

believed to be the result of earlier detection through screening and increased awareness, as well as improved treatment [2]. This is a big argument in favor of screening programs that has been focused on traditional imaging modalities of the breast as x-ray Mammography, which has been the standard imaging modality for decades [3]-[8]. Incidence rates of breast cancer have been increasing in the industrialized world following the increased life expectancy in those countries and the fact that many people are screened by methods that did not exist a few decades ago. The combination of the characteristics of breast cancer: high incidence, deadly disease, asymptomatic at earlier stages, and high survival rate if detected in early stages, makes the fight against the disease, through research and development of high-end technology in breast imaging devices, worthy.

Mammographic first signs of breast cancer usually appear in the form of clusters of microcalcifications. These tiny deposits of calcium can be visible long before any palpable lesion has developed and their early detection contributes to the success of the treatment. For diagnosis, radiologists generally rely on the evaluation of their shape, size, number and distribution. Malignant microcalcifications are typically very numerous, clustered, small, dot-like or elongated, variable in size, shape and density. Benign microcalcifications are generally larger, more rounded, smaller in number, more diffusely distributed, and more homogeneous in shape [9]. However, because of the small size of microcalcifications, the comparison and characterization of benign and malignant lesions represents a very complex problem even for an experienced radiologist [10].

The microcalcifications can arise in isolation or together with other areas of high density breast tissue, called masses. The term mass arises from the characteristic well-defined mammographic appearance, which tend to be brighter than the surroundings due to the high density within their boundaries. In order to be able to characterize a mass, radiologists generally rely on its contour and different kinds can be observed in mammograms (circumscribed, spiculated, microlobulated, with dense kernel). Usually circumscribed masses are related to benign lesions while spiculated masses are related to malignant lesions.

Mammography is generally accepted as the leader imaging modality of the breast, due to its high sensitivity and even higher specificity at low cost. Nevertheless, as the volumetric anatomical information is projected into a two-dimensional (2D) image plane, it can be hard to distinguish a breast tumor from overlying breast tissues. The presence of a tumor can be masked, which may delay the correct diagnosis and decrease the probability of a successful treatment, affecting the survival rate and increasing the costs of the future treatment. The overall breast density is known to be the main affecting factor of mammographic accuracy [11]. Dense breasts present the problem of poor detail on the detection and interpretation of the findings. In addition, x-rays are absorbed by typical dense malignant findings, however they are also absorbed by benign fibroglandular tissue resulting in false-positives and in the need for a recall that may

cause anxiety in women and unnecessary costs.

Alternative imaging modalities for breast cancer detection and diagnosis methods have become more common in the last 15 years: Positron Emission Mammography (PEM), Digital Breast Tomosynthesis (DBT), Ultrasound, and Magnetic Resonance Imaging (MRI). PEM is a very promising technique to provide functional information on breast cancer. This modality is still under development and since it makes use of radiotracers it is more appropriate to presurgical planning and monitoring response to therapy or recurrence. DBT is an emerging technique that may complement the mammography gaps [12]-[14]. This recent technology allows low-dose mammograms to be acquired at different projection angles over a limited range, which can be reconstructed to yield a (compressed) 3D breast volume. Therefore, the image acquisition is free of superposition between tissues and abnormalities, but it is still under investigation whether DBT images are better interpreted by the man or by the machine. In addition, it still exposes the patient to ionizing radiation, though in lower doses than usual mammography. Ultrasound emits sound waves and picks up the echoes as they bounce off body tissues. The echoes are converted by computer software into grayscale images of low resolution. In breast ultrasound, a gel is placed over the skin of the breast and a handheld instrument called a transducer is rubbed with gel and pressed against the skin. Breast ultrasound is used to clarify the type of certain lesions found during screening, diagnostic mammograms or on physical examination [15]. Ultrasound imaging lacks the resolution and contrast of mammography; however, it is ionizing radiation-free and hence more commonly used in younger women.

MRI of the breast has been shown to be the most sensitive modality for imaging high-risk women, offering valuable information about breast conditions that cannot be obtained by other imaging modalities, such as mammography or ultrasound [16], [15], [17]. In the context of screening it is yet to be determined whether the higher sensitivity of breast MRI will result in stronger reduction of breast cancer mortality. MRI scans use magnets and radio waves instead of x-rays to produce very detailed, cross-sectional pictures of the body. MRI does not use ionizing radiation, the energy from the radio waves is absorbed and then released in a pattern formed by the type of body tissue and by diseases as breast cancer. Dynamic contrast-enhanced magnetic resonance imaging (DCE-MRI) of the breast is especially robust for the diagnosis of cancer in high-risk young women with dense breasts. Imaging analysis is based on the enhancement pattern of lesions in dynamic breast MRI and on morphological changes. With these two criteria, breast MRI is highly sensitive in detecting breast cancer. However, its specificity may be compromised since several benign masses take up contrast agent in a similar way as malignant lesions do. DCE-MRI techniques are based on the injection of an MR contrast agent and acquisition of T1-weighted images over time, which provides information on the rate of passage of the agent between the blood and tissues. Tumor lesions are more vascularized due to angiogenesis than the surrounding normal tissue, and therefore these areas are distinguished from the background

[3]. For the analysis of breast MRI data, both the importance of morphology and of kinetic parameter assessment have been emphasized [18], [19]. However, the MR acquisition time is limited by the time of the contrast bolus passage, resulting in a trade-off between high spatial or temporal resolution. Therefore, a choice of focusing the image analysis on either morphologic features or kinetic enhancement must be made.

## **II CAD in Mammography and Breast MRI**

Early signs of breast cancer have become more apparent on mammograms, due to improvements in the acquisition techniques. However, the accuracy of the overall breast examination depends on both the quality of the images and the ability of the radiologist to interpret those images. During manual screening of a large number of mammograms, radiologists on visual inspection may get easily worn out, missing out vital clues while studying the scans. Double reading of screening mammograms provides greater sensitivity than single reading without increasing recall rates [20]. However, the number of radiologists required for double reading approach will be huge and many nations might not be able to meet this requirement. To minimize these effects, tremendous effort has been made to automate the process of mammographic screening.

Computer-aided detection (CADE) and diagnosis (CADx) involve the application of computerized analysis to the process of medical image interpretation. CADE and CADx systems for breast imaging may provide a practical help, particularly to mammographers who have limited experience. A radiologist uses the output from a computerized analysis of medical images as a second opinion in detecting and classifying lesions, with the final diagnosis being made by the radiologist. The computer output must be at a sufficient performance level, and displayed in a user-friendly format for effective and efficient use by the radiologist. The CAD performance by computers does not have to be comparable to or better than that by physicians, but needs to be complementary to that by physicians. It should be noted that here, CAD refers to the whole field and comprises both CADE and CADx. CAD systems are strongly needed in order to support the radiologists in the process of detecting lesions, interpreting the increased amount of image data, annotating features to classify, assessing extent of disease, and making diagnostic decisions for subsequent patient care [21]. Advances in computer vision, artificial intelligence, and computer technology, along with recognized medical screening needs and the availability of large databases of cases, has made the field of CADE and CADx grown substantially since the mid-1980s, with many comprehensive reviews written [22]-[31].

Fig. 1 shows how CAD is usually embedded in the clinical cycle of breast imaging. Typically the flow of data circulates from the imaging systems to a Picture Archiving and Communication

System (PACS) where the images are hosted until they are observed in reading station. It is presented a CAD integration scheme with possibility of operation outside the health provider. The images are transferred from PACS to the CAD server where the algorithms for detection and classification lead to a proposal of diagnosis that reaches the radiologist reading station.

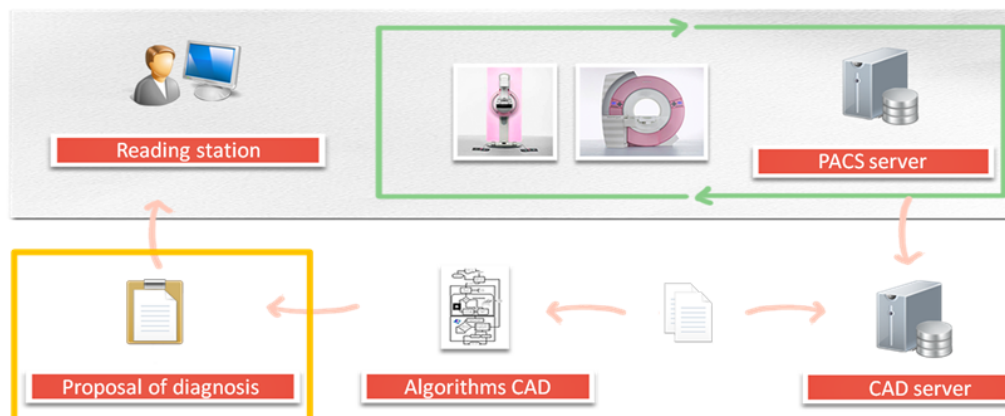


Figure 1: CAD embedded in the clinical cycle of breast imaging. The input images need to be stored and available for review with the integration of CAD and PACS.

The CADe for mammography is by far the most mature among all medical imaging analysis systems. It detects abnormalities or suspicious regions, and marks them with different labels indicating different features to be analyzed [32]. It can only assist the radiologist to make a decision but in both, observer studies and clinical evaluations, CADe is reported to increase the number of cancers detected by approximately 10%, which is comparable to double reading by two radiologists [33], [34]. A great deal of research has also been spent on developing CADx for breast ultrasound [35], [36], but for specific pathological lesions. Since MRI involves the acquisition of much more images compared to mammogram and ultrasound, development of breast MRI CAD is far more challenging, but also very helpful.

The general process of CAD for mammograms refers to image pre-processing, definition of region of interest (ROI), feature extraction and selection, classification and labeling of a ROI into benign, malignant or normal. This can be done by intelligent navigation tools to improve workflow.

The particular task of CADe is to focus the attention of the radiologist on suspicious areas, to reduce the oversight error. It can only assist the radiologist to make a decision, but the use of a CADe system can be comparable to double reading by two radiologists, and it has been shown to help finding more cancers [34], [28]. To detect abnormalities, most of the algorithms consist of: first, detection of suspicious ROIs on the mammogram, and second, its classification as mass, microcalcifications or normal tissue. The first stage is designed to have a very high sensitivity and a large number of false positives per image (FPI) is acceptable, since they are expected to be removed in stage two [37]-[39]. The ultimate goal of any CADx system is to be robust enough for clinical application and to provide reliable results that go

beyond detecting suspicious areas, but focusing on its recognition giving the impression about the severity level of the lesion. Computer assistance in its wider sense additionally comprises automated or semi-automated procedures such as image preprocessing, image registration, image segmentation, color-overlay, feature extraction, feature selection, machine learning, and 3D rendering techniques.

The intrinsic data variability and the interaction between the human observer and CADx systems induce the image interpretation to be very subjective. In this context, the validation of medical image processing approaches is required to highlight the inherent characteristics and behaviors of a method, in order to evaluate performance and limitations, and to compare it with different existing approaches. This requires having validation datasets with real clinical images for which the reference result has to be known. This “ground truth” can represent a contour outlined around a finding in case of CADe, or the nature of the abnormality (benign or malignant) for CADx systems. The choice of suitable metrics for the validation process is another crucial aspect [40].

The performance of detection algorithms in CADe is usually measured with sensitivity (Number of True Positive Marks / Number of Lesions) and the number of FPI (2.1). A true positive is a mark made by the CADe system that corresponds to the location of a lesion. A false positive is a mark made by the CADe that does not correspond to the correct location. The sensitivity versus FPI for different thresholds of detection is called a Free-Response Receiver Operating Characteristic (FROC) curve and this is generally used to report the performance of the detection algorithm [41]. Generally, the bigger the area under the curve the better but, despite the consistent use of evaluation methods in the literature, direct comparison of systems for detecting mammographic abnormalities is difficult because few studies have been reported on a common database [28].

$$FPI = \frac{\text{Number of False Positive Marks}}{\text{Number of Images}} \quad (2.1)$$

The aim of automatic diagnosis in CADx systems is to find a sufficiently good algorithm to support the radiologist decisions and to improve the overall sensitivity (2.2) and specificity (2.3). This can be evaluated by the Receiver Operating Characteristics (ROC), which allows computing as well the accuracy (ratio of correct diagnosis and total number of cases) and the area under the ROC curve. In case of ROC analysis, the reference result in validation datasets is usually the histological proof. However, alternatives do exist such as comparing CADx performance with BI-RADS grade used by the radiologists. This can be a multiclass evaluation against each BI-RADS grade, or a two class problem by following biopsy recommendations only. In the latter case the datasets can be divided into the categories: probably malignant and biopsied; probably benign and non biopsied.

$$\text{Sensitivity} = \frac{\text{Number of True Positives}}{(\text{Number of True Positives} + \text{Number of False Negatives})} \quad (2.2)$$

$$\text{Specificity} = \frac{\text{Number of True Negatives}}{(\text{Number of True Negatives} + \text{Number of False Positives})} \quad (2.3)$$

Based on the inspection of mammograms and often supplemental ultrasound and magnetic resonance images, radiologists give a recommendation for the subsequent patient management. Based on the level of suspicion of malignancy of the lesions found in the mammograms, usually a recommendation is made for a follow-up examination or, in the case of higher suspicion of malignancy, for a breast biopsy invasive removal and pathological testing of a suspicious area of the breast [29]. The positive predictive value (PPV) measures the percentage of all breast biopsies (diagnosed as positive for cancer) that are in fact positive for cancer (true positives) [33]. The PPV for diagnostic breast imaging is reported to be usually less than 30%, but there are substantial differences between the performance of radiologists from North America and Europe [29], [42], [43]. Unnecessary biopsies are both physically and emotionally traumatic for the patient; add unnecessary expenses and workload of radiologists, surgeons and pathologists. Improving PPV can have a substantial positive effect on patient care and on the healthcare system [33].

### **III Commercial CAD for Mammography and Breast MRI**

#### **Mammography CADe**

The R2<sup>TM</sup> Image Checker<sup>TM</sup> (nowadays property of Hologic, Inc.) was the first commercial CADe system approved by the *Food and Drug Administration* (FDA) intended to mark regions of interest on routine screening mammograms, and it was reported to have 98.5% of sensitivity at 0.5 FPI for microcalcification clusters detection and 86% sensitivity at 0.24 FPI for spiculated masses. In spite of rising the diagnostic sensitivity of the radiologists when using the system, the PPV of the interpretations decreased due to the high number of FPI [44].

A study by Gur et al. [45] reported that introducing the R2 CADe into this practice was not associated with statistically significant changes in recall and breast cancer detection rates, both for the entire group of radiologists and for the subset of radiologists who interpreted a high number of mammograms. Also, the work of Morton et al. [46] determines prospectively the effect of the same CADe system, stating that the use of CADe improved the detection of breast cancer, with an acceptable increase in the recall rate and a minimal increase in the number of biopsies with benign results. The study by Jiang et al. [47] shows that the use of CADe eliminated two-thirds of the substantial disagreements in which two radiologists recommended

biopsy and routine screening in the same patient ( $P < 0.05$ ).

Several companies such as Siemens, Hewlett Packard Co., Eastman Kodak Health Group (Carestream Health, Inc. since 2007), Sterling Diagnostic Imaging, GE, Lockheed Martin and Hologic were factoring mammography equipments for clinical imaging, which are usually combined with CAD systems for microcalcifications and mass detection. In spite of a variety of CADe systems in mammography are commercially available, only iCAD<sup>TM</sup> SecondLook<sup>TM</sup>, Confirma Inc. (acquired by Merge) CADstream<sup>TM</sup> and R2<sup>TM</sup> Image Checker<sup>TM</sup>, have obtained the FDA approval in the United States.

The Standard Mammogram Form (SMF) [48] is an image normalization framework that eliminates the current limitations of the imaging process and relies only on anatomical breast structures. The SMF<sup>TM</sup> Workstation developed by Mirada Solutions embeds the quantification of the amount of non-fat and fat tissue for each pixel, temporal registration of the breast, reconstruction of the uncompressed breast and localizing microcalcification clusters in 3D [49]. This system obtained a microcalcification cluster detection rate of 95% TP with 0.38 FPI.

Two other CADe systems for mammography were evaluated by Lauria et al. in [50] as an aid for radiological diagnosis over microcalcification clusters. The tested systems were the commercial iCAD<sup>TM</sup> SecondLook<sup>TM</sup> [51] and the CALMA [34] (Computer Assisted Library in MAMmography) research project. Three radiologists were asked to read mammographic images with and without the support of the CADe systems. The area  $A_z$  under the ROC curves increased by 0.03 on average when radiologists were supported by CAD ( $P < 0.05$ ). The conclusion was that both can be used in practise to improve the sensitivity values of conventional reading (radiologist alone). The average values of the  $A_z$  were: 0.86 for readers alone, 0.88 with the support of SecondLook<sup>TM</sup> ( $P < 0.05$ ) and 0.90 with the support of CALMA ( $P < 0.05$ ). It was not possible to establish a strong dependence on the skill of the readers, but for what sensitivity is concerned, it was observed that the less experienced one was more helped by CADe. Also, the radiologists spent a lot of time in attempting to synchronize the reading of film with CADe. Moreover, the two CAD systems were not compared directly in terms of sensitivity and specificity values, because it would have been necessary to collect a significantly larger number of images to obtain a statistically significant difference [52].

## Mammography CADx

Promising CADx prototypes are being developed and investigated in mammography. However, while considerable evidence has been collected that CADx have the potential to improve the diagnostic performance of radiologists, still no commercial CADx system is available today and open issues remain [29].

## Breast MRI CADe

In breast MRI studies, CADe provides a viable solution for reviewing thousands images in a standard study, with image processing and reporting tools to streamline the process. The CADstream™ was the first FDA approved CADe system developed by Confirma, Inc. for the automated data analysis, image management, and interpretation of breast MRI. It assists radiologists in the interpretation, standardization and reporting of these data-intensive studies. Nowadays, core features of CADstream include adaptive image registration (2D/3D), multiplanar reformatting, subtractions, angiogenesis maps, maximum intensity projections (MIP), volume summaries and it also incorporates ACR BI-RADS atlas for manual lesion classification [53].

Another commercial CADe in breast MRI is the fTP (full-time-point) pharmacokinetic analysis software platform by CADsciences. It provides various perspectives of the enhanced lesions to assist its interpretation. Similarly to CADstream, the display is mainly based on the enhancement kinetic features, such as the wash-out patterns, of voxels with the percent enhancement above a pre-set threshold. The morphological features as defined on BI-RADS lexicon [53], as well as the final diagnostic impression, will have to be evaluated by radiologists [32]. These CADe systems for MRI of the breast presently in use, generally display the suspicious lesions based on an enhancement above a threshold level, as well as the enhancement kinetics from the lesion [54]-[56]. Analyses of morphological features are left to the radiologist, who needs to combine all the information in order to make a final diagnostic decision. These commercial systems are in fact display systems [19]. The properties in the enhancement kinetics of lesions measured by DCE-MRI, either using fitting parameters from pharmacokinetic models or raw enhancement data, have been extensively investigated. On the other hand, the work in quantitative morphological analysis of lesions is much less [32].

## Breast MRI CADx

Although the essential information may be extracted with CADe, it would be helpful to add capabilities for differentiating among groups of lesions. To automate lesion classification, features extracted by computer-based image analysis have been investigated as diagnostic aids, with mathematical descriptors related with the ones visually used by radiologists. This approach can be developed towards the quantitative analysis of textural, morphological and kinetic enhancement features [21]. Currently, the exception to the existent CADe systems designed for DCE-MRI of the breast is the DynaCAD™ from Invivo Corporation [57]. Even though it solely relies on morphological analysis, a fully-automated classification is possible in the clinical practice making it the first breast MRI CADx in the market. The research behind this system is based on fractal theory as described by Penn et al. in [32].

## IV CADe and CADx Typical Schemes

Experience gives the radiologist the perceptual and cognitive skills to know what information to look for and how to interpret that information on the basis of the accumulation of knowledge from previous encounters with the same types of images. What makes their task difficult is the fact that, besides the highly texturized structure of the mammograms, the degree of natural anatomic dissimilarity is high. The radiologists will never be able to recognize all possible variations no matter how long they practice and how many images they see [59], which emphasizes the need for machine aid. The development of CADe systems has reached the point where extremely valuable information is offered to the clinician in the detection of lesions, at the earliest possible stage. In addition, it is important to realize that the reliability of CADx systems should be close to perfection, since it can have very serious implications. This section frames typical CADe and CADx based on classes of methods found on the state-of-art in computer-aided tools for breast imaging.

### CADe

A typical CADe can be described by the flowchart in Fig. 2. The different steps involved in the detection of features and its classification into microcalcifications or masses are presented.

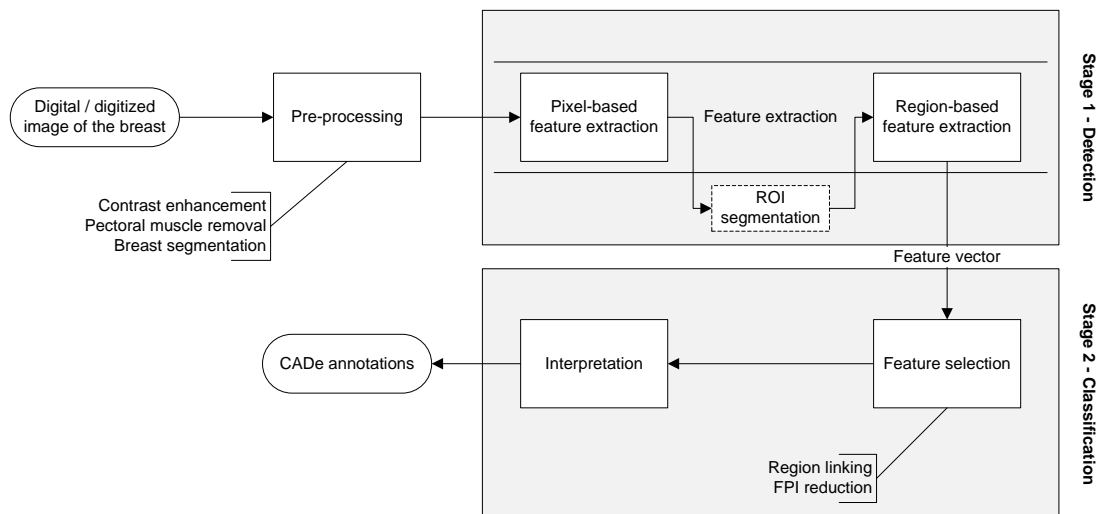


Figure 2: Flowchart of a typical CADe system in breast imaging. Borders of optional processing steps are dashed.

First block includes digitalization of the mammograms with different sampling and quantization rates, or direct acquisition to digital images by Full Field Digital Mammography (FFDM) [14]. The digitized/digital mammogram can be de-noised and enhanced. In this sense, contrast

enhancement can be considered a pre-processing step in breast CAD schemes. The pectoral muscle removal and the breast segmentation are also important steps. The pectoral muscle is a mass of tissue on which the breast rests. It usually appears slightly brighter compared to the rest of the breast tissue in mediolateral oblique view mammograms. This may cause biased detection of findings, particularly with masses, and it is often removed during mammogram pre-processing [60]. Breast segmentation by watershed transform [61], or recently discussed breast density estimation [62], are interesting examples of pre-processing steps.

## CADx

The task of discriminating benign and malignant lesions is usually modeled as a two-class classification problem. Most diagnosis algorithms in CADx approaches start with a ROI containing the lesion that shall be classified. The ROI may have been delineated manually by a radiologist or automatically by a CADe system. It usually is a rectangular subimage cut from a mammogram. Most CADx systems include steps for lesion segmentation, feature extraction, feature selection, and finally classification. Figure 3 shows a flowchart of a typical CADx system. The output may be the likelihood of malignancy, or a recommendation for biopsy or follow-up. In many systems, no automatic selection of features is done, while other approaches do not require an explicit segmentation of the lesion from the background tissue in the ROI. Some approaches use multiple ROIs containing the lesion cut from different mammographic projections e.g., craniocaudal (CC) and mediolateral oblique (MLO). Others use the information from additional modalities or from previous examinations on a temporal analysis of changes. The information about the clinical case can be optionally omitted from the scheme. In case of usage, patient data as age, history of cases or cancer risk, are embedded in the CADx scheme together with annotations about lesions found and BI-RADS grading by radiologists [29].

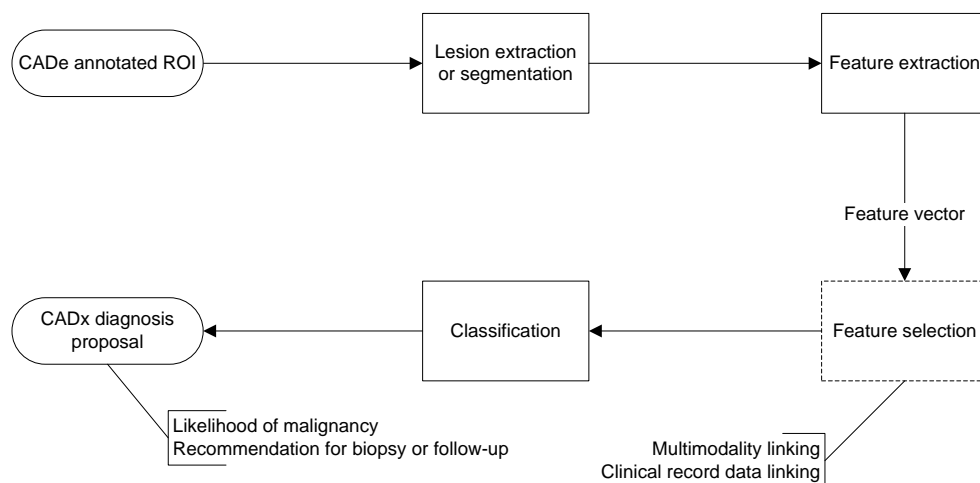


Figure 3: Flowchart of a typical CADx system in breast imaging. Borders of optional processing steps are dashed.

The organization of the next Section V closely follows the design of typical CADe and CADx systems, as illustrated in Fig. 2 and Fig. 3, respectively. Various methods are employed for the automatic extraction of features representing attributes of clustered microcalcifications and mammographic masses. While the methods used for lesion segmentation and feature extraction differ for clustered microcalcifications and mammographic masses, approaches for the remaining steps of feature selection and classification usually can be applied to both types of lesions.

## **V Survey on CADe and CADx Methods**

This section provides a survey on methods of image processing and analysis that have been developed to approach the problem of detection and diagnosis of masses and microcalcifications. It concentrates on this important type of breast lesions, and does not cover less common types like architectural distortions. These methods comprise: pixel and region-based feature extraction or segmentation, morphology and texture features, multiscale analysis, wavelet transforms, multifractal analysis, feature selection, an assortment of classifiers and other recently proposed methods. This section is organized by CADe and CADx methods in mammography and breast MRI. In particular it is studied the DCE-MRI, which is the most sensitive technique for the diagnosis of cancer in high-risk women, and also the most researched CAD-related technique for MRI. Nevertheless, microcalcifications are not visible in MRI due to the limited spatial resolution of this imaging modality and also the minuscule size of these important findings in breast. Therefore, even though in the scope of mammography the survey includes microcalcifications and masses, in breast MRI only the CADe and CADx on masses are covered.

### **V.A Feature extraction for CADe detection of clustered microcalcifications in Mammography**

#### **Stage 1 - Detection**

Radiologists employ a number of image characteristics on the discrimination of the findings and researchers have attempted to emulate that process. The first apparent characteristic is the region intensity or luminance. It is known that if a region differs in luminance from its surroundings by less than 2%, it is indistinguishable to human eye [65]. Although microcalcifications usually appear brighter than their surroundings, in a dense breast their contrast is quite low to be distinguished. Especially in some denser breasts of younger women, suspicious areas are almost invisible and other dense structures, as hypertrophied lobules or fibrous strands, may

easily be misinterpreted as microcalcifications. This is the major problem that most of the algorithms have to overcome.

The aim of contrast enhancement is to increase the contrast of microcalcifications over a threshold [66]. Usually, this kind of approach is globally oriented affecting all the image changes, and not precise enough to distinctively affect light details as microcalcifications. The major problem with these algorithms is that for an image, some regions may be under-enhanced that can cause false negatives while some regions may be over-enhanced resulting in false positives as noise [22].

Additional features were designed by Brake et al. [67] to capture image characteristics including isodensity, location and contrast, to classify between lesions and normal tissue. Tourassi et al. [68] used a template matching technique where each ROI of a database served as a template and mutual information was used as a metric of similarity to decide if a ROI contained a mass. These two approaches are mass oriented (see Section V.B). However, since microcalcifications have a variety of small sizes, shapes, and distributions, they make simple template matching a weaker option. Mathematical morphology [69]-[71] has been suggested as an efficient method for local contrast enhancement, being applicable for extracting only small light details without affecting other image details. Other strategies have been proposed for detecting microcalcifications, including contour-based model [72], random field models [73], fuzzy logic [74], [75] and artificial neural networks [76]-[80]. The micro size, low contrast and fuzzy nature of microcalcifications, makes its automated detection a field of heavy research. It is not only important to suppress the noise, to enhance the contrast between ROIs and background, but to extract and select features to identify the microcalcifications.

Detection of microcalcifications based on multi-scale analysis had been employed by a number of authors through wavelet transforms [81]-[85]. A reason why wavelets have been so effective is that microcalcifications appear as small bright dots on the mammogram and can be viewed as point discontinuities. Wavelet methods rely on pre-processing the image using a sub-band decomposition filterbank. The coefficients in the sub-band images which correspond to high spatial frequencies are selectively weighted to enhance the microcalcifications. A new image with enhanced microcalcifications is created with the inverse wavelet transform. Wavelets have finite square supports and are ideal for capturing point discontinuities, but not edges [23]. This explains the success in the detection of microcalcifications, whereas for the detection of masses these methods are not so effective [50].

Microcalcifications have less texture when compared to breast background. The parenchymal and ductal patterns in mammograms have high local self-similarity which is the basic property of fractal objects [86]. These tissue patterns can be reproduced synthetically by fractal models, and extracted from the original image. The abnormalities are considered as structural

deviations from the global regularity of the background, and this statistical approach already improved tumor classification in doubtful cases for expert radiologists [87] with MRI. The microcalcifications, which are not possible to be seen in MRI but in mammography due to the higher spatial resolution of the latter technique, can be enhanced by the fractal approach. The conventional fractal modeling of breast background tissues for the enhancement of microcalcifications is presented by Li et al. [86]. In terms of contrast and noise level, fractal modeling of breast background tissues was more helpful to enhance microcalcifications, compared to morphological operations and partial wavelet reconstruction approaches [86]. When self-similar geometrical objects as fractals are evaluated, the irregularities can be verified by analyzing their fluctuations at different resolutions. This property was found in medical images of breasts, by fractal dimension (FD), a value describing how the irregular structure of objects is replicated in scales. Since the cancer grows in an unexpected way, we can also expect malignant masses to have high FD, if we focus exclusively on morphology. This assumption comes from the Box-Counting algorithm applied to fractal dimension estimation [88] or, for example, FD can be estimated by the differences among values of gray of neighboring pixels in the images [89].

Multifractal theory can be considered an extension of fractal theory, where some natural phenomena (including natural images) might be better described. The multifractal spectrum summarizes both simple and multiple degrees of scaling. Scaling refers to the propagation of energy when the images are inspected at various resolutions. Monofractals are homogeneous in the sense that they have the same scaling properties, characterized by only one regularity exponent throughout the entire signal or image. In contrast, multifractals require a larger and theoretically infinite, number of indices or fractal dimensions to characterize their scaling properties. This can potentially give us more information about the image compared to the single fractal dimension [90]. More generally, this approach is capable of describing image features from local and global point of view, and be used for both, texture analysis for detection and classification. In a preliminary study [91] on the application of the multifractal image analysis to mammography, it was shown that the presence of microcalcifications led to changes in the local mammographic texture and multifractal scaling behavior. This was accomplished through multifractal detrended fluctuation analysis (MF-DFA). Recently, Soares et al. [58] confirmed the existence of multiple degrees of scaling in MRI of the breast, by using the scaling dynamics as discriminatory descriptors of irregularly for mass CADx.

## Stage 2 - Classification

General enhancement techniques not only enhance microcalcifications but also background structure and noise. In addition, most of these methods will have to include some sort of

noise removal to reduce the FPI. This is similar to the Stage 2 of the mass CAdE methods. The main aim in this case is to classify ROIs as either containing microcalcifications (positive ROI) or normal tissue (negative ROI). Various schemes have been developed for this purpose.

Nagel et al. [37] compared the performance of three methods for reducing FPI: rule-based method, neural network, and both techniques combined. They reported that the combined method was more efficient in eliminating FPI because each of the two stages eliminated different types of false-positives. Zheng et al. [92] developed a multistage algorithm including Gaussian filtering, nonlinear global thresholding for calcification detection and feature-based neural network for classification. Zhang et al. [93] applied a shift-invariant artificial neural network. Several methodologies have been proposed for the microcalcification characterization problem such as decision trees [94] or k-nearest neighbours [95]. Papadopoulos et al. [96] used a rule-based system, an artificial neural network (ANN) and a support vector machine (SVM) for the characterization of clustered microcalcifications. The best performance was achieved with SVM methodology is that the training procedure always converges to a specific solution corresponding to the global minimum of the objective function. In ANN the existence of several poor local minima that may trap the training procedure constitutes a considerable drawback. The effectiveness of SVM was also tested with great potential for classification, but here mass lesions were characterized by fractal dimension estimation methods. El-Naqa et al. [97] used support vector machines to detect microcalcification clusters. An improvement of the method was published by Wei et al. [98] using a relevance vector machine for microcalcifications CADx.

Wavelet transform is able to extracting microcalcifications also giving the spatial information of the detected object. In classification of microcalcifications wavelets still have an important role [82], [99]. Decision making is done by extracting features as a first stage by computing wavelet coefficients and classification using a classifier trained on the extracted features. Tsai et al. [100] detected microcalcifications by wavelet-based reconstruction and morphological features, having PCA evaluation on those features and BNN as final classifier. Detection of microcalcification by meta-heuristic algorithms was proposed by Thangavel and Karnan [101]. They used ant colony optimization (ACO) and genetic algorithm (GA) for identification of suspicious regions in mammograms. The method relies on the feature of bilateral asymmetry.

Sankar and Thomas proposed the method that uses fractal modeling of mammograms based on mean and variance to detect microcalcifications [102]. On a preliminary research by Kestener et al. [103] a multifractal spectrum is computed by the modulus maxima wavelet transform (MMWT) method, based on the continuous wavelet transform, and the methodology is applied to the classification of microcalcifications. Multifractal image analysis by Ramírez-Cobo and Vidakovic [85], focused solely on whole the image background and not on microcalcifications. Numerically stability problems induced attempting to overcome this difficulty in Wendt et al. [104] on generic non-medical images. Their multifractal formalism is based on wavelet leaders

Table I: Representative selection of microcalcifications CADe in Mammography

Authors	Year	Dataset size	Database	Features	Feature Selection and Classifier	$A_z$	TPF, FPI
Nagel et al. [37]	1998	50	Private	Featureless	Ruled-based and ANN	-	83%, 0.8
El-Naqa et al. [97]	2003	1120	University of Chicago	Pixel-based	SVM	-	94%, 1
Thangavel and Karnan [101]	2005	161	MIAS	Bilateral asymmetry	ACO vs GA	-	85%, 6
Papadopoulos et al. [96]	2005	105 25	Nijmegen; MIAS	Morphology	Ruled-based, SVM and ANN	0.81 0.79	-
Sankar and Thomas [102]	2007	111	MIAS	Fractal-based	Mean and variance	-	82%, 0.2
Tsai et al. [100]	2011	716	Private	Wavelet-based reconstruction morphology	PCA BNN	-	97%, 0.1
Thangaraju et al. [71]	2012	370	MIAS and DDSM	Hessian matrix	Foveal method	-	98%, 0.7
Oliver et al. [78]	2012	297 190	MIAS and Private	Bank of filters, dictionary of morphological features	Pixel-based Gentleboost classifier	-	80%, 1

instead of wavelet coefficients. An interesting work would be to compare both approaches in the context of mammogram images, as stated in [85].

Oliver et al. [78] created a word dictionary, which is obtained by convolving patches containing a microcalcification with a bank of filters. This dictionary allows characterizing examples of known microcalcifications and will be subsequently in unknown images. The words of the dictionary were used as input to the Gentleboost classifier. Testing mammograms are classified pixel-by-pixel by this trained classifier. Hence, the detection problem is translated to a pixel-based classification approach.

Table I provides a summary of a representative selection of various microcalcifications CADe algorithms in Mammography. Since most authors do not report the performance for stage 1 of the detection algorithm, the performance is measured at the CADe output.

## V.B Feature extraction for CADe detection of masses in Mammography

### Stage 1 - Detection

Detection algorithms (see Fig. 2, stage 1 - detection) can generally be considered to be of two classes of feature extraction: pixel-based or region-based [23]. The primary advantage of using pixel-based methods is that, since the features are extracted for each pixel from the local neighborhood of the pixel, a large sampling number is obtained to train a classifier. Then, the most suspiciously located pixels can be grouped together into regions, generally by collecting

connected pixels. This can be seen as the feature selection step in CADe (see Fig. 2, stage - classification). Optionally, a FPI reduction step can be applied followed by a classifier. These grouped pixels can be annotated to stand for the existence of possible lesions.

Radiologists characterize masses by their shape and margin properties, once well defined in at least two different projections. A number of researchers have focused on the detection of spiculated masses with higher likelihood of malignancy. Since they are characterized by spicules radiating in all directions, some approaches calculate the edge orientations at each pixel. Thus, each pixel is represented by a feature vector, which represents the strongest edge orientation at the pixel. The edge orientation itself can be computed in a variety of different ways. Kegelmeyer et al. [105] developed the idea of using the local edge orientation histogram feature as a normal mammogram exhibits a tissue structure that radiates in a particular orientation from the nipple to the chest, it would have edge orientations primarily in that direction. While in regions containing spiculated lesions, edges would exist in many different orientations. Mudigonda et al. [106] proposed a method for the detection of masses in mammographic images based on the analysis of iso-intensity contour groups, and subsequent inspection of texture flow-field information to eliminate false positives. Nakagawa et al. [107] used active contours models calculating the forces of the snakes, one related to edge intensity and the other based on grey-level information. Shi et al. [108] used level sets for accurately finding the border of the lesions and morphological, textural, and spiculation features for mass characterization. The main drawback of this approach is the assumption that masses have uniform density compared to the local background.

Karssemeijer et al. [109] detected stellate distortions by a statistical analysis of a map of pixel orientations. The orientation at each pixel was computed from the response of three filter kernels, which are second-order, directional derivatives of a Gaussian kernel in the directions. However, small masses may be missed if the neighborhood is too large and parts of large masses may be missed if the neighborhood is too small. To address this problem Liu et al. [110] developed a multi-resolution algorithm for the detection of spiculated masses using wavelets, due to the difficulty in estimating the size of the neighborhood that should be used to compute the local features of spiculated masses. A multiresolution representation of a mammogram using the discrete wavelet transform was generated and four features at each resolution for each pixel were extracted. Pixels were then classified using a binary classification tree. Not restricted in spiculated masses, Li et al. [111] developed a method for lesion site selection using morphological enhancement and stochastic model-based segmentation technique. A finite generalized Gaussian mixture distribution was used to model histograms of mammograms. The Expectation Maximization (EM) algorithm was used to determine the parameters of the model. The segmentation was achieved by classifying pixels using a new Bayesian relaxation labeling technique without a false positive reduction step. Heath and Bowyer [112] developed a mass

detection algorithm which was based on an Average Fraction Under the Minimum (AFUM) filter, which was designed to find the degree to which the surrounding region of a point radially decreases in intensity. This follows a different approach of first extracting features from the image and threshold them in a posterior step. Varela et al. [113] used features based on the iris filter output, together with gray level, texture, contour-related and morphological features.

Pixel-based feature extraction for detection also has inherent disadvantages. It does not take into account the spatial arrangement of the pixels, which is a very important factor to discriminate masses from normal tissue. In contrast, region-based feature extraction for detection takes into account the spatial information. Segmentation [114] or filtering techniques [115] can be applied to ROIs, which optionally could come from the output of a previous pixel-based extraction step. Features are then extracted for each region that is classified as suspicious or not. These features are directly correlated with important diagnostic information like shape and texture of the extracted regions. The main disadvantage is that if a classifier is used, there are fewer samples for training it as compared to the pixel-based class.

Qian et al. [116] developed a multi-resolution and multi-orientation wavelet transform for the detection of masses and spiculation analysis. It was observed that traditional wavelet transforms cannot extract directional information which is crucial for a spiculation detection task and thus, they introduced a directional wavelet transform. They show that at coarser resolutions, features such as the central mass region can be easily detected, whereas at finer resolutions detailed directional features such as spicules can be localized. Zhang et al. [76] noted that the presence of spiculated lesions led to changes in the local mammographic texture. They proposed that such a change could be detected in the Hough domain. They partitioned an image into overlapping ROIs and computed the Hough transform for each ROI. Local changes in mammographic texture were detected by thresholding to determine the presence of a spiculated mass. Zwiggelaar et al. [117] described a technique to characterize patterns of linear structures using principal component analysis and factor analysis. They created statistical models of spiculations created using ROIs containing spiculated masses. Sampat et al. [118] proposed a new class of linear filters, spiculated lesion filters, for the detection of converging lines or spiculations. These filters are highly specific narrowband filters, which are designed to match the expected structures of spiculated masses. As a part of this algorithm, the authors employ a radon transform of the image and filtering in the radon domain to enhance spicules on mammograms. Finally, a FPI reduction step is done by using oriented difference-of-Gaussian (DoG) filters to identify and create a likelihood map of potential normal structures.

A major limitation of both pixel-based and region-based methods is that the analysis is not done over a continuous range of scales. Cancerous lesions are stochastic biological phenomena which manifest in images as having various structures occurring at different sizes and over ranges of spatial scales. The boundaries of masses require a more localized approach, though the sharp-

ness, and hence the scales of interpretation of the lesion boundaries can vary considerably. Moreover, the spiculations that are associated with many cancerous lesions occur with different widths, lengths, and densities, which suggests that their characterization will require analysis over scales [23]. Timp et al. [73] presented automated detection of temporal changes in mammographic masses between consecutive screening rounds. Difference features and similarity features were designed to realize the interval change analysis.

There are several surveys in mammographic CADe that identify other classes of methods [24], [25], [30]. Segmentation is usually mixed with feature extraction for detection of masses in mammography, and the classification stage is often included on methods categorized as detection methods. Rangayyan et al. [25] were not particularly focused on masses but on the analysis of multiple subtle signs of cancer as bilateral asymmetry, architectural distortion not covered in the present work. They also joint detection and classification in methods comparison. Cheng et al. [24] cover qualitatively the general enhancement of mammographic images, the detection and classification of masses, and underlying computer vision techniques. Oliver et al. [30] presents a division between unsupervised and supervised segmentation techniques. Region-based methods are included in the unsupervised group together with counter-based methods and clustering methods. Counter-based are in fact edge detection methods that we stated already as region-based because they rely on boundaries of regions. Clustering methods can be performed pixel-wise or region-wise [119]. Model-based supervised methods, rely on the prior knowledge about the object and background regions to be detected or segmented. These often include a training stage and therefore we categorize them on Stage 2 - Classification.

## Stage 2 - Classification

The purpose of the classification of suspicious regions as mass or normal tissue is to reduce the number of FPI that were produced at the end of the first stage. The Stage 2- Classification strongly depends on Stage 1-Detection steps to extract features that feed the training of a classifier. Independently from the pixel-based or region-based features previously extracted, the use of decision trees was very common on early research on classification of masses [110]. Kegelmeyer et al. [105] trained a binary decision tree with texture and gradient features. Székely et al. [120] also used a decision tree to classify a sliding window to contain mass or normal tissue. In a first segmentation the feature vector is calculated and passed to a set of decision trees that classifies the image segment. Then markov random field (MRF) is used in a refined segmentation to improve the results. Wei et al. [121] developed a classifier using multiresolution texture features and linear discriminant analysis (LDA) for the classification task.

A general example of model-based classification methods is the pattern matching. The training is usually based on images containing the object to identify. The prototypes of possible masses are created based on the characteristics or physical features of the targeted masses. Freixenet et al. [122] used a probabilistic template matching scheme to detect masses. The shape of a deformable template was learnt from real mass samples, followed by a Bayesian scheme to adapt it to the real contours of the mammogram. Tourassi et al. [68] also used a template matching technique where each ROI of a database served as a template and mutual information (MI) was used as a similarity measure to decide if a query ROI contained a mass. MI-based template matching also shown to be flexible for robust translation across modalities [123]. However, template matching usually results in a large set of possible masses, a majority of which are false positives.

Christoyianni [124] used a radial-based function neural network (RBFNN) to classify features estimated using independent component analysis (ICA). They consider every region of mammograms to be generated by a set of independent images, namely the source regions, that are estimated using ICA techniques. Varela et al. [113] merged a feature set into a backpropagation neural network (BNN) classifier to reduce the number of false positives. Krishnapuram et al. [125] proposed a multiple-instance learning (MIL) algorithm that automatically selects a small set of useful features for diagnosis. Guo et al. [126] presented a study of fractal-based methods for texture characterization of mass lesions and architectural distortion. SVM was used as the pattern classification method for classification of masses. Campanini et al. [127] presented an SVM-based featureless approach for mass detection in digital mammograms. Instead of extracting features from ROIs, the authors used a multiresolution, overcomplete wavelet representation to codify the image with redundancy of information. West et al. [128] investigated the effect of classifier diversity and demonstrated that most of the improvement occurred with ensembles formed from 3-5 different classifiers.

Table II provides a summary of a representative selection of mass CADe algorithms in Mammography. The performance is measured at the CADe output.

## V.C Classification for CADx diagnosis of microcalcifications and masses in Mammography

Classification in CADx provides the answer whether microcalcification and masses are benign or malignant. Every classifier has its own advantages in classifying specific data as microcalcifications [98], and various classification techniques have been used for classifying masses. Most of the techniques used are supervised methods of machine learning [129] as: decision trees, LDA, SVM, ANN and Bayesian networks.

Table II: Representative selection of mass CADE in Mammography

Authors	Year	Dataset size	Database	Features	Feature Selection and Classifier	$A_z$	TPF, FPI
Kegelmeyer et al. [105]	1994	85	DDSM	Pixel-based and texture	Decision tree	-	97%, 0.28
Zwiggelaar et al. [117]	1999	56	Private	Pixel-based	PCA	-	80%, 0.23
Brake et al. [67]	2000	340 772	Nijmegen DDSM	Region-based isodensity	ANN	-	75%, 0.1
Mudigonda et al. [106]	2001	56	MIAS	Pixel-based Iso-intensity	Texture flow-field	-	81%, 2.2
Liu et al. [110]	2001	38	MIAS	Pixel-based wavelet	Decision tree	-	84%, 1
Tourassi et al. [68]	2003	1465	DDSM	MI template matching	SVM	0.87	-
Campanini et al. [127]	2004	512	DDSM	Wavelet coding	SVM	-	80%, 1.1
Sampat et al. [118]	2005	171	DDSM; MIAS	Spiculation filter	DoG	- -	88%, 2.7 84%, 3
Székely et al. [120]	2006	160	Private	Pixel-based and texture	Decision tree	-	90%, -
Varela et al. [113]	2007	394	Private	Region-based, Irish Filter, texture, morphology	BNN	-	97%, 3.8
Guo et al. [126]	2009	117	MIAS	Fractal-based	SVM	0.84	-

Most of the features in CADx are designed to capture the shape and margin characteristics of masses or microcalcifications, as mathematical descriptors of malignancy. Morphologic features are directly inspired by characteristics for which a radiologist looks. On the other hand, texture features have been designed to capture important differences between malignant and benign masses that may not be evident to human eye. Thus, texture features have the potential to capture characteristics that are important diagnostically but are not easily extracted visually [23].

ANN was applied in the study by Chan et al. [130], with results showing computerized methods able to capture the changes in the texture of the tissue surrounding malignancy, which were not visually apparent on mammograms. Later in [131], they decided to join morphologic features that described the size, contrast, and shape of microcalcifications and their variations within a cluster. They also used a genetic algorithm and LDA to select the best feature subset from the multi-dimensional feature spaces. Veldkamp et al. [95] used cluster shape features, cluster position features, and distribution features for the classification of microcalcifications. They used a sequential forward selection procedure for feature selection and a  $k$ -nearest-neighbor (kNN) classification scheme. One limitation of using shape features is the strong dependence on the accuracy of a segmentation algorithm [132]. If the contrast is very poor on microcalcifications, the segmentation may not be very accurate. Therefore, some research studies do not use shape features, as the work with image structure by Dhawan et al. [133]. Kallergi [134] developed a classification method that used ANN based on fourteen morphological (for individual microcalcifications) and distributional (for the clusters) features shown to achieve good performance. Kim and Yoon [135] evaluated recursive feature elimination-based support

vector machine (SVM-RFE) to improve classification accuracy. SVM-RFE incorporates feature selection in a recursive elimination manner to obtain a ranking of features that are particularly meaningful to SVMs and the top ranked features are chosen for classification.

De Santo et al. [136] used multiple classifier system (MCS). One classifier is devised for the classification of individual microcalcifications while the second one classifies the entire cluster. The first evaluates the following features: compactness, roughness, border gradient strength and local contrast. The classifier for clusters of microcalcifications evaluates the following features: mass density of the cluster, average mass of the microcalcifications and the centre mass of the cluster, standard deviation of the masses of the microcalcifications and standard deviation of distance between microcalcifications and center of mass. The final output was a weighted combination of the outputs of both classifiers. Radiologists do not look at every individual calcification to make a diagnosis but tend to focus more relevantly on the global properties of a cluster to make a diagnosis [23]. Soltanian-Zadeh et al. [137] compared four groups of features namely, multi-wavelet-based features, wavelet-based features, Haralick-based texture features and shape features, according to their discriminant power in separating microcalcifications severities. Within each group, a feature-selection procedure based on genetic algorithms was employed to identify the most-suitable features for use with a kNN classifier. Ren [77] proposed a new strategy namely balanced learning with optimized decision making to enable effective learning from imbalanced samples, which is further employed to evaluate the performance of ANN and SVM in the computer diagnosis of microcalcifications.. Although ANN outperforms SVM without balanced learning, the performance from the two classifiers becomes very comparable when both optimized decision making and balanced learning are employed.

Rangayyan et al. [138] used morphological features to characterize the roughness of tumor boundaries. They studied shape factors and edge acutance for the classification of manually segmented masses as benign or malignant, and spiculated or circumscribed. Later in [139], features are computed through an iterative procedure for polygonal modeling of the mass boundaries. Two features comprising spiculation index and fractional concavity were developed and combined with the global shape feature of compactness. Sahiner et al. [119] aimed to characterized mammographic mass margins according to BI-RADS spiculated and circumscribed categories. The features were evaluated with respect to the individual annotations by radiologists. Guliato et al. [140] implemented fuzzy region growing methods for mass segmentation and classification by the degree of inhomogeneity around the mass boundary, correlated with the likelihood of malignancy of the tumor. The authors obtained a benign/malignant classification sensitivity of 80% with a specificity of 90%. Lim and Er [141] studied the classification of masses using generalized dynamic fuzzy neural networks (GDFNN) with features based on the gray-level co-occurrence matrix.

Some authors have extracted texture and gradient features in a transform domain rather than

in the spatial domain, since they would be more discriminatory than features computed in the spatial domain. Sahiner et al. [142] proposed the rubber band straightening transformation (RBST) to transform a band of pixels surrounding the mass to a rectangular strip. They extracted texture features from the RBST image based on the SGLD matrices to classify masses as benign or malignant. Hadjiiski [143] classified masses using texture features extracted from the RBST image. They tested the performance of a hybrid classifier consisting of the unsupervised adaptive resonance theory (ART) network cascaded with the supervised LDA with claimed superior performance against Bayesian belief network (BNN), starting with manually segmented ROIs. Zheng et al. [144] applied a BNN and neural network on a common database and with the same genetic algorithm. The results show that the performance of the two techniques were at the same level, and pointed out that CADx in masses might be more dependent on feature selection and training database than on a particular classifier. Malar et al. [79] investigated the extreme learning classification with a single layer feed forward network (SLFFN), with superior performance over BNN or SVM, on wavelet-based extracted features.

Timp et al. [145] discussed how the inclusion of temporal change information affects a mass CADx system. SVM was also employed as a classifier. Besides the topic of temporal changes, content-based image retrieval (CBIR) [146], [147], multimodal and multiview approaches are becoming popular. Park et al. [147] investigated whether using a fractal dimension as a quantitative measure to assess the texture similarity of reference-image regions selected by a CBIR. Drukker et al. [148] proposed a multimodal CADx using mammograms and breast sonography. However, classification performance depended on specific methods for combining features from multiple images per lesion.

Table III and Table IV gives a representative selection of CADE algorithms in Mammography, respectively, for microcalcifications and mass diagnosis. The CADx performance is measured at the CADE output.

#### V.D CADx diagnosis of masses in DCE-MRI of the breast

Dynamic contrast-enhanced magnetic resonance of the breast has been an increasingly used technique with high sensitivity for breast cancer detection [150]. The biggest limitation of any breast MRI technique when compared with Mammography or DBT is the reduced spatial-resolution which relatively induces a lack on specificity. This is also compromised by the dynamics of the contrast agent in benign cases, making it difficult to discriminate between benign and malignant lesion. This is the main reason why the most recent research works have been focused more on CADx than CADE.

MRI requires significant time for image acquisition, processing and interpretation, with several

Table III: Area under the ROC curve  $A_z$  of a representative selection of microcalcifications CADx in Mammography

Authors	Year	Dataset size	Database	Features	Feature Selection and Classifier	$A_z$
Dhawan et al. [133]	1996	191	Private	Image structure	GA and BNN	0.86
Chan et al. [131]	1998	145	Private	Texture and morphology	GA and LDA	0.89
Veldkamp et al. [95]	2000	90	Nijmegen	Region-based shape	kNN	0.83
De Santo et al. [136]	2003	102	Nijmegen	Pixel-based and region-based	MCS	0.79
Kallergi [134]	2004	100	DDSM	Region-based morphology	ANN	0.98
Soltanian-Zadeh et al. [137]	2004	103	Nijmegen	Pixel-based multi-wavelet	GA and kNN	0.89
Karahaliou et al. [132]	2007	100	DDSM	Pixel-based texture	kNN	0.96
Kim and Yoon [135]	2009	347	DDSM	MI template matching	SVM-RFE	0.90
Ren [77]	2012	748	DDSM	Region-based shape	Balanced learning with ANN vs. SVM	0.94
Dheeba et al. [80]	2012	322 216	MIAS; Private	Texture	SONN	0.98 0.91

Table IV: Area under the ROC curve  $A_z$  of a representative selection of mass CADx in Mammography

Authors	Year	Dataset size	Database	Features	Feature Selection and Classifier	$A_z$
Sahiner et al. [142]	1998	168	Private	SGLD matrices RBST texture features	LDA	0.94
Hadjiiski [143]	1999	348	Private	RBST texture features	ART and LDA	0.81
Zheng et al. [144]	1999	433	-	Region-based	GA and BNN	0.87
Rangayyan et al. [139]	2000	54	MIAS and Alberta program	Modeling contours, spiculation, concavity, compactness	LDA	0.82
Lim and Er [141]	2004	343	DDSM	Pixel-based texture	GDFNN	0.87
Drukker et al. [148]	2005	100	Private	Region-based shape	BNN	0.92
Timp et al. [145].	2007	465	Dutch screening program	Temporal difference and similarity features	SVM	0.77
Guliatto et al. [149]	2008	111	MIAS and Alberta program	Texture and shape as in [139] Polygonal modeling contours preserves spicules	LDA	0.94
Park et al. [147]	2009	843	Private	Fractal-based	kNN	0.87
Malar et al. [79]	2012	120	MIAS	Pixel-based wavelet	SLFFN	0.98

hundred images per case [151]. Research on detection systems resulted in CADe mainly focus to help on this task [152]. Contrarily to the previous subsection related with CADe in mammography, this section combines detection and classification of features in one in order to identify masses. As mentioned in the beginning of the section, microcalcifications are not visible in MRI and only the computer-aided detection on masses is covered in this subsection.

The clinical diagnosis have been done by visual examination of morphology features and contrast-enhancement kinetics (functional features) using descriptors established in the BI-RADS lexicon [53]. Malignant lesions tend to have more irregular shape, spiculated margins, and heterogeneous inner enhancement [153]. A lesion with enhancement kinetics of rapid initial rise, followed by a drop-off with time (washout) in the delayed phase, has high PPV for malignancy [58]. Although BI-RADS provides a useful criteria, the priority and weights on different morphological features are not standardized.

The subjective clinical evaluation that is too much focused on reporting the findings qualitatively, plus the time consuming task for radiologists to analyze functional features, makes CADx a valuable aid [154]. Automatic detection and classification of breast lesions using advanced computational methods should reduce inter-observer variability and assist the radiologists in the clinical workflow. Considering the high throughput of images in the clinical routine the potential of CAD is evident, to reduce the subjectivity in human interpretation by improving specificity and possibly sensitivity, through a quantitative measurement, and quicken the workflow for the breast MRI analysis [58].

This subsection correspondingly follows the classes of methods already mentioned in mass CAD in mammography, but in recent research works feature extraction and classification a jointly framed. The simplest heuristic model used to distinguish between malignant and benign lesions in DCE-MRI is known as the three-time-points (3TP), [18], [155], [156], where points are selected along the time-intensity sequence during contrast uptake to characterize the enhancement slope and the washout rate. The enhancement pattern in the 3TP method varies according to the imaging protocol, but it allows a pixel-by-pixel kinetic analysis from the intensity values. Combining certain physiological parameters with a mathematical model of the temporal kinetics of the signal, parameter maps can be displayed. These depend on the overall shape of the tissue curves, and thus reflect tissue physiology only indirectly. In addition, the accuracy of the 3TP method is nearly insensitive to the temporal sampling rate of the acquired data, as shown in [157], which makes it preferable to apply the 3TP on data acquired by standard imaging protocols that suffer from low temporal resolution. Albeit providing only an imperfect gold standard which does not necessarily reflect the biological truth, the 3TP represents a clinical routine for visual examination of DCE-MRI data, and hence may serve as a reference model.

In the last sixteen years, a plethora of detection algorithms and classifiers have been proposed

for CAD of breast lesions in DCE-MRI. In 1997, Sinha et al. [158] proposed a multi-feature analysis method which makes use of three classes (kinetics, morphology and texture) for feature classification and use, for lesion classification, linear discriminant analysis together with linear discriminant stepwise regression. The automated interpretation approach based on enhancement variance dynamics proposed by Chen et al. [159] used linear discriminant analysis for lesion classification after feature extraction. Later in [54], Chen et al. used the fuzzy c-means clustering technique for segmentation of breast lesions. Pediconi et al. [160] investigated a novel color-coded signal intensity curve software. It allowed lesions to be visualized as false color maps which correspond to conventional signal intensity time curves. The high performance results are based on qualitative assessments considering all histologically confirmed lesions.

Morphology, texture and kinetic (temporal) features are important fields of research in feature extraction in DCE-MRI. For quantitative morphology analysis, Gilhuijs et al. [161] employed radial gradient histogram and other shape measures, using round-robin (RR) to classify the lesions. Yao et al. proposed in [162] a pixel-by-pixel classification method based on texture analysis and wavelet transform for tumour evaluation in breast DCE-MRI. In [163], Zheng et al. used spatiotemporal enhancement pattern and Fourier transformation to analyze two-dimensional images of breast tumors.

Artificial neural networks have been one of the most investigated approaches for the classification of breast lesions in DCE-MRI [164]-[166]. A primary advantage of using a neural network for classification is that the user is not required to select features or choose an appropriate model for the data. Szabó et al. [167] used an ANN to retrospectively determine the discriminative ability of kinetic, morphologic and combined MRI features. Inputs to the ANN included four morphologic and nine kinetic features from biopsy-proven breast lesions. The model derived from the most relevant input variables, called the minimal model, gave the best results. Natkemper et al. [168] analyzed various machine learning methods using four morphologic and five kinetic tumor features. It was provided a comparison between unsupervised and supervised classification: k-means clustering and self-organising maps also known as Kohonen Maps (unsupervised classifiers) and, Fisher discriminant analysis, kNN, SVM and decision trees (supervised classifiers). It was found that contour and wash-out type features determined by the radiologists lead to the best classification results with SVM. Moreover, it has been shown that SVM lead to a better performance than a variety of other machine learning techniques when applied in discrimination of breast lesions [168]-[170]. In [171], Gal et al. presented a study showing that textural and kinetic, rather than morphology, features are the most important for lesion classification and again SVM classifiers with sigmoid kernel performs better than other well-known classifiers.

A comparison between the classification of kinetic patterns on malignant breast lesions done by k-means and the classification by the 3TP, as reported in [172], is discussed by Lee et al. in [173]. Levman and Martel [174] introduced the custom radial basis function vector machine and have shown that using kinetic features it leads to a slightly better performance than SVM with radial basis function kernel.

Meinel et al. [175] described that the specificity of the radiologist was significantly improved when aided by a CAD system based on a BNN developed by them. The feature extraction was also based on lesion shape, texture and enhancement kinetics information. The best result achieved was with BNN alone. However, results for human readers with and without the CADx model were also evaluated. When only the first abnormality shown to human readers was included, ROC analysis yielded area under the ROC of 0.91 with ANN assistance and 0.82 without the assistance.

A classification of small contrast enhancing focal lesions in dynamic MRI using a combination of morphological criteria and dynamic analysis based on unsupervised vector-quantification was performed by Schlossbauer et al. [176]. In small MR-mammographic lesions, dynamic analysis with vector quantization alone tends to result in a higher diagnostic accuracy compared with combined morphologic and dynamic analysis. Yao et al. proposed in [162] a pixel-by-pixel classification method based on texture analysis and wavelet transform for tumor evaluation in breast DCE-MRI, but with a very small dataset. In [163], Zheng et al. used spatial-temporal enhancement pattern and Fourier transformation to analyze breast tumors.

Deurloo *et al.* [177] combined in clinical reading in MRI by radiologists with computer-calculated probability of malignancy of each lesion into an linear regression (LR) model. Inputs to the LR included the four best features from a set of six morphologic and three temporal features. Either biopsy-proven lesions or lesions showing transient enhancement were included in the study. The study of Deurloo et al. [177] revealed that the specificity of the radiological interpretation with the combined model is not as high as that of pathological analysis of specimens obtained at fine needle aspiration (FNA) and biopsy. Clinical application of computer analysis can, therefore, not be expected to replace FNA or biopsy. However, in situations when FNA or biopsy is not possible to perform, application of computerized analysis may be used to increase specificity.

As mentioned before, the only fully-automated classification with reported use in the clinical practice is the one available in CADx system DynaCAD which solely relies on morphological analysis. The research behind this system is based on fractal theory as described by Penn et al. in [178], and focused on assessing the margin sharpness of the breast lesions, which is only one of the possible ways to analyze tissues in the breast [58], [159], [161]. The potential problem with the fractal dimension approach is that distinct fractal sets may share the same fractal

dimension values with different appearances or texture patterns [179]. Moreover, sharp changes of the patterns of enhancement on border slices of a segmented tumor are known to occur with most of the techniques based on slice by slice assessment of the morphology. This results in lower specificity, probably caused by partial volume or the recently studied morphological blooming effect [178]. Blooming evaluates the transition of the margin to the surroundings by a progradient unsharpness of lesion borders, however, the spatial volumetric dependency was not investigated and multifractal approach has been also neglected as in [154]. Morphological blooming achieved the sensitivity of 80% with 2.46 false positives per non-cancerous breast [178].

The multifractal analysis provides a spectrum of fractal dimensions, characterizing multiple irregularities that can potentially provide more information about the image compared to the single fractal dimension [180], without being exclusively focused on lesion margins as in [181]. In this sense, Soares et al. [58] proposed a multifractal analysis with the extraction of features in tri-dimensional (3D) volumes of interest. It was shown how multifractal analysis may depend on the concept of lacunarity, when used for the description of the spatial distribution of the pixel intensities in image volumes with multiscaling behaviors. This method named Multifractal Scaling Exponent Lacunarity Analysis (MF-SELA) gave better results when compared with 3TP in the same dataset. The performance is likely to improve when taking full advantage of the 3D nature of the MRI data. Gilhuijs et al. [161] compared 3D with 2D analysis using a representative slice through the middle of the lesion. 3D was found to result in higher performance for the majority of the shape-based features. However, the manual lesion segmentation employed there would limit the inclusion of this technique in an automated CAD. Automatic segmentation has been shown to be useful when evaluating state-of-art features in 2D or 3D [182], as in volumetric analysis by Chen et al. [182]. This is mainly due to the fact that these features rely on lesion morphology, and segmentation reduces the influence of normal tissue of the breast surrounding a tumor on that features.

Features in spatiotemporal space by Lee et al. [154] with SVM-RFE, or the recent work in textural-kinetics by Agner et al. [183] with probabilistic boosting tree (PBT) classifier, revealed promising results. These are interesting works in the field by the manner they challenge to investigate differentiation that was not attainable using conventional approaches in which spatial or temporal features were extracted separately.

Table V provides a representative selection of CADx algorithms in DCE-MRI. The CADx performance is measured at the CAde output. Only relevant studies with biopsy-proven cases were selected.

Table V: Area under the ROC curve  $A_z$  of a representative selection of mass CADx in DCE-MRI

Authors	Year	Dataset size	Features	Classifier	Sensitivity Specificity	Accuracy	$A_z$
Sinha et al. [158]	1997	43	Kinetics Morphology Texture	LDA	95% 93%	94%	-
Szabó et al. [167]	2004	105	Kinetics Morphology Texture	Minimal ANN model	-	-	0.80
Chen et al. [159]	2004	121	Kinetics Morphology Texture	LDA	-	-	0.80
Pediconi et al. [160]	2005	68	Pixel-based	False color map	92.6% 85.7%	91.2%	-
Nattkemper et al. [168]	2005	74	Contour and Wash-out	SVM	-	-	0.88
Deurloo et al. [177]	2005	100	Kinetics Morphology	LRA	-	-	0.91
Chen et al. [182]	2007	121	Texture	LRA	-	-	0.86
Meinel et al. [175]	2007	80	Kinetics Morphology Texture	BNN	-	-	0.97
Schlossbauer et al. [176].	2008	47	Kinetics vector quantization	LDA	-	-	0.76
Levman and Martel [174]	2008	94	Kinetics	SVN	62.5% 78.6%	74.5%	0.74
Lee et al. [154]	2010	111	Spatio- temporal	SVM-RFE	76% 80%	-	0.88
Agner et al. [183]	2011	41	Textural- kinetics	PBT	95% 82%	90%	0.92
Soares et al. [58]	2013	35	Multifractal- based	SVM	-	-	0.96

## VI Conclusion

In this article, we provide a comprehensive review of computer-aided detection (CADe) and diagnosis (CADx) schemes developed for two complementary imaging modalities as mammography and breast MRI (in particular, DCE-MRI of the breast). Radiological imaging is one of the most effective means of early detection of breast cancer. However, the differentiation between benign and malignant findings is still difficult. Computer-aided medical imaging analysis (CAD) arises in this sense. Computerized software models known as CADe have been proposed to help to assist radiologists in locating and identifying possible abnormalities. CADx are decision aids to radiologists in characterizing findings from radiologic images identified either by a radiologist or CADe. It should not be forgotten that CAD techniques can serve only as a double-reading aid and cannot replace human readers, but they can have impact in places where expert radiologists cannot be present like in under development countries.

Wavelets and multiscale analysis play an important role on the detection of microcalcifications in CADe mammography. To aim mammographic detection of masses, region-based features and pattern matching CADe are reported to be successful. Nevertheless, the field of CADe in mammography for the detection of most common abnormalities can be seen as solid. On the

base of this statement are the examples of knowledge transfer between research institutes and universities to industrial and commercialized CAde systems in mammography.

In breast MRI and in mammography there is a whole range of classifiers, but most of the existing CADx models incorporate ANNs. Although ANNs are powerful in terms of their predictive abilities, usually their parameters do not carry any real-life interpretation.

The results of CADx in mammography, though encouraging, are not yet conclusive enough to warrant a credible clinical usage. The state-of-art methods show that the accuracy of cancer detection has indeed improved with introduction of CADx. There is still a long way to go for implementation of the same in a clinical setting as it already happen in mammography on CAde. Almost all of the existing CADx schemes are trained and tested on retrospectively collected cases that may not represent the real clinical practice. Large prospective studies are required to evaluate the performance of CADx systems in real life before employing them in a clinical setting.

Most of the commercial CAD systems in breast MRI are advertized as CADx, but not based on learning. On the other side, what can be found on the present thesis is that almost no scientific research on CAde exists nowadays. Detection and characterization of breast lesions in DCE-MRI with the aforementioned methods for CADx is relatively easily interpretable. However, the studies in table V are still limited on the number of proven lesions and in fact the findings should be validated prospectively in a larger population. DCE-MRI is without doubt a valuable technique with room for improvement in false positive reduction and sensitivity increasing. In this sense, researchers had been investing lot of effort in first, to characterize breast lesions as radiologists usually do, and more recently to investigate differentiation between lesions through unconventional approaches as multifractal, textural-kinetics and spatio-temporal analysis on region or volumes of interest. In addition, usually the surroundings (background) of the lesions are not included in the analysis of texture complexity [58]. Moreover, a CADx system should also work as a second-opinion for the radiologist and therefore focus on a comprehensive set of characteristics of the lesions, including features that are indistinguishable to the human eye.

An objective comparative performance evaluation of the existing CADx schemes is difficult because the reported performances depend on the dataset used in the computerized framework building. One approach to a systematic performance comparison would be to use large and consistent, publicly available datasets for testing purposes. The public databases available for mammography are good examples that should be replicable to MRI. A large number of clinical cases with lesions must be used as the gold standard to develop a computerized scheme for CAD. Databases with adequate numbers of cases are usually not available to researchers, specially having ground truth based on histology or pathological proofs.

In the future, well-designed and executed studies which specifically evaluate the addition of CADx to MRI clinical cycle are needed to determine whether or not the use of CAD provides a positive clinical benefit to the patients; similarly to what have been shown through the role of CADe in mammography. With the aim to incorporate all possible information from different sources when making recommendations to radiologists, more CAD multimodal approaches should be investigated.

## References

- [1] J. Ma and A. Jemal, "Breast Cancer Statistics," in *Breast Cancer Metastasis and Drug Resistance*, A. Ahmad, Ed. Springer New York, 2013, pp. 1–18.
- [2] L. Tabar, M. Yen, B. Vitak, H. Chen, R. Smith, and S. Duffy, "Mammography service screening and mortality in breast cancer patients: 20-year follow-up before and after introduction of screening," *The Lancet*, vol. 361, no. 9367, pp. 1405–1410, 2003.
- [3] M. Reddy and R. Given-Wilson, "Screening for breast cancer," *Womens Heal. Med.*, vol. 3, no. 1, pp. 22–27, Jan. 2006.
- [4] L. Wyld and C. E. Ingram, "Screening of the population for breast cancer," *Surg. Oxf.*, vol. 25, no. 6, pp. 254–256, Jun. 2007.
- [5] D. Schopper and C. de Wolf, "How effective are breast cancer screening programmes by mammography? Review of the current evidence," *Eur. J. Cancer*, vol. 45, no. 11, pp. 1916–1923, Jul. 2009.
- [6] P. Skaane, "Studies comparing screen-film mammography and full-field digital mammography in breast cancer screening: updated review," *Acta Radiol. Stockh. Swed. 1987*, vol. 50, no. 1, pp. 3–14, Jan. 2009.
- [7] A. M. J. Bluekens, R. Holland, N. Karssemeijer, M. J. M. Broeders, and G. J. den Heeten, "Comparison of Digital Screening Mammography and Screen-Film Mammography in the Early Detection of Clinically Relevant Cancers: A Multicenter Study," *Radiology*, vol. 265, no. 3, pp. 707–714, Jan. 2012.
- [8] P. Skaane, A. I. Bandos, R. Gullien, E. B. Eben, U. Ekseth, U. Haakenaasen, M. Izadi, I. N. Jebsen, G. Jahr, M. Krager, L. T. Niklason, S. Hofvind, and D. Gur, "Comparison of Digital Mammography Alone and Digital Mammography Plus Tomosynthesis in a Population-based Screening Program," *Radiology*, vol. 267, no. 1, pp. 47–56, Jan. 2013.
- [9] F. van Gelderen, *Understanding X-Rays: A Synopsis of Radiology*. Springer, 2004.
- [10] E. Pisano, M. Yaffe, B. Hemminger, R. Hendrick, L. Niklason, A. Maidment, C. Kimme-Smith, S. Feig, E. Sickles, and M. Braeuning, "Current status of full-field digital mammography," *Acad. Radiol.*, vol. 7, no. 4, pp. 266–280, 2000.
- [11] E. D. Pisano, R. E. Hendrick, M. J. Yaffe, J. K. Baum, S. Acharyya, J. B. Cormack, L. A. Hanna, E. F. Conant, L. L. Fajardo, L. W. Bassett, and others, "Diagnostic accuracy of digital versus film mammography: exploratory analysis of selected population subgroups in DMIST," *Radiology*, vol. 246, no. 2, p. 376, 2008.
- [12] J. M. Park, E. A. Franken Jr, M. Garg, L. L. Fajardo, and L. T. Niklason, "Breast tomosynthesis: present considerations and future applications," *Radiographics*, vol. 27, no. S1, p. S231, 2007.
- [13] H. J. Teertstra, C. E. Loo, M. A. A. J. van den Bosch, H. van Tinteren, E. J. T. Rutgers, S. H. Muller, and K. G. A. Gilhuijs, "Breast tomosynthesis in clinical practice: initial results," *Eur. Radiol.*, vol. 20, no. 1, pp. 16–24, Jan. 2010.
- [14] R. Schulz-Wendtland, G. Dilbat, M. Bani, P. Fasching, K. Heusinger, M. Lux, C. Loehberg, B. Brehm, M. Hammon, M. Saake, P. Dankerl, S. Jud, C. Rauh, C. Bayer, M. Beckmann, M. Uder, and M. Meier-Meitingner, "Full Field Digital Mammography (FFDM) versus CMOS Technology, Specimen Radiography System (SRS) and Tomosynthesis (DBT) - Which System Can Optimise Surgical Therapy?," *Geburtshilfe Frauenheilkd.*, vol. 73, no. 05, pp. 422–427, Jun. 2013.
- [15] L. S. Gold, G. Klein, L. Carr, L. Kessler, and S. D. Sullivan, "The emergence of diagnostic imaging technologies in breast cancer: discovery, regulatory approval, reimbursement, and adoption in clinical guidelines," *Cancer Imaging*, vol. 12, no. 1, pp. 13–24, 2012.
- [16] E. Warner, D. B. Plewes, K. A. Hill, P. A. Causer, J. T. Zubovits, R. A. Jong, M. R. Cutrara, G. DeBoer, M. J. Yaffe, S. J. Messner, W. S. Meschino, C. A. Piron, and S. A. Narod, "Surveillance of BRCA1 and BRCA2 Mutation Carriers With Magnetic Resonance Imaging, Ultrasound, Mammography, and Clinical Breast Examination," *JAMA J. Am. Med. Assoc.*, vol. 292, no. 11, pp. 1317–1325, Sep. 2004.
- [17] L. Moy, K. Elias, V. Patel, J. Lee, J. Babb, H. Toth, and C. Mercado, "Is breast MRI helpful in the evaluation of inconclusive mammographic findings?," *Am. J. Roentgenol.*, vol. 193, no. 4, p. 986, Oct. 2009.

- [18] C. Kuhl, P. Mielcareck, S. Klaschik, C. Leutner, E. Wardelmann, J. Gieseke, and H. H. Schild, "Dynamic Breast MR Imaging: Are Signal Intensity Time Course Data Useful for Differential Diagnosis of Enhancing Lesions?1," *Radiology*, vol. 211, no. 1, pp. 101–110, Apr. 1999.
- [19] S. Behrens, H. Laue, M. Althaus, T. Boehler, B. Kuemmerlen, H. K. Hahn, and H.-O. Peitgen, "Computer assistance for MR based diagnosis of breast cancer: present and future challenges," *Comput. Med. Imaging Graph.*, vol. 31, no. 4–5, pp. 236–247, Jun. 2007.
- [20] J. J. James, F. J. Gilbert, M. G. Wallis, M. G. C. Gillan, S. M. Astley, C. R. M. Boggis, O. F. Agbaje, A. R. Brentnall, and S. W. Duffy, "Mammographic Features of Breast Cancers at Single Reading with Computer-aided Detection and at Double Reading in a Large Multicenter Prospective Trial of Computer-aided Detection: CADET II1," *Radiology*, vol. 256, no. 2, pp. 379–386, Jan. 2010.
- [21] M. L. Giger, "Computerized analysis of images in the detection and diagnosis of breast cancer," *Semin. Ultrasound CT MRI*, vol. 25, no. 5, pp. 411–418, Oct. 2004.
- [22] H. Cheng, X. Cai, X. Chen, L. Hu, and X. Lou, "Computer-aided detection and classification of microcalcifications in mammograms: a survey," *Pattern Recognit.*, vol. 36, no. 12, pp. 2967–2991, 2003.
- [23] M. Sampat, M. Markey, and A. Bovik, "Computer-Aided Detection and Diagnosis in Mammography," in *Handbook of image and video processing*, vol. 10, Elsevier Academic Press, 2005, pp. 1195–1217.
- [24] H. D. Cheng, X. J. Shi, R. Min, L. M. Hu, X. P. Cai, and H. N. Du, "Approaches for automated detection and classification of masses in mammograms," *Pattern Recognit.*, vol. 39, no. 4, pp. 646–668, Apr. 2006.
- [25] R. M. Rangayyan, F. J. Ayres, and J. E. L. Desautels, "A review of computer-aided diagnosis of breast cancer: Toward the detection of subtle signs," *J. Frankl. Inst.*, vol. 344, no. 3–4, pp. 312–348, May 2007.
- [26] M. Bazzocchi, F. Mazzeola, C. Del Frate, F. Girometti, and C. Zuiani, "CAD systems for mammography: a real opportunity? A review of the literature," *Radiol. Med. (Torino)*, vol. 112, no. 3, pp. 329–353, 2007.
- [27] H. Fujita, Y. Uchiyama, T. Nakagawa, D. Fukuoka, Y. Hatanaka, T. Hara, G. N. Lee, Y. Hayashi, Y. Ikedo, X. Gao, and X. Zhou, "Computer-aided diagnosis: The emerging of three CAD systems induced by Japanese health care needs," *Comput. Methods Programs Biomed.*, vol. 92, no. 3, pp. 238–248, Dec. 2008.
- [28] Jinshan Tang, R. M. Rangayyan, Jun Xu, I. El Naqa, and Yongyi Yang, "Computer-aided detection and diagnosis of breast cancer with mammography: recent advances," *IEEE Trans. Inf. Technol. Biomed.*, vol. 13, no. 2, pp. 236–251, 2009.
- [29] M. Elter and A. Horsch, "CADx of mammographic masses and clustered microcalcifications: a review," *Med. Phys.*, vol. 36, no. 6, pp. 2052–2068, Jun. 2009.
- [30] Arnau Oliver, Jordi Freixenet, Joan Martí, Elsa Pérez, Josep Pont, Erika R.E. Denton, and Reyer Zwiggelaar, "A review of automatic mass detection and segmentation in mammographic images," *Med. Image Anal.*, vol. 14, no. 2, pp. 87–110, Apr. 2010.
- [31] K. Ganesan, U. R. Acharya, C. K. Chua, L. C. Min, K. T. Abraham, and K.-H. Ng, "Computer-aided breast cancer detection using mammograms: a review," *IEEE Rev. Biomed. Eng.*, vol. 6, pp. 77–98, 2013.
- [32] K. Nie, J.-H. Chen, H. J. Yu, Y. Chu, O. Nalcioglu, and M.-Y. Su, "Quantitative Analysis of Lesion Morphology and Texture Features for Diagnostic Prediction in Breast MRI," *Acad. Radiol.*, vol. 15, no. 12, pp. 1513–1525, Dec. 2008.
- [33] R. M. Nishikawa, "Current status and future directions of computer-aided diagnosis in mammography," *Comput. Med. Imaging Graph.*, vol. 31, no. 4–5, pp. 224–235, 2007.
- [34] S. R. Amendolia, M. G. Bisogni, U. Bottigli, A. Ceccopieri, P. Delogu, M. E. Fantacci, A. Marchi, V. M. Marzulli, R. Palmiero, and S. Stumbo, "The CALMA project: a CAD tool in breast radiography," *Nucl. Inst Methods Phys. Res.*, vol. 460, no. 1, pp. 107–112, 2001.
- [35] D.-R. Chen and Y.-H. Hsiao, "Computer-aided Diagnosis in Breast Ultrasound," *J. Med. Ultrasound*, vol. 16, no. 1, pp. 46–56, 2008.
- [36] Y. Guo, "Computer-aided detection of breast cancer using ultrasound images," *Grad. Theses Diss.*, p. 635, 2010.
- [37] R. Nagel, R. Nishikawa, J. Papaioannou, and K. Doi, "Analysis of methods for reducing false positives in the automated detection of clustered microcalcifications in mammograms," *Med. Phys.*, vol. 25, p. 1502, 1998.

- [38] S.-N. Yu, K.-Y. Li, and Y.-K. Huang, "Detection of microcalcifications in digital mammograms using wavelet filter and Markov random field model," *Comput. Med. Imaging Graph.*, vol. 30, no. 3, pp. 163–173, Apr. 2006.
- [39] M. Jirari, "Computer Aided System For Detecting Masses In Mammograms," Ph.D. thesis, Kent State University, 2008.
- [40] A. Mencattini, M. Salmeri, G. Rabottino, and S. Salicone, "Metrological Characterization of a CADx System for the Classification of Breast Masses in Mammograms," *Instrum. Meas. IEEE Trans.*, vol. 59, no. 11, pp. 2792–2799, 2010.
- [41] S. Yu and L. Guan, "A CAD system for the automatic detection of clustered microcalcifications in digitized mammogram films," *IEEE Trans. Med. Imaging*, vol. 19, no. 2, pp. 115–126, Feb. 2000.
- [42] J. G. Elmore, C. Y. Nakano, T. D. Koepsell, L. M. Desnick, C. J. D'Orsi, and D. F. Ransohoff, "International Variation in Screening Mammography Interpretations in Community-Based Programs," *J. Natl. Cancer Inst.*, vol. 95, no. 18, pp. 1384–1393, Sep. 2003.
- [43] R. D. Rosenberg, B. C. Yankaskas, L. A. Abraham, E. A. Sickles, C. D. Lehman, B. M. Geller, P. A. Carney, K. Kerlikowske, D. S. M. Buist, D. L. Weaver, W. E. Barlow, and R. Ballard-Barbash, "Performance Benchmarks for Screening Mammography," *Radiology*, vol. 241, no. 1, pp. 55–66, Jan. 2006.
- [44] J. Roehrig, T. Doi, A. Hasegawa, B. Hunt, J. Marshall, H. Romsdahl, A. Schneider, R. Sharbaugh, and W. Zhang, "Clinical results with R2 imagechecker system," *Comput. Imaging Vis.*, vol. 13, pp. 395–400, 1998.
- [45] D. Gur, J. H. Sumkin, H. E. Rockette, M. Ganott, C. Hakim, L. Hardesty, W. R. Poller, R. Shah, and L. Wallace, "Changes in Breast Cancer Detection and Mammography Recall Rates After the Introduction of a Computer-Aided Detection System," *J. Natl. Cancer Inst.*, vol. 96, no. 3, pp. 185–190, Apr. 2004.
- [46] M. J. Morton, D. H. Whaley, K. R. Brandt, and K. K. Amrami, "Screening Mammograms: Interpretation with Computer-aided Detection—Prospective Evaluation1," *Radiology*, vol. 239, no. 2, pp. 375–383, Jan. 2006.
- [47] Y. Jiang, R. M. Nishikawa, R. A. Schmidt, A. Y. Toledano, and K. Doi, "Potential of Computer-aided Diagnosis to Reduce Variability in Radiologists' Interpretations of Mammograms Depicting Microcalcifications1," *Radiology*, vol. 220, no. 3, pp. 787–794, Jan. 2001.
- [48] R. Highnam and M. Brady, *Mammographic Image Analysis*. Springer, 1999.
- [49] M. Yam, M. Brady, R. Highnam, C. Behrenbruch, R. English, and Y. Kita, "Three-dimensional reconstruction of microcalcification clusters from two mammographic views," *IEEE Trans. Med. Imaging*, vol. 20, no. 6, pp. 479–489, 2001.
- [50] A. Lauria, R. Palmiero, G. Forni, M. E. Fantacci, M. Imbriaco, A. Sodano, and P. L. Indovina, "A study on two different CAD systems for mammography as an aid to radiological diagnosis in the search of microcalcification clusters," *Eur. J. Radiol.*, vol. 55, no. 2, pp. 264–269, Aug. 2005.
- [51] A. Malich, D. Vogel, M. Facius, C. Marx, M. G. Freesmeyer, D. Sauner, A. Hansch, S. O. R. Pfeleiderer, M. Fleck, and W. A. Kaiser, "Evaluation of the primary diagnosis with a CAD-system in mammography," *RöFo Fortschritte Auf Dem Geb. Röntgenstrahlen Nukl.*, vol. 175, no. 9, pp. 1225–1231, Sep. 2003.
- [52] J. W. Hoffmeister, S. K. Rogers, M. P. DeSimio, and R. F. Brem, "Determining efficacy of mammographic CAD systems," *J. Digit. Imaging*, vol. 15 Suppl 1, pp. 198–200, 2002.
- [53] E. A. Morris, "Illustrated breast MR lexicon," *Semin. Roentgenol.*, vol. 36, no. 3, pp. 238–249, Jul. 2001.
- [54] W. Chen, M. L. Giger, U. Bick, and G. M. Newstead, "Automatic identification and classification of characteristic kinetic curves of breast lesions on DCE-MRI," *Med. Phys.*, vol. 33, no. 8, pp. 2878–2887, Aug. 2006.
- [55] C. Lehman, S. Peacock, W. DeMartini, and X. Chen, "A new automated software system to evaluate breast MR examinations: improved specificity without decreased sensitivity," *Am. J. Roentgenol.*, vol. 187, no. 1, pp. 51–56, Jul. 2006.
- [56] K. Kinkel and N. Hylton, "Challenges to interpretation of breast MRI," *J. Magn. Reson. Imaging*, vol. 13, no. 6, pp. 821–829, Jun. 2001.
- [57] In vivo Corporation, "DynaCAD with ONCAD," 2009. [Online]. Available: <http://www.invivocorp.com/Literature/12723878336.pdf>. [Accessed: 14-Feb-2012].

- [58] F. Soares, F. Janela, M. Pereira, J. Seabra, and M. M. Freire, "3D Lacunarity in Multifractal Analysis of Breast Tumor Lesions in Dynamic Contrast-Enhanced Magnetic Resonance Imaging," *IEEE Trans. Image Process.*, vol. 22, no. 11, pp. 4422–4435, 2013.
- [59] E. A. Krupinski, "The Future of Image Perception in Radiology Synergy between Humans and Computers," *Acad. Radiol.*, vol. 10, no. 1, pp. 1–3, 2003.
- [60] K. Ganesan, U. R. Acharya, K. C. Chua, L. C. Min, and K. T. Abraham, "Pectoral muscle segmentation: A review," *Comput. Methods Programs Biomed.*, vol. 110, no. 1, pp. 48–57, Apr. 2013.
- [61] K. Wei, W. Guangzhi, and D. Hui, "Segmentation of the breast region in mammograms using watershed transformation," in *Proceedings of 27th Annual International Conference of the Engineering in Medicine and Biology Society*, 2005, pp. 6500–6503.
- [62] S. D. Tzikopoulos, M. E. Mavroforakis, H. V. Georgiou, N. Dimitropoulos, and S. Theodoridis, "A fully automated scheme for mammographic segmentation and classification based on breast density and asymmetry," *Comput. Methods Programs Biomed.*, vol. 102, no. 1, pp. 47–63, Apr. 2011.
- [63] F. Soares, M. M. Freire, M. Pereira, F. Janela, and J. Seabra, "The Role of Self-Similarity for Computer Aided Detection Based on Mammogram Analysis," in *Biomedical Diagnostics and Clinical Technologies: Applying High-Performance Cluster and Grid Computing*, IGI Global, 2011, pp. 181–199.
- [64] G. Peters, *Computer-aided detection for digital breast tomosynthesis*. 2007.
- [65] J. Dengler, S. Behrens, and J. Desaga, "Segmentation of microcalcifications in mammograms," *IEEE Trans. Med. Imaging*, vol. 12, no. 4, pp. 634–642, 1993.
- [66] T. Soni, J. Zeidler, and W. Ku, "Performance evaluation of 2-D adaptive prediction filters for detection of small objects in image data," *IEEE Trans. Image Process.*, vol. 2, no. 3, pp. 327–340, 1993.
- [67] G. te Brake, N. Karssemeijer, and J. Hendriks, "An automatic method to discriminate malignant masses from normal tissue in digital mammograms," *Phys. Med. Biol.*, vol. 45, pp. 2843–2857, 2000.
- [68] G. Tourassi, R. Vargas-Voracek, D. Catarious Jr, and C. Floyd Jr, "Computer-assisted detection of mammographic masses: A template matching scheme based on mutual information," *Med. Phys.*, vol. 30, p. 2123, 2003.
- [69] M. A. Duarte, A. V. Alvarenga, C. M. Azevedo, A. F. C. Infantosi, and W. C. A. Pereira, "Automatic microcalcifications segmentation procedure based on Otsu's method and morphological filters," in *Pan American Health Care Exchanges*, 2011, pp. 102–106.
- [70] M. Mustra, M. Grgic, and K. Delac, "Enhancement of microcalcifications in digital mammograms," in *2012 19th International Conference on Systems, Signals and Image Processing (IWSSIP)*, 2012, pp. 248–251.
- [71] B. Thangaraju, I. Vennila, and G. Chinnasamy, "Detection of microcalcification clusters using Hessian matrix and foveal segmentation method on multiscale analysis in digital mammograms," *J. Digit. Imaging*, vol. 25, no. 5, pp. 607–619, Oct. 2012.
- [72] I. Bankman, W. Christens-Barry, D. Kim, and I. Weinberg, "Automated recognition of microcalcification clusters in mammograms," presented at the PROCEEDINGS-SPIE THE INTERNATIONAL SOCIETY FOR OPTICAL ENGINEERING, 1993, p. 731.
- [73] N. Karssemeijer, "Recognition of clustered microcalcifications using a random field model," in *Proceedings of SPIE*, 1905, vol. 776, p. 1993.
- [74] Y. Heng-Da Cheng, R. Freimanis, and D. Paliy, "A novel approach to microcalcification detection using fuzzy logic technique," *IEEE Trans. Med. Imaging*, vol. 17, no. 3, 1998.
- [75] H. D. Cheng and H. Xu, "A novel fuzzy logic approach to mammogram contrast enhancement," *Inf. Sci.*, vol. 148, no. 1–4, pp. 167–184, Dec. 2002.
- [76] W. Zhang, K. Doi, M. L. Giger, R. M. Nishikawa, and R. A. Schmidt, "An improved shift-invariant artificial neural network for computerized detection of clustered microcalcifications in digital mammograms," *Med. Phys.*, vol. 23, no. 4, pp. 595–601, Apr. 1996.
- [77] J. Ren, "ANN vs. SVM: Which one performs better in classification of MCCs in mammogram imaging," *Knowl.-Based Syst.*, vol. 26, pp. 144–153, Feb. 2012.
- [78] A. Oliver, A. Torrent, X. Lladó, M. Tortajada, L. Tortajada, M. Sentís, J. Freixenet, and R. Zwiggelaar, "Automatic microcalcification and cluster detection for digital and digitised mammograms," *Knowl.-Based Syst.*, vol. 28, pp. 68–75, Apr. 2012.

- [79] E. Malar, A. Kandaswamy, D. Chakravarthy, and A. Giri Dharan, "A novel approach for detection and classification of mammographic microcalcifications using wavelet analysis and extreme learning machine," *Comput. Biol. Med.*, vol. 42, no. 9, pp. 898–905, Sep. 2012.
- [80] J. Dheeba and S. T. Selvi, "A Swarm Optimized Neural Network System for Classification of Microcalcification in Mammograms," *J. Med. Syst.*, vol. 36, no. 5, pp. 3051–3061, Oct. 2012.
- [81] R. N. Strickland and Hee Il Hahn, "Wavelet transforms for detecting microcalcifications in mammograms," *IEEE Trans. Med. Imaging*, vol. 15, no. 2, pp. 218–229, Apr. 1996.
- [82] T. Wang and N. Karayiannis, "Detection of microcalcifications in digital mammograms using wavelets," *IEEE Trans. Med. Imaging*, vol. 17, no. 4, pp. 498–509, 1998.
- [83] W. Zhang, H. Yoshida, R. Nishikawa, and K. Doi, "Optimally weighted wavelet transform based on supervised training for detection of microcalcifications in digital mammograms," *Med. Phys.*, vol. 25, p. 949, 1998.
- [84] H. Moradmand, S. Setayeshi, A. R. Karimian, M. Sirous, and M. E. Akbari, "Comparing the Performance of Image Enhancement Methods to Detect Microcalcification Clusters in Digital Mammography," *Iran. J. Cancer Prev.*, vol. 5, no. 2, pp. 61–68, Apr. 2012.
- [85] P. Ramírez-Cobo and B. Vidakovic, "A 2D wavelet-based multiscale approach with applications to the analysis of digital mammograms," *Comput. Stat. Data Anal.*, vol. 58, pp. 71–81, Feb. 2013.
- [86] H. Li, K. Liu, and S. Lo, "Fractal modeling and segmentation for the enhancement of microcalcifications in digital mammograms," *IEEE Trans. Med. Imaging*, vol. 16, no. 6, pp. 785–798, 1997.
- [87] A. I. Penn, L. Bolinger, M. D. Schnall, and M. H. Loew, "Discrimination of MR images of breast masses with fractal-interpolation function models," *Acad. Radiol.*, vol. 6, no. 3, pp. 156–163, Mar. 1999.
- [88] P. Dey and S. Mohanty, "Fractal dimensions of breast lesions on cytology smears.," *Diagn. Cytopathol.*, vol. 29, no. 2, 2003.
- [89] D. Chen, R. Chang, C. Chen, M. Ho, S. Kuo, S. Chen, S. Hung, and W. Moon, "Classification of breast ultrasound images using fractal feature," *Clin. Imaging*, vol. 29, no. 4, pp. 235–245, 2005.
- [90] E. Nilsson, "Multifractal-based Image Analysis with applications in Medical Imaging," M.Sc. dissertation, Umeå University, 2007.
- [91] F. Soares, M. M. Freire, M. Pereira, F. Janela, and J. Seabra, "Towards the detection of microcalcifications on mammograms through Multifractal Detrended Fluctuation Analysis," in *Proceedings of the IEEE Pacific Rim Conference on Communications, Computers and Signal Processing*, 2009, pp. 677–681.
- [92] B. Zheng, Y. Chang, M. Staiger, W. Good, and D. Gur, "Computer-aided detection of clustered microcalcifications in digitized mammograms," *Acad. Radiol.*, vol. 2, no. 8, pp. 655–662, 1995.
- [93] W. Zhang, K. Doi, M. Giger, Y. Wu, R. Nishikawa, and R. Schmidt, "Computerized detection of clustered microcalcifications in digital mammograms using a shift-invariant artificial neural network," *Med. Phys.*, vol. 21, p. 517, 1994.
- [94] M. Bottema and J. Slavotinek, "Detection and classification of lobular and DCIS (small cell) microcalcifications in digital mammograms," *Pattern Recognit. Lett.*, vol. 21, no. 13–14, pp. 1209–1214, 2000.
- [95] W. Veldkamp, N. Karssemeijer, J. Otten, and J. Hendriks, "Automated classification of clustered microcalcifications into malignant and benign types," *Med. Phys.*, vol. 27, p. 2600, 2000.
- [96] A. Papadopoulos, D. Fotiadis, and A. Likas, "Characterization of clustered microcalcifications in digitized mammograms using neural networks and support vector machines," *Artif. Intell. Med.*, vol. 34, no. 2, pp. 141–150, 2005.
- [97] I. El-Naqa, Y. Yang, M. N. Wernick, N. P. Galatsanos, and R. M. Nishikawa, "A support vector machine approach for detection of microcalcifications," *IEEE Trans Med Imaging*, vol. 21, no. 12, pp. 1552–1563, 2003.
- [98] L. Wei, Y. Yang, R. M. Nishikawa, and Y. Jiang, "A study on several Machine-learning methods for classification of Malignant and benign clustered microcalcifications," *IEEE Trans. Med. Imaging*, vol. 24, no. 3, pp. 371–380, 2005.
- [99] B. Zheng, W. Qian, and L. Clarke, "Digital mammography: mixed feature neural network with spectral entropy decision for detection of microcalcifications," *IEEE Trans. Med. Imaging*, vol. 15, no. 5, pp. 589–597, 1996.
- [100] N. C. Tsai, H. W. Chen, and S. L. Hsu, "Computer-aided diagnosis for early-stage breast cancer by using Wavelet Transform," *Comput. Med. Imaging Graph.*, vol. 35, no. 1, pp. 1–8, 2011.

- [101] K. Thangavel and M. Karnan, "Computer aided diagnosis in digital mammograms: detection of microcalcifications by meta heuristic algorithms," *GVIP J.*, vol. 5, no. 7, pp. 41–55, 2005.
- [102] D. Sankar and T. Thomas, "Fractal Modeling of Mammograms Based on Mean and Variance for the Detection of Microcalcifications," in *International Conference on Conference on Computational Intelligence and Multimedia Applications, 2007*, 2007, vol. 2, pp. 334–348.
- [103] P. Kestener, J. M. Lina, P. Saint-Jean, and A. Arneodo, "Wavelet-based multifractal formalism to assist in diagnosis in digitized mammograms," *Image Anal Ster.*, vol. 20, no. 3, pp. 169–174, 2001.
- [104] H. Wendt, S. G. Roux, S. Jaffard, and P. Abry, "Wavelet leaders and bootstrap for multifractal analysis of images," *Signal Process.*, vol. 89, no. 6, pp. 1100–1114, Jun. 2009.
- [105] W. Kegelmeyer, J. Pruneda, P. Bourland, A. Hillis, M. Riggs, and M. Nipper, "Computer-aided mammographic screening for spiculated lesions.," *Radiology*, vol. 191, no. 2, p. 331, 1994.
- [106] N. R. Mudigonda, R. M. Rangayyan, and J. E. L. Desautels, "Detection of breast masses in mammograms by density slicing and texture flow-field analysis," *IEEE Trans. Med. Imaging*, vol. 20, no. 12, pp. 1215–1227, 2001.
- [107] T. Nakagawa, T. Hara, H. Fujita, T. Iwase, T. Endo, and K. Horita, "Automated contour extraction of mammographic mass shadow using an improved active contour model," *Int. Congr. Ser.*, vol. 1268, pp. 882–885, Jun. 2004.
- [108] J. Shi, B. Sahiner, H.-P. Chan, J. Ge, L. Hadjiiski, M. A. Helvie, A. Nees, Y.-T. Wu, J. Wei, C. Zhou, Y. Zhang, and J. Cui, "Characterization of mammographic masses based on level set segmentation with new image features and patient information," *Med. Phys.*, vol. 35, no. 1, pp. 280–290, 2008.
- [109] N. Karssemeijer and G. M. te Brake, "Detection of stellate distortions in mammograms," *IEEE Trans. Med. Imaging*, vol. 15, no. 5, pp. 611–619, Oct. 1996.
- [110] S. Liu, C. Babbs, and E. Delp, "Multiresolution detection of spiculated lesions in digital mammograms," *IEEE Trans. Image Process.*, vol. 10, no. 6, pp. 874–884, 2001.
- [111] H. Li, Y. Wang, K. J. R. Liu, S.-C. B. Lo, and M. T. Freedman, "Computerized radiographic mass detection. I. Lesion site selection by morphological enhancement and contextual segmentation," *IEEE Trans. Med. Imaging*, vol. 20, no. 4, pp. 289–301, 2001.
- [112] M. Heat and K. Bowyer, "Mass detection by Relative Image Intensity (AFUM)," in *5th International Workshop on Digital Mammography ed MJ Yaffe (Medical Physics Publishing) pp*, 2000, pp. 219–25.
- [113] C. Varela, P. G. Tahoces, A. J. Méndez, M. Souto, and J. J. Vidal, "Computerized detection of breast masses in digitized mammograms," *Comput. Biol. Med.*, vol. 37, no. 2, pp. 214–226, Feb. 2007.
- [114] T. Berber, A. Alpkocak, P. Balci, and O. Dicle, "Breast mass contour segmentation algorithm in digital mammograms," *Comput. Methods Programs Biomed.*, vol. 110, no. 2, pp. 150–159, May 2013.
- [115] G. Kom, A. Tiedeu, and M. Kom, "Automated detection of masses in mammograms by local adaptive thresholding," *Comput. Biol. Med.*, vol. 37, no. 1, pp. 37–48, Jan. 2007.
- [116] W. Qian, L. Li, L. Clarke, R. A. Clark, and J. Thomas, "Digital mammography: Comparison of adaptive and nonadaptive CAD methods for mass detection," *Acad. Radiol.*, vol. 6, no. 8, pp. 471–480, Aug. 1999.
- [117] R. Zwiggelaar, T. C. Parr, J. E. Schumm, I. W. Hutt, C. J. Taylor, S. M. Astley, and C. R. M. Boggis, "Model-based detection of spiculated lesions in mammograms," *Med. Image Anal.*, vol. 3, no. 1, pp. 39–62, Mar. 1999.
- [118] M. P. Sampat, A. C. Bovik, G. J. Whitman, and M. K. Markey, "A model-based framework for the detection of spiculated masses on mammography," *Med. Phys.*, vol. 35, no. 5, pp. 2110–2123, May 2008.
- [119] B. Sahiner, L. M. Hadjiiski, H.-P. Chan, C. Paramagul, A. Nees, M. Helvie, and J. Shi, "Concordance of computer-extracted image features with BI-RADS descriptors for mammographic mass margin," 2008, vol. 6915, p. 69151N–69151N–6.
- [120] N. Szekely, N. Toth, and B. Pataki, "A hybrid system for detecting masses in mammographic images," *Instrum. Meas. IEEE Trans.*, vol. 55, no. 3, pp. 944–952, 2006.
- [121] D. Wei, H. Chan, M. Helvie, B. Sahiner, N. Petrick, D. Adler, and M. Goodsitt, "Classification of mass and normal breast tissue on digital mammograms: multiresolution texture analysis," *Med. Phys.*, vol. 22, p. 1501, 1995.

- [122] J. Freixenet, A. Oliver, R. Martí, X. Lladó, J. Pont, E. Pérez, E. R. E. Denton, and R. Zwigelaar, "Eigendetection of masses considering false positive reduction and breast density information," *Med. Phys.*, vol. 35, no. 5, pp. 1840–1853, May 2008.
- [123] M. A. Mazurowski, J. Y. Lo, B. P. Harrawood, and G. D. Tourassi, "Mutual information-based template matching scheme for detection of breast masses: From mammography to digital breast tomosynthesis," *J. Biomed. Inform.*, vol. 44, no. 5, pp. 815–823, Oct. 2011.
- [124] I. Christoyianni, A. Koutras, E. Dermatas, and G. Kokkinakis, "Computer aided diagnosis of breast cancer in digitized mammograms," *Comput. Med. Imaging Graph.*, vol. 26, no. 5, pp. 309–319, Sep. 2002.
- [125] B. Krishnapuram, J. Stoeckel, V. Raykar, B. Rao, P. Bamberger, E. Ratner, N. Merlet, I. Stainvas, M. Abramov, and A. Manevitch, "Multiple-Instance Learning Improves CAD Detection of Masses in Digital Mammography," in *Digital Mammography*, E. A. Krupinski, Ed. Springer Berlin Heidelberg, 2008, pp. 350–357.
- [126] Q. Guo, J. Shao, and V. Ruiz, "Characterization and classification of tumor lesions using computerized fractal-based texture analysis and support vector machines in digital mammograms," *Int. J. Comput. Assist. Radiol. Surg.*, vol. 4, no. 1, pp. 11–25, 2009.
- [127] R. Campanini, D. Dongiovanni, E. Iampieri, N. Lanconelli, M. Masotti, G. Palermo, A. Riccardi, and M. Roffilli, "A novel featureless approach to mass detection in digital mammograms based on support vector machines," *Phys. Med. Biol.*, vol. 49, p. 961, 2004.
- [128] D. West, P. Mangiameli, R. Rampal, and V. West, "Ensemble strategies for a medical diagnostic decision support system: A breast cancer diagnosis application," *Eur. J. Oper. Res.*, vol. 162, no. 2, pp. 532–551, Apr. 2005.
- [129] R. O. Duda, P. E. Hart, and D. G. Stork, *Pattern Classification*. John Wiley & Sons, 2012.
- [130] H.-P. Chan, B. Sahiner, N. Petrick, M. A. Helvie, K. L. Lam, D. D. Adler, and M. M. Goodsitt, "Computerized classification of malignant and benign microcalcifications on mammograms: texture analysis using an artificial neural network," *Phys. Med. Biol.*, vol. 42, no. 3, p. 549, Mar. 1997.
- [131] H.-P. Chan, B. Sahiner, K. L. Lam, N. Petrick, M. A. Helvie, M. M. Goodsitt, and D. D. Adler, "Computerized analysis of mammographic microcalcifications in morphological and texture feature spaces," *Med. Phys.*, vol. 25, no. 10, pp. 2007–2019, 1998.
- [132] A. Karahaliou, S. Skiadopoulos, I. Boniatis, P. Sakellaropoulos, E. Likaki, G. Panayiotakis, and L. Costaridou, "Texture analysis of tissue surrounding microcalcifications on mammograms for breast cancer diagnosis," *Br J Radiol*, vol. 80, no. 956, pp. 648–656, Aug. 2007.
- [133] A. P. Dhawan, Y. Chitre, and C. Kaiser-Bonasso, "Analysis of mammographic microcalcifications using gray-level image structure features," *IEEE Trans. Med. Imaging*, vol. 15, no. 3, pp. 246–259, 1996.
- [134] M. Kallergi, "Computer-aided diagnosis of mammographic microcalcification clusters," *Med. Phys.*, vol. 31, no. 2, pp. 314–326, 2004.
- [135] S. Yoon and S. Kim, "Mutual information-based SVM-RFE for diagnostic classification of digitized mammograms," *Pattern Recognit. Lett.*, vol. 30, no. 16, pp. 1489–1495, Dec. 2009.
- [136] M. De Santo, M. Molinara, F. Tortorella, and M. Vento, "Automatic classification of clustered microcalcifications by a multiple expert system," *Pattern Recognit.*, vol. 36, no. 7, pp. 1467–1477, Jul. 2003.
- [137] H. Soltanian-Zadeh, F. Rafiee-Rad, and S. Pourabdollah-Nejad D, "Comparison of multiwavelet, wavelet, Haralick, and shape features for microcalcification classification in mammograms," *Pattern Recognit.*, vol. 37, no. 10, pp. 1973–1986, Oct. 2004.
- [138] R. M. Rangayyan, N. M. El-Faramawy, J. E. L. Desautels, and O. A. Alim, "Measures of acutance and shape for classification of breast tumors," *IEEE Trans. Med. Imaging*, vol. 16, no. 6, pp. 799–810, 1997.
- [139] P. R. M. Rangayyan, N. R. Mudigonda, and J. E. L. Desautels, "Boundary modelling and shape analysis methods for classification of mammographic masses," *Med. Biol. Eng. Comput.*, vol. 38, no. 5, pp. 487–496, Sep. 2000.
- [140] D. Guliato, R. M. Rangayyan, W. A. Carnielli, J. A. Zuffo, and J. E. L. Desautels, "Segmentation of breast tumors in mammograms using fuzzy sets," *J. Electron. Imaging*, vol. 12, no. 3, pp. 369–378, 2003.
- [141] W. K. Lim and M. J. Er, "Classification of mammographic masses using generalized dynamic fuzzy neural networks," *Med. Phys.*, vol. 31, no. 5, pp. 1288–1295, May 2004.

- [142] B. Sahiner, H. P. Chan, N. Petrick, M. A. Helvie, and M. M. Goodsitt, "Computerized characterization of masses on mammograms: the rubber band straightening transform and texture analysis," *Med. Phys.*, vol. 25, no. 4, pp. 516–526, Apr. 1998.
- [143] L. Hadjiiski, B. Sahiner, H. P. Chan, N. Petrick, and M. Helvie, "Classification of malignant and benign masses based on hybrid ART2LDA approach," *IEEE Trans. Med. Imaging*, vol. 18, no. 12, pp. 1178–1187, Dec. 1999.
- [144] B. Zheng, Y.-H. Chang, X. H. Wang, W. F. Good, and D. Gur, "Application of a Bayesian belief network in a computer-assisted diagnosis scheme for mass detection," 1999, vol. 3661, pp. 1553–1561.
- [145] S. Timp, C. Varela, and N. Karssemeijer, "Temporal Change Analysis for Characterization of Mass Lesions in Mammography," *IEEE Trans. Med. Imaging*, vol. 26, no. 7, pp. 945–953, 2007.
- [146] B. Zheng, "Computer-Aided Diagnosis in Mammography Using Content-Based Image Retrieval Approaches: Current Status and Future Perspectives," *Algorithms*, vol. 2, no. 2, p. 828, 2009.
- [147] S. C. Park, X.-H. Wang, and B. Zheng, "Assessment of Performance Improvement in Content-based Medical Image Retrieval Schemes Using Fractal Dimension," *Acad. Radiol.*, vol. 16, no. 10, pp. 1171–1178, Oct. 2009.
- [148] K. Drukker, K. Horsch, and M. L. Giger, "Multimodality Computerized Diagnosis of Breast Lesions Using Mammography and Sonography1," *Acad. Radiol.*, vol. 12, no. 8, pp. 970–979, Aug. 2005.
- [149] D. Guliato, R. M. Rangayyan, J. D. Carvalho, and S. A. Santiago, "Polygonal Modeling of Contours of Breast Tumors With the Preservation of Spicules," *IEEE Trans. Biomed. Eng.*, vol. 55, no. 1, pp. 14–20, 2008.
- [150] C. A. Méndez, F. Pizzorni Ferrarese, P. Summers, G. Petralia, and G. Menegaz, "DCE-MRI and DWI Integration for Breast Lesions Assessment and Heterogeneity Quantification," *Int. J. Biomed. Imaging*, vol. 2012, 2012.
- [151] C. Wood, "Computer Aided Detection (CAD) for breast MRI," *Technol. Cancer Res. Treat.*, vol. 4, no. 1, pp. 49–53, Feb. 2005.
- [152] C. Meeuwis, S. M. van de Ven, G. Stapper, A. M. Fernandez Gallardo, M. A. A. J. van den Bosch, W. P. T. M. Mali, and W. B. Veldhuis, "Computer-aided detection (CAD) for breast MRI: evaluation of efficacy at 3.0 T," *Eur. Radiol.*, vol. 20, no. 3, pp. 522–528, Mar. 2010.
- [153] M. D. Schnall, J. Blume, D. A. Bluemke, G. A. DeAngelis, N. DeBruhl, S. Harms, S. H. Heywang-Köbrunner, N. Hylton, C. K. Kuhl, E. D. Pisano, P. Causer, S. J. Schnitt, D. Thickman, C. B. Stelling, P. T. Weatherall, C. Lehman, and C. A. Gatsonis, "Diagnostic Architectural and Dynamic Features at Breast MR Imaging: Multicenter Study1," *Radiology*, vol. 238, no. 1, pp. 42–53, Jan. 2006.
- [154] S. H. Lee, J. H. Kim, N. Cho, J. S. Park, Z. Yang, Y. S. Jung, and W. K. Moon, "Multilevel analysis of spatiotemporal association features for differentiation of tumor enhancement patterns in breast DCE-MRI," *Med. Phys.*, vol. 37, no. 8, pp. 3940–3956, Aug. 2010.
- [155] F. W. Flickinger, J. D. Allison, R. M. Sherry, and J. C. Wright, "Differentiation of benign from malignant breast masses by time-intensity evaluation of contrast enhanced MRI," *Magn. Reson. Imaging*, vol. 11, no. 5, pp. 617–620, 1993.
- [156] E. Furman-Haran, D. Grobgeld, R. Margalit, and H. Degani, "Response of MCF7 human breast cancer to tamoxifen: evaluation by the three-time-point, contrast-enhanced magnetic resonance imaging method.," *Clin. Cancer Res.*, vol. 4, no. 10, pp. 2299–2304, Oct. 1998.
- [157] J. U. Fluckiger, M. C. Schabel, and E. V. R. DiBella, "The effect of temporal sampling on quantitative pharmacokinetic and three-time-point analysis of breast DCE-MRI," *Magn. Reson. Imaging*, vol. 30, no. 7, pp. 934–943, Sep. 2012.
- [158] S. Sinha, F. Lucas Quesada, N. Debruhl, J. Sayre, D. Farria, D. Gorczyca, and L. Bassett, "Multifeature analysis of Gd-enhanced MR images of breast lesions," *J. Magn. Reson. Imaging*, vol. 7, no. 6, pp. 1016–1026, Nov. 1997.
- [159] W. Chen, M. Giger, L. Lan, and U. Bick, "Computerized interpretation of breast MRI: Investigation of enhancement-variance dynamics," *Med. Phys.*, vol. 31, no. 5, p. 1076, Apr. 2004.
- [160] F. Pediconi, C. Catalano, F. Venditti, M. Ercolani, L. Carotenuto, S. Padula, E. Moriconi, A. Roselli, L. Giacomelli, M. A. Kirchin, and R. Passariello, "Color-coded automated signal intensity curves for detection and characterization of breast lesions: preliminary evaluation of a new software package for integrated magnetic resonance-based breast imaging," *Invest. Radiol.*, vol. 40, no. 7, pp. 448–457, Jul. 2005.

- [161] K. G. Gilhuijs, M. L. Giger, and U. Bick, "Computerized analysis of breast lesions in three dimensions using dynamic magnetic-resonance imaging," *Med. Phys.*, vol. 25, no. 9, pp. 1647–1654, Sep. 1998.
- [162] J. Yao, J. Chen, and C. Chow, "Breast Tumor Analysis in Dynamic Contrast Enhanced MRI Using Texture Features and Wavelet Transform," *IEEE J. Sel. Top. Signal Process.*, vol. 3, no. 1, pp. 94–100, Feb. 2009.
- [163] Y. Zheng, S. Englander, S. Baloch, E. Zacharaki, Y. Fan, M. Schnall, and D. Shen, "STEP: Spatiotemporal enhancement pattern for MR-based breast tumor diagnosis," *Med. Phys.*, vol. 36, no. 7, pp. 3192–3204, Jul. 2009.
- [164] C. McLaren, W. Chen, K. Nie, and M. Su, "Prediction of Malignant Breast Lesions from MRI Features: A Comparison of Artificial Neural Network and Logistic Regression Techniques," *Acad. Radiol.*, vol. 16, no. 7, pp. 842–851, Jul. 2009.
- [165] R. Lucht, M. Knopp, and G. Brix, "Classification of signal-time curves from dynamic MR mammography by neural networks," *Magn. Reson. Imaging*, vol. 19, no. 1, pp. 51–57, Jan. 2001.
- [166] T. Twellmann, O. Lichte, and T. W. Nattkemper, "An adaptive tissue characterization network for model-free visualization of dynamic contrast-enhanced magnetic resonance image data," *IEEE Trans Med Imaging*, vol. 24, no. 10, pp. 1256–1266, Oct. 2005.
- [167] B. K. Szabó, M. K. Wiberg, B. Boné, and P. Aspelin, "Application of artificial neural networks to the analysis of dynamic MR imaging features of the breast," *Eur. Radiol.*, vol. 14, no. 7, pp. 1217–1225, Jul. 2004.
- [168] T. W. Nattkemper, B. Arnrich, O. Lichte, W. Timm, A. Degenhard, L. Pointon, C. Hayes, and M. O. Leach, "Evaluation of radiological features for breast tumour classification in clinical screening with machine learning methods," *Artif. Intell. Med.*, vol. 34, no. 2, pp. 129–139, Jun. 2005.
- [169] J. Levman, T. Leung, P. Causer, D. Plewes, and A. L. Martel, "Classification of Dynamic Contrast-Enhanced Magnetic Resonance Breast Lesions by Support Vector Machines," *IEEE Trans Med Imaging*, vol. 27, no. 5, pp. 688–696, May 2008.
- [170] A. Basavanahally, S. Doyle, and A. Madabhushi, "Predicting classifier performance with a small training set: Applications to computer-aided diagnosis and prognosis," in *Proceedings of the IEEE International Symposium on Biomedical Imaging: From Nano to Macro*, 2010, pp. 229–232.
- [171] Y. Gal, A. Mehnert, A. Bradley, D. Kennedy, and S. Crozier, "Feature and Classifier Selection for Automatic Classification of Lesions in Dynamic Contrast-Enhanced MRI of the breast," in *Proceedings of the 2009 Digital Image Computing: Techniques and Applications*, 2009, pp. 132–139.
- [172] E. Furman-Haran and H. Degani, "Parametric analysis of breast MRI," *J. Comput. Assist. Tomogr.*, vol. 26, no. 3, p. 376, May 2002.
- [173] S. H. Lee, J. H. Kim, J. S. Park, and W. K. Moon, "Optimal Clustering of Kinetic Patterns on Malignant Breast Lesions: Comparison between K-means Clustering and Three-time-points Method in Dynamic Contrast-enhanced MRI," in *Proceedings of the 29th Annual International Conference of the IEEE Engineering in Medicine and Biology Society*, 2007, pp. 2089–2093.
- [174] J. Levman and A. Martel, "Computer-aided diagnosis of breast cancer from magnetic resonance imaging examinations by custom radial basis function vector machine," in *Proceedings of the 32nd Annual International Conference of the IEEE Engineering in Medicine and Biology Society*, 2010, pp. 5577–5580.
- [175] L. A. Meinel, A. H. Stolpen, K. S. Berbaum, L. L. Fajardo, and J. M. Reinhardt, "Breast MRI lesion classification: improved performance of human readers with a backpropagation neural network computer-aided diagnosis (CAD) system," *J. Magn. Reson. Imaging JMRI*, vol. 25, no. 1, pp. 89–95, Jan. 2007.
- [176] T. Schlossbauer, G. Leinsinger, A. Wismuller, O. Lange, M. Scherr, A. Meyer-Baese, and M. Reiser, "Classification of Small Contrast Enhancing Breast Lesions in Dynamic Magnetic Resonance Imaging Using a Combination of Morphological Criteria and Dynamic Analysis Based on Unsupervised Vector-Quantization," *Invest. Radiol.*, vol. 43, no. 1, pp. 56–64, Jan. 2008.
- [177] E. E. Deurloo, S. H. Muller, J. L. Peterse, A. P. E. Besnard, and K. G. A. Gilhuijs, "Clinically and Mammographically Occult Breast Lesions on MR Images: Potential Effect of Computerized Assessment on Clinical Reading1," *Radiology*, vol. 234, no. 3, pp. 693–701, Jan. 2005.
- [178] A. Penn, S. Thompson, R. Brem, C. Lehman, P. Weatherall, M. Schnall, G. Newstead, E. Conant, S. Ascher, E. Morris, and E. Pisano, "Morphologic Blooming in Breast MRI as a Characterization of

- Margin for Discriminating Benign from Malignant Lesions," *Acad. Radiol.*, vol. 13, no. 11, pp. 1344–1354, Nov. 2006.
- [179] H. O. Peitgen, H. Jürgens, and D. Saupe, *Chaos and Fractals: New Frontiers of Sciences*. Springer, 1993.
- [180] R. Lopes and N. Betrouni, "Fractal and multifractal analysis: A review," *Med. Image Anal.*, vol. 13, no. 4, pp. 634–649, Aug. 2009.
- [181] A. Penn, S. Thompson, M. Schnall, M. Loew, and L. Bolinger, "Fractal discrimination of MRI breast masses using multiple segmentations," in *Proceedings of SPIE*, 2000, vol. 3979, pp. 959–966.
- [182] W. Chen, M. Giger, H. Li, U. Bick, and G. Newstead, "Volumetric texture analysis of breast lesions on contrast-enhanced magnetic resonance images," *Magn. Reson. Med.*, vol. 58, no. 3, pp. 562–571, 2007.
- [183] S. C. Agner, S. Soman, E. Libfeld, M. McDonald, K. Thomas, S. Englander, M. A. Rosen, D. Chin, J. Noshier, and A. Madabhushi, "Textural Kinetics: A Novel Dynamic Contrast-Enhanced (DCE)-MRI Feature for Breast Lesion Classification," *J. Digit. Imaging*, vol. 24, no. 3, pp. 446–463, Jun. 2011.



## Chapter 3

# **Review and Performance Evaluation of Multifractal Approaches for Computer-aided Detection of Microcalcification Clusters in Mammograms**

This chapter consists of the following article:

Review and Performance Evaluation of Multifractal Approaches for Computer-aided Detection of Microcalcification Clusters in Mammograms

Filipe Soares, Filipe Janela, Manuela Pereira, João Seabra and Mário M. Freire

Article submitted for publication in an international peer-reviewed IEEE journal, 2013.



# Review and Performance Evaluation of Multifractal Approaches for Computer-aided Detection of Microcalcification Clusters in Mammograms

Filipe Soares, Filipe Janela, Manuela Pereira, João Seabra and Mário M. Freire, *Member, IEEE*

**Abstract**—Computer-aided detection of mammographic patterns often relies on texture characterization. Yet texture characterization has so far rarely been based on a multifractal image analysis in the scope of breast cancer. This article reviews and investigates a generalization for the two-dimensionality (2D) of the main three multifractal methods recently proposed: Multifractal Detrended Fluctuation Analysis (MF-DFA), Modulus Maxima Wavelet Transform (MMWT) and Wavelet Leaders Multifractal Formalism (WLMF). After these methods have been suitably applied in synthetic multifractal surfaces, our goal is to evaluate if such generalizations can be used for the extraction of important clinical elements for breast cancer detection, namely microcalcifications, in a proposed common framework. The detection performance of the methods is evaluated by Free-Response Operating Characteristic analysis and their computational costs are also compared. Within a set of 290 clinical images from two public databases, the employed methods were able to successfully distinguish microcalcification clusters from the background. Reported results show that 2D MF-DFA outperforms the other two wavelet-based variants of multifractal analysis, independently from the spatial resolution of the images in the database. Nevertheless, 2D WLMF is computationally more efficient having average detection performance. By depicting the multifractal behavior in gray scale images, the inspection of singularities and their fluctuations at multiple resolutions revealed that the multifractal study is very important for the characterization of the underlying complexity of microcalcifications. Multifractal mammogram analysis provides useful information for computer-aided detection.

**Index Terms**—Computer-aided detection; Mammography; Multifractal Image Analysis; Detrended Fluctuation Analysis; Wavelet Leaders; Modulus Maxima Wavelet Transform.

## I. INTRODUCTION

**B**REAST cancer is curable if detected in early stages and given proper treatment. Screening by mammography has

This work was partially funded by the Fundação para a Ciência e a Tecnologia through the grant SFRH/BDE/15624/2006, by Siemens S.A. Healthcare Sector, by Instituto de Telecomunicações and by University of Beira Interior, Portugal. *Asterisk indicates corresponding author.*

\*Filipe Soares is with Siemens S.A. Healthcare Sector, 4456-901 Perafita, Portugal (e-mail: filipecruzsoares@gmail.com).

Filipe Janela and João Seabra are with Siemens S.A. Healthcare Sector, 4456-901 Perafita, Portugal.

Filipe Soares, Manuela Pereira and Mário M. Freire are with Instituto de Telecomunicações, Department of Computer Science, University of Beira Interior, 6201-001 Covilhã, Portugal.

lead to a reduction in breast cancer mortality of up to 30%. However, statistics show that 60-80% of biopsies are performed on benign cases and approximately 25-40% of malignant cases are missed [1], [2].

The detection and diagnosis of breast cancer with mammography consists of two steps. The first is the asymptomatic screening, in which suspicious areas in a mammogram may be identified. The second is the diagnostic mammography, in which symptomatic women with some abnormality receive specific view mammograms and possibly ultrasound or magnetic resonance imaging. The result of the latter imaging step determines the need for biopsy [3].

Mammographic first signs of breast cancer usually appear in the form of clusters of microcalcifications. These tiny deposits of calcium can be visible long before any palpable lesion has developed and their early detection contributes to the success of the treatment. For diagnosis, radiologists generally rely on their shape, size, number and distribution. Malignant calcifications are typically very numerous, clustered, small, dot-like or elongated, variable in size, shape and density. Benign calcifications are generally larger, more rounded, smaller in number, more diffusely distributed, and more homogeneous in shape [4]. However, because of the small size of microcalcifications, the comparison and characterization of benign and malignant lesions represents a very complex problem even for an experienced radiologist [5].

In almost 50% of the mammograms the presence of microcalcifications in conjunction with other mammographic readings is an early sign of breast cancer. Microcalcifications in isolation would account for about 30% of cancer detection. On screening studies, 90% of nonpalpable in situ ductal carcinomas and 70% of nonpalpable minimal carcinomas are detected on microcalcifications alone. Microcalcifications are found using high-resolution imaging techniques or, in the case of mammography, using direct radiological magnification, because they are the smallest structures identified on mammograms. Clinically, their size varies in the range of 0.1-1.0 mm, and the average diameter is about 0.3 mm. The smaller ones (0.1-0.2 mm) can hardly be seen due to lack of spatial resolution in image acquisition and noise. Moreover, some parts of the background, such as dense tissue, may be brighter than the microcalcifications in the fatty part of the

breast. Nevertheless, the existence of microcalcifications in a mammogram is often a sign of abnormality, whether or not they appear in independent clusters or associated with other patterns of high density breast tissue, called masses [5]–[7].

The two-dimensional nature of mammography makes it very difficult to distinguish a breast tumor from overlying breast tissues. The mammographic findings are generally hard to discover because of their superimposition on the breast parenchymal textures. Moreover, breast density is known to be the most affecting factor for mammographic accuracy [8].

The complex anatomy of the breast and, therefore, the highly textured structure of the mammograms imply the need for reliable image processing tools to assist the process of detection and diagnosis. Concerning the discomfort and risk of mammography and, more importantly, of core biopsy exams, screening programs must seek a good sensitivity and acceptable specificity on the reports [9]. The variability between cases increases the difficult task that the human decision maker faces when reporting on a mammogram, which emphasizes the need for machine aid. The development of Computer-Aided Detection (CADE) systems has reached the point where extremely valuable information is offered to the clinician in the detection of lesions, at the earliest possible stage. It can only assist the radiologist to make a decision, but the use of a CADE system can be comparable to double reading by two radiologists, and it has been shown to help finding more cancers [6], [10].

#### *A. Review of Prior Work on Detection of Mammographic Abnormalities*

The task of CADE systems is to focus the attention of the radiologist on suspicious areas. To detect abnormalities, most of the algorithms consist of: first, detection of suspicious regions on the mammogram, and second, its classification as mass, microcalcifications or normal tissue. The first stage is designed to have a very high sensitivity and a large number of false positives per image (FPI) is acceptable, since they are expected to be removed in stage two [11]–[13].

The performance of detection algorithms in CADE is usually measured with sensitivity (Number of True Positive Marks / Number of Lesions) and the number of FPI (Number of False Positive Marks / Number of Images). A true positive is a mark made by the CADE system that corresponds to the location of a lesion. A false positive is a mark made by the CADE that does not correspond to the correct location. The sensitivity versus FPI is called a Free-Response Receiver Operating Characteristic (FROC) curve and this is generally used to report the performance of the detection algorithm [14]. Generally, the bigger the area under the curve the better but, despite the consistent use of evaluation methods in the literature, direct comparison of systems for detecting mammographic abnormalities is difficult because few studies have been reported on a common database [10].

Radiologists employ a number of image characteristics on the discrimination and researchers have attempted to emulate that process. The first apparent characteristic is the region intensity. In a dense breast the contrast is quite low so that the

human eye is able to distinguish. The aim of simple contrast enhancement methods is to increase the contrast of microcalcifications over a threshold [15]. The major problem with this kind of algorithms is that for an image, some regions may be under-enhanced that can cause false negatives while some regions may be over-enhanced resulting in false positives as noise [16]. Additional features were designed by Brake et al. [17] to capture image characteristics including iso-density, location and contrast, to classify between lesions and normal tissue. Tourassi et al. [18] used a template matching technique where each region of interest (ROI) of a database served as a template and mutual information was used as a metric of similarity to decide if a ROI contained a mass. Other strategies have been proposed for detecting microcalcifications, including mathematical morphology [19]–[21], random field models [22] and artificial neural networks [23]–[26].

A major limitation of pixel-based and region-based detection methods is that the analysis is not done over a continuous range of scales. Cancerous lesions are stochastic biological phenomena which manifest in images as having various structures occurring at different sizes and over ranges of spatial scales. Moreover, the spiculations that are associated with many cancerous lesions occur with different widths, lengths, and densities, which suggest that their characterization will require multi-scale analysis [27]. In this sense, a number of authors employed wavelet transforms for the detection of microcalcifications [28]–[31]. Wavelet methods rely on pre-processing the image using a sub-band decomposition filterbank. The coefficients in the sub-band images which correspond to high spatial frequencies are selectively weighted to enhance the calcifications. A reason why wavelets have been so effective is that microcalcifications appear as small bright dots on the mammogram and can be viewed as point discontinuities. Wavelets have finite square supports and are ideal for capturing point discontinuities, but not edges [27]. This explains the success in the detection of calcifications, whereas for the detection of masses these methods are not so effective.

Microcalcifications have less structure when compared to the breast background. The parenchymal and ductal patterns in mammograms possess structures with high local self-similarity which is the basic property of fractal objects [32]. These tissue patterns can be constructed by fractal models, and be taken out from the original image, as the microcalcification information will be enhanced. The abnormalities are considered as structural deviations from the global regularity of the background, and this statistical approach improved tumor classification in doubtful cases for expert radiologists [33] with magnetic resonance imaging. Also with mammography [32], in terms of contrast and noise level, fractal modeling of breast background tissues was more helpful to extract mammographic patterns and to enhance microcalcifications, compared to morphological operations and partial wavelet reconstruction approaches.

Multifractal theory can be considered an extension of fractal theory, where some natural phenomena might be better

described. The multifractal spectrum summarizes both simple and multiple degrees of scaling. Scaling refers to the propagation of energy when the images are inspected at various resolutions. Monofractals are homogeneous in the sense that they have the same scaling properties, characterized by only one regularity exponent throughout the entire signal or image. In contrast, multifractals require a larger and theoretically infinite, number of indices to characterize their scaling properties. This can potentially give us more information about the image compared to the single fractal dimension [34]. The existence of multiple degrees of scaling in magnetic resonance images of the breast was suggested by Derado et al. [35], and confirmed by Soares et. al. [36] making use of the scaling dynamics as discriminatory descriptors.

### *B. Multifractal Image Analysis*

Texture characterization is now often envisaged by measuring the fluctuations, with respect to space, of the regularity of the image intensity. Multifractal image analysis allows the extraction of relevant information directly from image regions which regularity differs from the background [34]. Multifractal image analysis permits the sharp distinction between edge points and isolated points. Although both types of points differ from background, edge points are locally connected, while the isolated ones are not [37]. This multifractal approach exploits both the local regularity of a finding, and the global distribution of its regularity. Furthermore, the multifractal spectrum translates a regularity-based texture characterization by the quantity and quality of irregularities in the analyzed data.

The problem of the detection of microcalcifications in digitized mammograms was addressed in [38] with wavelet-based multifractal theory using the Modulus Maxima Wavelet Transform (MMWT). Defined from a continuous wavelet transform, this is undoubtedly a very promising method presenting high precision in the scaling analysis, in spite of being computationally and conceptually complex, especially for high-dimensional objects.

A reliable alternative to MMWT is the Multifractal Detrended Fluctuation Analysis (MF-DFA) method, introduced in 2002 for time series [39]. The MF-DFA has the advantage of being less sensitive to the temporal resolution of the time series [40]. Moreover, it is suggested that when no a priori knowledge of the fractal properties of a process exists, choosing MF-DFA is recommended. There are also evidences in [40] that MF-DFA provides similar results to MMWT but it is simpler and more accurate for short artificial signals.

A recent alternative for wavelet-based multifractal analysis called Wavelet Leader Multifractal Formalism (WLMF) [41] is theoretically backed up by a strong mathematical framework. In addition, being defined from a discrete wavelet transform, WLMF easily enables its theoretical and practical extensions to higher dimension [41], [42].

MMWT, WLMF and MF-DFA methods are highly effective to characterize statistical data, such as heart rhythms or seismic patterns [43]. However, the extension of these methods to more general cases is nowadays an open problem,

namely on the detection of microcalcifications addressed herein and generally in two-dimensional (2D) image scope.

In a preliminary study [44] on the application of the multifractal image analysis to mammography with MF-DFA, we have shown that the presence of microcalcifications led to changes in the local mammographic texture and multifractal scaling behavior. In this article the main three multifractal methods recently presented in literature are investigated in a generalization for the two-dimensionality. After these methods have been suitably applied in synthetic multifractal surfaces, our goal is to evaluate if such generalizations can be used for the extraction of important clinical elements for breast cancer detection, namely microcalcifications, by depicting the multifractal behavior in gray scale images of mammograms.

### *C. Overview of the Article*

In this article, we present a new model for CADE of microcalcification clusters in mammography, using the multifractal formalism focused in the properties of microcalcifications. We review and investigate the 2D extension of three multifractal methods to address the problem of texture characterization of microcalcifications in relation to their surroundings, thus presenting a new approach to be combined with other diagnostic tools. No image representation was used to compute the associated fractal dimension; instead, the image itself is studied in terms of multifractal features. This work should not be confused with the multifractal image analysis by Ramírez-Cobo and Vidakovic [31], focused solely on the image background and not on microcalcifications. Finally, it is also proposed a technique to reduce the false positives due to normal linear structures e.g., blood vessels. This is accomplished by using self-similarity analysis to identify and create a likelihood map of potential structures to remove.

This article is organized as follows. Section II describes the proposed detection model and three multifractal approaches. Experimental results and discussion are given in Section III and IV, respectively. Section V concludes on the value of multifractal mammogram analysis for CADE.

## II. DETECTION MODEL AND MULTIFRACTAL APPROACHES

In this section, the mathematical background of the new model is described for 2D detection of microcalcification clusters in mammograms. The theoretical basis of MMWT, WLMF and MF-DFA is presented together with our modifications for the specific problem of microcalcifications.

Fig. 1 illustrates the flowchart of the proposed model for the detection of abnormalities. The mammogram is pre-processed to locate the skin-line of the breast. The feature extraction is the core of the model as it is detailed in section B. A clustering process of microcalcifications and self-similarity analysis finish the workflow.

### *A. Pre-Processing and Breast Region Detection*

A mammogram mainly contains two distinct regions: the exposed breast region and the unexposed non-breast region. In order to avoid the time consuming analysis of the complete

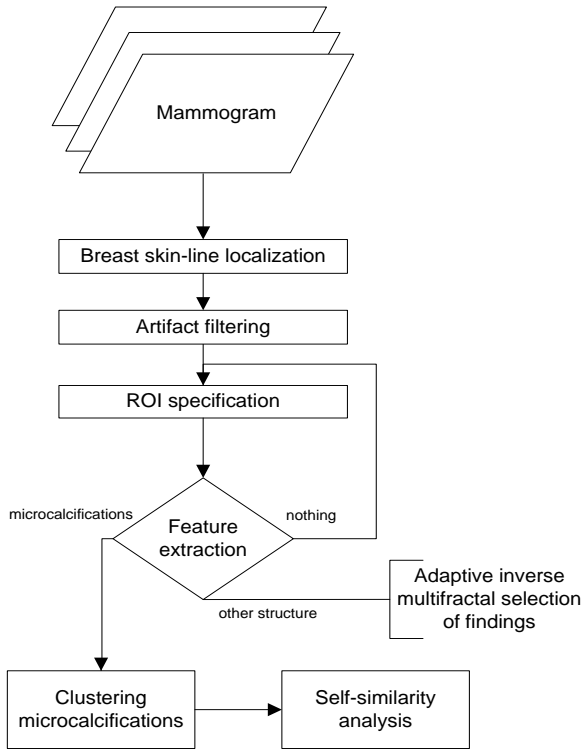


Fig. 1. Proposed microcalcification detection model. The first three blocks of the flow are pre-processing steps before the core feature extraction, where the method for multifractal image analysis is employed. The clustering and self-similarity analysis aim for false positive reduction.

mammogram, the first step of the system is the segmentation of the exposed breast region. The subsequent processing calculation is reduced and radiopaque artifacts are removed at the same time.

The implementation of the breast skin-line localization was based on the work presented in [45], [46]. Particularly, it followed the algorithm proposed in [45], which combines the global thresholding method for a coarse estimation of breast region and morphological operations for exact positioning of the breast boundary. It takes the advantage of the Watershed Transformation [47] which has substantially higher robustness with respect to noise, compared with the Region Growing method by pixel aggregation segmentation depicted in [46]. The watershed transformation is one kind of morphological operation which combines the Region Growing and edge detection techniques [45].

The gradient image should be filtered before computing its Watershed Transform. Noise suppression was applied to enhance image and calcification contrast. The overall noise reduction is achieved by Median Filtering [47]. In order to improve the performance of the method in the detection of the breast border, and to compensate for the intensity fall-off due to thickness variation, a double thresholding is applied to gray levels obtained as in [48]. First, the gray level histogram of the entire mammogram is calculated. The peaks at the higher and

lower gray levels correspond to both unexposed and exposed non-breast regions, respectively. The residual levels of the gradient image match the potential edge region, where the watershed transformation has to be confined as in [45].

The exposed breast region is divided in ROIs by a grid of squares. The feature extraction was performed pixelwise for each grid element. Grid elements with pixels belonging to the unexposed regions were discarded, namely on the border zones of the breast skin-line.

### B. Multifractal-based Feature Extraction

A multifractal-based method is employed for the extraction of small-sized isolated details in mammograms. In this section three main methods are compared to derive features which are selected according to multifractal singularity information.

For the image analysis of mammograms, the measure of a region is defined as a function of the gray levels belonging to that region. Oppositely to the topological dimensions represented by a natural number of independent vectors, fractal elements are characterized by a real number related to the degree of irregularity of the signal, named fractal dimension. One of the most popular methods for its calculation is the box-counting, due to its simplicity and fast computing procedure [49]. Considering a 2D signal or surface region describing a mammogram image, the box-counting method is not appropriate since it gives only a relation between non-empty boxes and the box size, regardless of the signal level into the boxes. In case of multifractals, the signal value within the box is embedded into the process characterization. Instead of one quantity or measure,  $\mu$ , describing the phenomenon in all scales (as in case of fractals), a set of measures,  $\Sigma\mu_i$  (weight factors) depicting statistically the same phenomenon in different scales, have to be used for characterizing such structures.

First, the quantity called the coarse Hölder exponent  $\alpha$  is defined in (1), quantifying the strength of the singularities of the measure, describing the pointwise singularity (local regularity) of the object with the determined measure of the box  $\mu(box)$  and size of the box  $\varepsilon$ . The limiting value of  $\alpha$  is estimated as the slope of the linear regression line, taken from the plot corresponding points by bi-logarithmic diagram  $\log \mu(box)$  against  $\log \varepsilon$ .

$$\alpha = \frac{\log \mu(box)}{\log \varepsilon} \quad (1)$$

A single Hölder exponent denotes monofractality. Usually in the whole structure there are many boxes with the same  $\alpha$ . Once  $\alpha$  has been quantified, the limiting value of  $f(\alpha)$  is estimated by (2) as the slope of the linear regression line (similar to  $\alpha$  estimation), by the respective bi-logarithmic diagram where  $N_\varepsilon(\alpha)$  is the number of boxes of size  $\varepsilon$ .

$$f(\alpha) = \frac{-\log N_\varepsilon(\alpha)}{\log \varepsilon} \quad (2)$$

Such definition of  $f(\alpha)$  means that for each singularity  $\alpha$   $N_\varepsilon(\alpha)$  increases for decreasing  $\varepsilon$ . Then,  $f(\alpha)$  may be seen as the fractal dimension of the set of points or region that

corresponds to a singularity  $\alpha$ , and a graph of  $f(\alpha)$  plotted over subsets characterized by  $\alpha$  is called the multifractal spectrum of the measure  $\mu$ , describing the global distribution of singularities. For theoretical introductions to multifractal analysis, the reader is referred to e.g. [34].

1) *2D Multifractal Detrended Fluctuation Analysis*

The detrended fluctuation analysis is based on the identification of the scaling of the  $q^{\text{th}}$ -order moments that power-law depend on the signal length. In this sense, the methodological challenge is how to detect and quantify the scaling and correlation properties with mammographic images. This method was generalized to be capable of analyzing multifractal properties of objects with higher dimensions by Gu and Zhou [50]. The 2D MF-DFA method consists of the following stages, where a more detailed description of stage 1 and stage 2 can be found in [50]:

Stage 1: Consider a self-similar surface denoted by a two-dimensional array of gray levels  $f(i, j)$ , where  $i = 1, 2, \dots, M$  and  $j = 1, 2, \dots, N$ . The surface is partitioned into  $M_s \times N_s$  disjoint segments or boxes of lateral size  $s$ .

Stage 2: In each segment  $f_{v,w}$  identified by  $v$  and  $w$ , the cumulative sum of the gray levels is named  $u_{v,w}(i, j)$  where  $i, j$  are pixel coordinates and  $1 \leq i, j \leq s$ .

Stage 3: Local trend and detrended fluctuation function  $F(v, w, s)$  are evaluated for each segment as

$$F(v, w, s) = \sqrt{\frac{1}{s^2} \sum_{i=1}^s \sum_{j=1}^s [u_{v,w}(i, j) - \tilde{u}_{v,w}(i, j)]^2}, \quad (3)$$

where many fitting procedures ( $m$ -order two-dimensional polynomials)  $\tilde{u}$  can be used. Since the detrending is done by the subtraction of the fits from the profile, the order of the polynomials differs in their capability of eliminating trends in the series. Second-order was confirmed to be adequate for spurious free fitting with mammographic data, this way eliminating the influence of possible first-order trends in the original two-dimensional array, for scales larger than the segment size.

Stage 4: The  $q^{\text{th}}$ -order mean fluctuation function is obtained by averaging over all possible segments lengths  $s$ , that is,

$$F_q(s) = \left\{ \frac{1}{M_s N_s} \sum_{v=1}^{M_s} \sum_{w=1}^{N_s} [F(v, w, s)]^q \right\}^{\frac{1}{q}}, \quad (4)$$

where  $q$  can take any real value except zero. The parameter  $q$  can be seen as a focus control of a ‘‘microscope lens’’ for exploring different regions of irregularity.

Stage 5: The key property of  $F_q(s)$  is that for an image with self-similarity properties, a presence of a power-law scaling is revealed with a linear relationship on a double log plot within a significant range of  $s$ . Varying  $s$  in the range from 8 to  $\min(M, N)/4$  with the scaling relation between the detrended fluctuation function  $F_q$  and the size scale  $s$ , given by [39]:

$$F_q(s) \sim s^{h(q)}, \quad (5)$$

where the  $h(q)$  is called generalized Hurst exponent (for a

monofractal signal,  $h(q)$  is a constant).

The generalized Hurst exponent and the multifractal spectrum may be related via Legendre transform [51], deriving the multifractal parameters as

$$\alpha = h(q) + q \frac{dh(q)}{dq} \quad \text{and} \quad (6)$$

$$f(\alpha) = q[\alpha - h(q)] + 1. \quad (7)$$

2) *2D Modulus Maxima Wavelet Transform*

The 2D MMWT, originally developed in the multifractal scope by Arneodo et. al. [52], allows us to build an estimator that is based on the local maxima of the continuous wavelet transform. The wavelet transform is a powerful tool for characterizing the scaling properties of multifractal measures [53] and the MMWT had been proven effective to estimate the multifractal singularity spectrum. The basic idea is to describe the partition function over only the modulus maxima of the wavelet transform of the signal. The redundancy of the continuous wavelet transform is decreased by just keeping the positions and the coefficients of the wavelet transform at the local maxima.

A partition function  $\tau(q)$  is found from a power-law dependence depicted by expression (8) where the structure function  $S(q, s)$  is the sum of the  $q^{\text{th}}$  powers of the local maxima of the absolute modulus of the wavelet transform coefficients at scale  $s$ .

$$S(q, s) \propto s^{\tau(q)} \quad (8)$$

To precisely define what we mean by a local maximum of the wavelet transform modulus, let  $Wf(x)$  be the wavelet transform of a function  $f(x)$ . We call a local extremum any point  $x_0$  such that the derivative depicted by expression (9) has a zerocrossing at  $x = x_0$ , when  $x$  varies. We call a modulus maximum, any point  $x_0$  such that (10) occurs when  $x$  belongs to either a right or left neighborhood of  $x_0$ , and (11) when  $x$  belongs to the other side of the neighborhood of  $x_0$ . These points, also called multi-scale edge points, are points where the modulus is locally maximum with respect to its neighbors.

$$\frac{d(Wf(x))}{dx} \quad (9)$$

$$|Wf(x)| < |Wf(x_0)| \quad (10)$$

$$|Wf(x)| \leq |Wf(x_0)| \quad (11)$$

A function is not singular in any neighborhood where its wavelet transform has no modulus maxima at the finer scales [54]. We call maxima line, any connected curve in the scale space  $x$  along which all points are modulus maxima. At each scale, localized maxima in the modulus of the wavelet transform are identified. These are then connected across scales to form maxima lines, essentially ridges identifying maxima across scale. There is always at least one maxima ridge line pointing toward any singularity. Measuring the slope of the logarithm of the modulus maxima associated with

a singularity produces an estimate of  $\alpha$ . The wavelet power spectrum can be averaged over time to produce a global wavelet spectrum analogous to the Fourier energy spectrum [55].

The modulus maxima perform three useful tasks:

- 1) the existence of local maxima marks the existence of a singularity (or discontinuity, or edge) in the signal. In this sense the wavelet transform is similar to well-known edge-detectors in image processing;
- 2) these maxima form paths which at fine scales locate the edge in the original function;
- 3) the modulus of these maxima can characterize the edge via its regularity, i.e. estimate the order of singularity which has led its detection.

For a 2D wavelet transform, let the wavelet functions be  $\psi^1(x, y)$  and  $\psi^2(x, y)$ . Let equation (12) and (13),  $\psi_s^1$  and  $\psi_s^2$  be referred to as the detail images, since they contain horizontal and vertical details of the 2D image at scale  $s$ . The transform of  $f(x, y)$  at the scale  $s$  has two components defined by equation (14) and (15) where  $*$  is the convolution operation. The equation presented in (16) where  $\nabla$  is the gradient is straightforward.

$$\psi_s^1(x, y) = \frac{1}{s^2} \psi^1\left(\frac{x}{s}, \frac{y}{s}\right) \quad (12)$$

$$\psi_s^2(x, y) = \frac{1}{s^2} \psi^2\left(\frac{x}{s}, \frac{y}{s}\right) \quad (13)$$

$$W_s^1 f(x, y) = f * \psi_s^1(x, y) \quad (14)$$

$$W_s^2 f(x, y) = f * \psi_s^2(x, y) \quad (15)$$

$$\begin{pmatrix} W_s^1 f(x, y) \\ W_s^2 f(x, y) \end{pmatrix} = s \begin{pmatrix} \frac{\partial}{\partial x} (f * \theta_s)(x, y) \\ \frac{\partial}{\partial y} (f * \theta_s)(x, y) \end{pmatrix} = s \nabla (f * \theta_s)(x, y) \quad (16)$$

The Canny algorithm defines  $(x_0, y_0)$  to belong to an edge if  $\|\nabla f(x_0, y_0)\|$  is locally maximum at  $(x_0, y_0)$  in the direction of  $\nabla f(x_0, y_0)$ . The modulus of the gradient vector  $\nabla(f * \theta_s)(x, y)$  is proportional to the wavelet transform modulus. Edges are often interpreted as one class of singularities, and thus are related to the local maxima of the wavelet transform modulus, defined as the local maxima of the gradient. The main stages of the 2D MMWT are the following [52]:

Stage 1: the local maxima belong to curves in the  $(x, y)$  plane which are the edges of the image along each direction. Hence, edge points can be located from the two components, (14) and (15), of the wavelet transform. The edge information of the image is given by the local extrema or the modulus maxima of the detail images.

Stage 2: the calculation of MMWT is depicted in the search of local maxima using the Canny edge detector. For each scale of the wavelet representation and for each pixel in the image,

we check whether this pixel is a local modulus maximum along the gradient direction or not.

Stage 3: of the procedure consists in the construction of the Maxima Chain (MMWT Chain). Singularities are tracked and chained to one another by similarity of wavelet modulus and position.

Stage 4: Identification of the local maxima along the MMWT chains (MMMWT).

Stage 5: The MMMWT are disposed along connected curves across the scales (maxima lines) forming a WT skeleton: i) If the value of wavelet power is similar to the wavelet power of the smaller scale, ii) and if its position is close to the position of the smaller scale.

The computation of the partition function is defined directly from the MMMWT that belongs to the referred WT skeleton. The calculation of  $\alpha$  and  $f(\alpha)$  is now possible as suggested in [55].

### 3) 2D Wavelet Leaders Multifractal Formalism

The MMWT approach suffers from high computational costs, complex implementation and still lacks theoretical foundations. Recently, a new multifractal formalism based on wavelet leaders has been proposed in [41], [42]. It is constructed from the coefficients of an orthonormal Discrete Wavelet Transform (DWT) and hence benefits from low computational costs and a simple implementation. The WLMF is a new formulation in terms of the local suprema of the wavelet coefficients, or the leaders of the signal.

Let  $f(i, j)$  denote the 2D gray level image to be analyzed, and  $d_x^{(m)}(s, i, j)$  the  $L^1$ -normalized 2D DWT wavelet coefficients. Let us introduce a dyadic indexing of squares as

$$\lambda_{s, i, j} = \left\{ \left[ i2^s, (i+1)2^s \right], \left[ j2^s, (j+1)2^s \right] \right\}. \quad (17)$$

We can assume that each wavelet coefficient  $d_x^{(m)}$  is localized on those dyadic intervals. Finally, let the union of nine such adjacent dyadic intervals be

$$3^2 \lambda_{s, i, j} = \bigcup_{m, n \in \{-1, 0, 1\}} \lambda_{s, i+m, j+n}, \quad (18)$$

the finite quantities referred to as wavelet leaders are defined by

$$L_x(s, i, j) = \sup_{l=1, 2, 3, \lambda' \subset 3^2 \lambda_{s, i, j}} \left| d_x^{(m)}(\lambda') \right|, \quad (19)$$

they hence consist of the supremum of wavelet coefficients taken within the spatial neighborhood, and over all finer scales. The WLMF approach is based on structure functions, i.e., spatial averages of (the  $q^{\text{th}}$  order of) the leaders at a given scale  $2^s$  [42]:

$$S(2^s, q) = \frac{1}{n_j} \sum_{i, j} L_x(s, i, j)^q. \quad (20)$$

From (20), the scaling function  $\tau(q)$  is defined by

$$\tau(q) = \liminf_{2^s \rightarrow 0} \frac{\ln S(2^s, q)}{\ln(2^s)}. \quad (21)$$

Then, the multifractal spectrum can be estimated by the aforementioned Legendre transform [51].

To achieve high correlation with microcalcifications the

wavelet decomposition is employed in this study by using the scaling filter Least Asymmetric Daubechies of order 8, as recommended in [30], [56]. It accumulates more energy in those coefficients of the wavelet transform corresponding to details characterized by symmetry and finite length, as microcalcifications [30].

### C. Selection of Findings and False Positive Reduction

#### 1) Adaptive Inverse Multifractal Analysis

In multifractal-based digital image processing, we derive a two-dimensional multifractal transform for bi-directional mapping of pixel values from the input image (original domain) to the corresponding values of  $\alpha$  and  $f(\alpha)$  (transformed domain). By applying such procedure inversely, it is possible to extract details (pixels) belonging to particular image regions by the MF approach [57], [58].

The value  $\alpha$  gives the local information of the pointwise regularity: for a fixed measure (gray level intensity) each image pixel is characterized by its own value of  $\alpha$ . For instance, pixels having  $\alpha \cong 2$  belong to regions where the measure is regular, i.e., where the probability of the gray level intensity to change with scale is small. Points with  $\alpha \neq 2$  denote regions where the non-regular zones exist. The value of  $f(\alpha)$  describes the global information of the ROI regularity.

The decision whether an element is classified as a microcalcification candidate is not made by comparing empirically features like the minimum and a maximum size (in pixels) or a certain compactness varying with the size. Instead, for each element, the scaling proprieties related with the multifractal spectrum derived from MF-DFA, MMWT or WLMF, allow its selection by the adaptive analysis. By appropriate choice of a pair  $\alpha$  and  $f(\alpha)$ , details that represent regions with microcalcifications can be revealed as in Fig. 2.

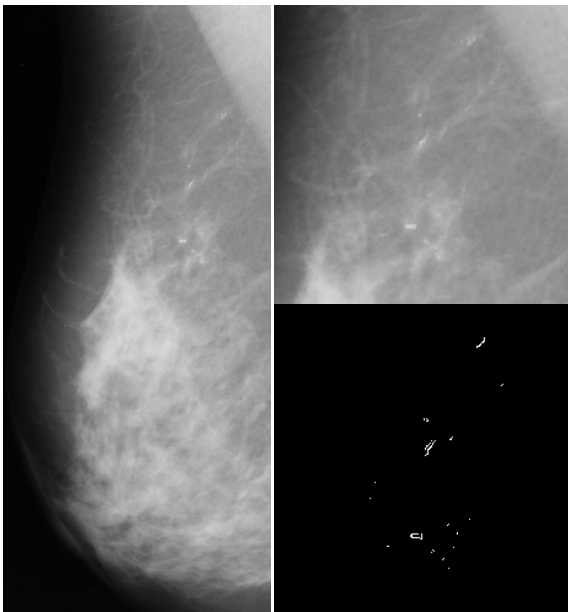


Fig. 2. Fragment of a mammogram and extracted microcalcifications.

#### 2) Clustering

A number of microcalcifications grouped together, defined as at least 3 microcalcifications within a  $1 \text{ cm}^2$  area [59], is termed as a cluster. After individual microcalcifications are extracted, cluster features can be used to group them. Cluster area and number of microcalcifications are the most popular features due to their simplicity and effectiveness. Zhang et al. [60] used morphology features, spatial features and the cluster description features.

The coordinates of the highest gray level pixel in a region of suspicious microcalcifications represent the input pattern in our clustering phase. It is followed the idea of Hojjatoleslami and Kittler [61] as the first step, in order to set the number of initial clusters to feed the main k-means clustering technique performed [62]. A threshold of  $1 \text{ cm}^2$  is used as discontinuity measure to distinguish a new cluster. If a cluster has more than four elements, all the objects are labeled as a cluster of microcalcifications.

#### 3) Self-similarity Analysis

Assessing the level of self-similarity present in the boundary of the relevant elements, detected via adaptive inverse multifractal analysis, is the main goal of the false positive reduction step described here. It comprises a Boundary Self-Similarity Analysis (BSSA) technique where the 2D shape of each element has to be converted to the one-dimensional form.

At the beginning of this phase the findings are presented as marks, a set of pixels corresponding to the selected relevant elements. Usually, some elements are distorted or subject to the effects of noise. A high pass Gaussian filter could be applied before the following phase. However, in the case of microcalcifications we do not want to filter the information more than in the first extraction phase and, since only the boundary matters in this step this has to be evaluated with a tracing algorithm. We perform the Moore-neighbor method to select the outer boundary of any connected component [63].

The BSSA technique requires the element to have a polygonal (closed) shape composed of at least 4 connected pixels. In order to create the boundary profile of the shape of original closed contour  $L$ , the centroid  $C$  of the polygon is calculated, followed by the computation of the distance between each point of the contour and this interior centroid point (see Fig. 3). The function of that distance is the signal used for the self-similarity analysis by Hurst estimation [64].

Calcifications that are irregular in shape, size or resemble small fragments of a broken glass, fall closer to the malignant category. Therefore, their boundary profile is not expected to be self-similar. A self-similar one belongs to connected elements with Hurst  $\cong 0.5$ , and it is not known to what extent this type of boundary should be associated with benign cases. To reduce the false positives we aim to eliminate linear structures (bigger than  $0.8 \text{ mm}$ ) with  $0.9 < \text{Hurst} < 1$ , that could represent vascular structures or other normal linear structures. A likelihood map of these potential normal structures is created and the corresponded pixels are subtracted from the preceding extraction (multifractal) phase.

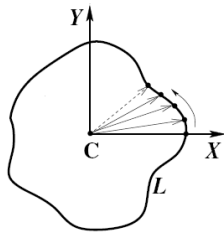


Fig. 3. Radius vectors with centroid in C to create the boundary profile of a microcalcification with closed contour L.

### III. RESULTS

#### A. Experiments

Public datasets are desirable to make a fair comparison between methods since the performance of a CAde can vary dramatically as it depends on factors such as the subtlety of cases and number. For that reason, the proposed methods of extraction have been applied to regions of interest in mammograms from the Mammographic Image Analysis Society (MiniMIAS) [65] and from the Digital Database for Screening Mammography (DDSM) [66]. Lesions containing clustered microcalcifications can appear in a mammogram together with other mammographic findings. Therefore, these datasets contain other abnormalities in addition to malignant clustered microcalcifications.

From the DDSM, the largest publicly available database of digitized mammograms, each abnormality was outlined by a radiologist and this was considered as the “ground truth” for the detection of spatial location of lesions. A set of 100 images from the DDSM database was used to test the detection algorithm. This set consists of 50 images of clustered microcalcification and 50 normal images. As for the MiniMIAS, 190 clinical cases were analyzed which 28 of them had microcalcifications. The location coordinates and radius of the abnormalities are outlined with respect to clusters rather than individual calcifications.

The 8-bit converted gray images were split and multiple ROIs of each mammogram (specified according to Section II.A.) were analyzed. For all the multifractal methods applied, the multi-scale analysis was performed varying the scale between 8 and 64 pixels, for each 256 x 256 ROI at different pixel sample rate ( $\mu\text{m}/\text{pixel}$ ) depending on the database scanner. Some of the detection results obtained and the spectral analysis are illustrated on the following figures.

Fig. 4 shows the multifractal spectrums estimated by the 2D MF-DFA with a cropped ROI size of 128 x 128 (blue squares) and 256 x 256 (black circles) containing microcalcifications, of a region from the mammogram mdb219 belonging to MiniMIAS, centered at the same coordinate. The spectrums denote the presence of multifractality as both plots are not limited to  $\alpha \cong 2$  scope. It can be seen that the curves are convex, monotonous decreasing and similar at different scales. Microcalcifications are small light local abnormalities. From the multifractal standpoint they are characterized by both high  $\alpha$  and low  $f(\alpha)$  values, because they represent sharp local

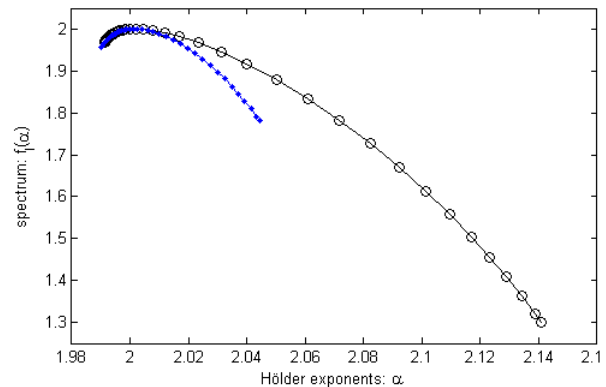


Fig. 4. Two cropped ROI sizes from the same MiniMIAS mammogram, 128 x 128 (blue squares) and 256 x 256 (black circles), and their multifractal spectrums  $f(\alpha)$  via Legendre transform with 2D MF-DFA.

changes of contrast and rare events in global sense. This property was commonly verified in the microcalcifications detected, independently of the multifractal method employed, in particular with 256 x 256 sized ROIs, which was therefore the default ROI size chosen. In general the microcalcifications appeared: ultra small and bright; with smooth surface (small variation of gray level inside) not belonging to surroundings (big variation of gray level from outside) with sharp changes in gray level just around the edge.

The mammograms mdb209, mdb219, mdb223 and mdb249 in Fig. 5(a) contain cases of subtle microcalcifications. The tissue is either fatty-glandular (first two) or dense-glandular (last two). A multifractal spectrum was estimated in ROIs of these mammograms by the 2D MF-DFA. Fig. 5(b) illustrates the correspondent Legendre spectrums. All the plots denote the presence of multifractality but the ones related with regions of denser mammograms present lower  $\alpha$  for the same  $f(\alpha)$ . This is understandable as it represents a weaker change in local contrast compared to fatty-glandular cases. An inverse multifractal analysis was adapted for  $f(\alpha) < 1.7$ , with  $\alpha < 2$  or  $\alpha > 2$ . This threshold value for  $f(\alpha)$  together with  $\alpha > 2$  was empirically found to be a good starting point for the disclosure of microcalcifications with no significant noise visible, as it is represented in Fig. 5(a), with respect to cases of miniMIAS database and using 2D MF-DFA. Moreover, this setting was derived from samples of both databases and also using 2D MMWT and 2D WLMF.

#### B. Detection Performance

The performance of the detection method was evaluated by Free-Response Receiver Operating Characteristic (FROC) analysis. For each dataset, the 2D MF-DFA was compared with the 2D MMWT and 2D WLMF. Different levels of thresholding were applied to  $f(\alpha)$  with the condition of  $\alpha > 2$ :  $f(\alpha) < 1.7$ ;  $f(\alpha) < 1.6$ ;  $f(\alpha) < 1.5$ ;  $f(\alpha) < 1.4$ . At each level a number of pixels which had been considered suspicious were extracted. By varying the threshold level, the sensitivity of the detection method is changed. If the output of the extraction was located within the annotation of the radiologist, it was

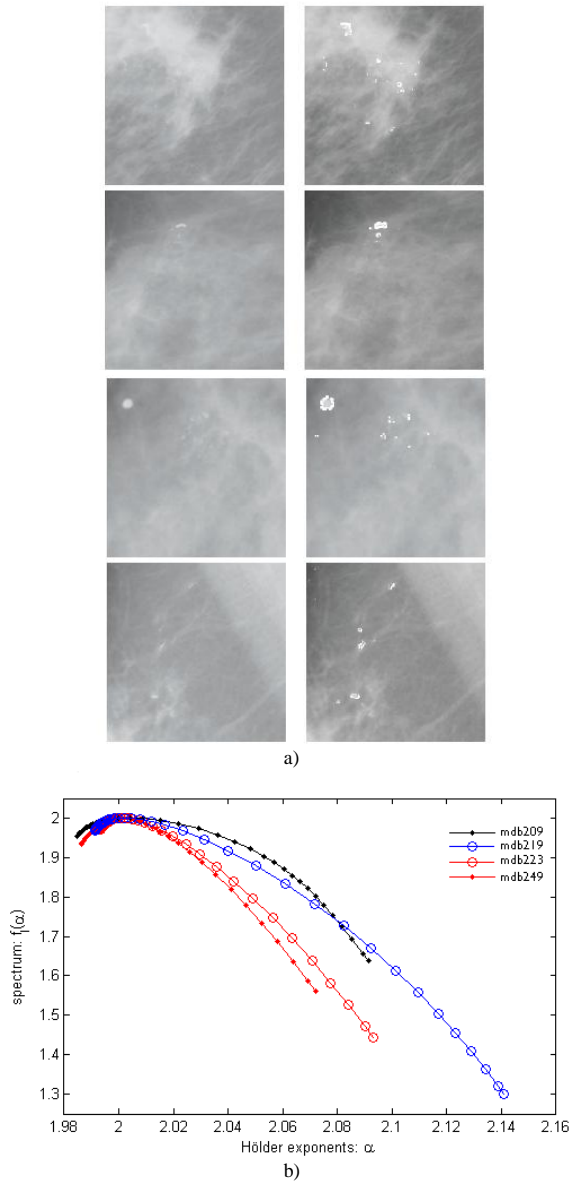


Fig. 5. (a) Detection of microcalcifications in mammogram ROIs. From top to bottom: mdb209, mdb219, mdb223 and mdb249. (b) Legendre spectrums with 2D MF-DFA.

counted as a true-positive spot on a confusion matrix. Table I presents this assessment of sensitivity of the CADE.

FROC curves are shown in Fig. 6. The 2D MF-DFA outperforms 2D MMWT, and 2D WLMF with both datasets. At the same  $f(\alpha)$  threshold level, the FPI differs depending on the multifractal approach. The best performance is reached with DDSM having bigger area under the curve. This can be due to the combination of a higher resolution on the images from DDSM ( $43.5\mu\text{m}/\text{pixel}$  or  $584\text{dpi}$ ) in comparison to MiniMIAS ( $200\mu\text{m}/\text{pixel}$  or  $127\text{dpi}$ ), and the usage of a method less sensitive to spatial resolution that reduces spurious detection at the same resolution level. If we analyze the result at 0.5 FPI, the best option reaches 85% of sensitivity

TABLE I  
ASSESSMENT OF SENSITIVITY

Case #	Tissue	Annotation	Area (pixel <sup>2</sup> )	Detection	Match	Class
1	Fatty	CALC	3141	true	true	TP
2	Dense	CALC	7238	true	true	TP
3	Dense	CALC	12867	true	true	TP
4	Dense	NORM		true	false	FP
5	Fatty	NORM		false	true	TN
6	Fatty	CALC	1661	true	true	TP
...	...	...	...	...	...	...
290	Dense	CALC	2463	false	false	FN

Assessment of sensitivity through the match between the detection and the annotation on the dataset. The classification of the match is presented for different densities of background tissue.

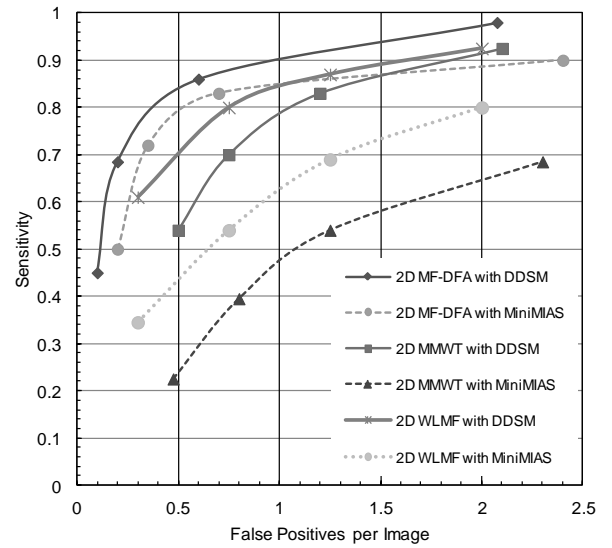


Fig. 6. FROC curves showing detection performance using the three multifractal methods on different datasets. 2D MF-DFA with DDSM has the best performance with bigger area under the curve. It points 85% of sensitivity for the detection of microcalcifications at 0.5 False Positives per Image.

with MF-DFA detecting microcalcifications. It is observed that the two wavelet-based methods are strongly dependent on the higher-resolution dataset to gain sensitivity.

It is also worth of notice that for the multifractal spectrum estimation several ranges of  $q$  were tested (results no shown), for the problem in study. An optimal microcalcification detection performance was reached at  $-1 < q < 1$  by the wavelet-based methods, and at  $-3 < q < 3$  by the 2D MF-DFA.

### C. Computational Efficiency

The computational efficiency of the three multifractal methods is presented in Fig. 7. The impact on CPU time in seconds (s) was measured on a 2.53GHz Intel® Core™ i5 M540 workstation. This performance was estimated at four FPI rates for the computationally more demanding DDSM, which is also the dataset yielding better FROC results.

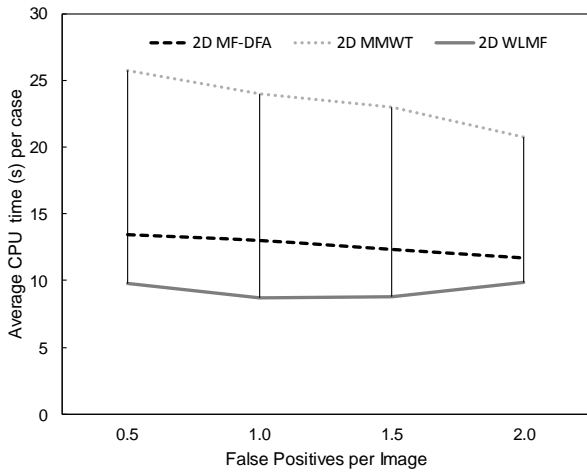


Fig. 7. Comparison of computational efficiency by CPU time in seconds (s) averaged per case in DDSM dataset, using the three multifractal methods.

MMWT are the slowest performer, getting faster for higher FPI. WLMF is more CPU efficient than MF-DFA with acceptable detection performance at FPI 1.5 (89%, see Fig. 6).

#### IV. DISCUSSION

Although the detection and diagnosis of microcalcifications are two fields that have improved significantly in recent years, there is still no stout differentiation between benign and malignant clusters of microcalcifications. However, each incremental improvement in the detection rate has a potentially significant impact on breast cancer screening.

Some of the factors that drastically influence the feature extraction results are: i) the variability of the anatomy of the breast - every mammogram has different properties related to different tissue types and correspondingly variable brightness in the mammographic appearance; ii) the imaging conditions - shot noise, quantum mottle, patient movement, low contrast in mammograms due to low X-ray dosage and glare; iii) faint microcalcifications are lost in a dense background; iv) the superposition of certain breast structures [67].

The role of fractal and multifractal analysis in signal processing, compared to classic signal processing, lies in the way of how the non-regularities are assumed [68]. The classic approach usually deals with a smoothed version of the image in order to suppress the noise and extract irregularities, such as edges. The multifractal-based image analysis tends to extract relevant information directly from the singularities. This approach exploits both local regularity of a given measure, described by the pointwise Hölder exponent  $\alpha$ , and the global distribution of the regularity in a whole scene, described by  $f(\alpha)$ . Herein, it was confirmed that ROIs selected in mammograms have multiple degrees of scaling by the observation of a multifractal spectrum.

Within a set of 290 clinical images from two public databases, the employed methods were able to successfully distinguished microcalcifications from the background. On the other hand, the commercial CADe system in [69] approved by the Food and Drug Administration was reported to have

98.5% of sensitivity at 0.5 FPI, whereas our best solution points to 85%; however this is with a non-public database. No results are known for public and comparable databases with the use of its algorithms and the results may vary considerably on different datasets. For example, clinical studies to evaluate the performance of commercial CADe systems have reported sensitivities ranging from 67% to 89% with the FPI ranging from 0.40 to 0.74 FPI [70], [71]. In the present study the results vary considerably between the two public datasets. This can be due to the spatial resolution of the digitized mammograms, although 2D MF-DFA was a solid performer for both datasets. The sensitivity reach 97% at 2 FPI mark for 2D MF-DFA with DDSM. Our experiments were parameterized independently from a database and we state that the results obtained here are above average literature [21], [23]–[26], specially using multiple databases [21], [24].

The proposed model is simultaneously highly robust and sensitive to important properties of microcalcifications, and can be used to detect them on the early stage of a possible breast cancer. The clear distinction between regions of normal tissue (monofractal) and regions with abnormalities (multifractal) mostly prevails for the mammograms in the analyzed dataset. If we focus on extraction of abnormalities, the main advantage of the multifractal approaches is resistance against noise, which is an important property for the particular microcalcification detection problem. Another big advantage is the optimization of performance compared with equally capable systems that face this type of breast cancer feature detection problem. This can happen due to the ability of removing the redundant features depending on the multifractal-based method: MMWT is able to decrease the redundancy of the wavelet transform by solely keeping the positions and coefficients of the continuous wavelet transform at the local maxima. The modulus maxima lines can characterize a detected element via its regularity, i.e. estimate the order of singularity that has led to its detection; WLMF only considers the coefficient leaders of the discrete wavelet transform; MF-DFA evaluates the scaling of the  $q^{\text{th}}$ -order moments by fluctuations in data segments with trends simply estimated by fitting.

It was verified that using any of the three multifractal-based methods, the image can be described from the local (pixel-based) and global (region-based) point of view, convening on higher detection quality. MF-DFA outperforms MMWT and is simpler to implement. However, when time in the clinical workflow is the priority, WLMF is an interesting option for screening with acceptable performance.

By the type of abnormalities disclosed on the images and the performance of the proposed microcalcification detection model, BSSA was able to minimize the FPI rates. One possible limitation of BSSA is not working for some unconventional shaped objects due to the radial function, which does not happen to be a problem in case of microcalcifications. Also note that calcifications arrayed in a line suggest deposits in a duct, and are usually no bigger than 0.8 mm, individually. This condition was included in BSSA.

The self-similarity degree featured in the boundaries of the

selected relevant elements may be an indicator of cancer, as it should be confirmed by a classification system. The Hurst parameter should be investigated more deeply in the future, and its role placed in the scope of computer-aided diagnosis [72]. Results not shown point to the tendency that averaged over all the malignant lesions and averaged over all the benign lesions, Hurst is higher for cancer. This has to be followed by extensive clinical validation to draw firm conclusions.

The pectoral muscle is a mass of tissue on which the breast rests. It usually appears slightly brighter compared to the rest of the breast tissue in mediolateral oblique view mammograms. This may cause biased detection of findings, particularly with masses, and it is often removed during mammogram pre-processing [73]. Although in our proposed detection model the pectoral muscle was retained, since no microcalcifications were detected in this region using the multifractal methods. It is arguable that skipping this step may affect computational time for feature extraction. However, top methods for pectoral muscle identification also introduce additional time complexity in the pre-processing step [74], [75]. Further investigations on the shortcomings and benefits of pectoral muscle removal should be done in the future for microcalcification detection.

The images from DDSM and MiniMIAS were digitized by scanners from screen-film mammograms. It might be a significant complementary work if the proposed algorithm could be tested on databases of full-field digital mammograms, with reported benefits on diagnostic accuracy in women less than 50 years old [76].

## V. CONCLUSION

Experience helps the radiologist to know what and where to look for when reading a mammogram: opacity near the mammary duct, the tissue surrounding the opacity or nipple alterations in the surrounding area. However, with regard to microcalcifications, it is very difficult to compare the distribution of texture, their value, and the possible order or disorder between regions of the same mammogram.

We proposed a new model for the detection of microcalcification clusters in mammography using the multifractal formalism. It is reviewed and investigated the 2D extension of three multifractal methods to address the problem of texture characterization of microcalcifications in relation to their surroundings. In addition, it was also proposed a technique to reduce the false positives by using clustering and self-similarity analysis to identify and create a likelihood map of potential structures to remove.

The results from this study suggest that the multifractal characterization of features as proposed here can be useful for a computer-aided breast cancer detection system. The procedure of inspecting singularities and their fluctuations at multiple resolutions revealed that multifractal information is of very importance. The inclusion of a classifier should play a role for disambiguation of results and stronger false positive reduction. On the other side, false negative marks of microcalcifications occur mainly in mammograms with low image contrast and can easily be recognized as non-cancer in a

final decision process focused on the cluster shape, density and size.

The high sensitivity of the multifractal-based detection of clustered microcalcifications can lead to a gain in confidence by the radiologist to rely on CADe to find these abnormalities and, therefore, to reduce the need of searching the image with a magnifying glass (or electronic zoom). This would allow radiologists just to check the computer-detected clusters of microcalcifications and then to look for mass lesions when reading the mammograms, reducing the fatigue and increasing the productivity of the experts.

## REFERENCES

- [1] L. Tabar, M. Yen, B. Vitak, H. Chen, R. Smith, and S. Duffy, "Mammography service screening and mortality in breast cancer patients: 20-year follow-up before and after introduction of screening," *The Lancet*, vol. 361, no. 9367, pp. 1405–1410, 2003.
- [2] A. M. J. Bluekens, R. Holland, N. Karssemeijer, M. J. M. Broeders, and G. J. den Heeten, "Comparison of Digital Screening Mammography and Screen-Film Mammography in the Early Detection of Clinically Relevant Cancers: A Multicenter Study," *Radiology*, vol. 265, no. 3, pp. 707–714, Jan. 2012.
- [3] R. M. Nishikawa, "Current status and future directions of computer-aided diagnosis in mammography," *Computerized Medical Imaging and Graphics*, vol. 31, no. 4–5, pp. 224–235, 2007.
- [4] F. van Gelderen, *Understanding X-Rays: A Synopsis of Radiology*. Springer, 2004.
- [5] E. Pisano, M. Yaffe, B. Hemminger, R. Hendrick, L. Niklason, A. Maidment, C. Kimme-Smith, S. Feig, E. Sickles, and M. Braeuning, "Current status of full-field digital mammography," *Academic Radiology*, vol. 7, no. 4, pp. 266–280, 2000.
- [6] S. R. Amendolia, M. G. Bisogni, U. Bottigli, A. Ceccopieri, P. Delogu, M. E. Fantacci, A. Marchi, V. M. Marzulli, R. Palmiero, and S. Stumbo, "The CALMA project: a CAD tool in breast radiography," *Nuclear Inst. and Methods in Physics Research, A*, vol. 460, no. 1, pp. 107–112, 2001.
- [7] C. Boggis and S. Astley, "Computer-assisted mammographic imaging," *Breast Cancer Res*, vol. 2, no. 6, p. 392, 2000.
- [8] E. D. Pisano, R. E. Hendrick, M. J. Yaffe, J. K. Baum, S. Acharyya, J. B. Cormack, L. A. Hanna, E. F. Conant, L. L. Fajardo, L. W. Bassett, and others, "Diagnostic accuracy of digital versus film mammography: exploratory analysis of selected population subgroups in DMIST," *Radiology*, vol. 246, no. 2, p. 376, 2008.
- [9] L. J. Warren Burhenne, S. A. Wood, C. J. D'Orsi, S. A. Feig, D. B. Kopans, K. F. O'Shaughnessy, E. A. Sickles, L. Tabar, C. J. Vyborny, and R. A. Castellino, "Potential contribution of computer-aided detection to the sensitivity of screening mammography," *Radiology*, vol. 215, no. 2, pp. 554–562, May 2000.
- [10] Jinshan Tang, R. M. Rangayyan, Jun Xu, I. El Naqa, and Yongyi Yang, "Computer-aided detection and diagnosis of breast cancer with mammography: recent advances," *IEEE Transactions on Information Technology in Biomedicine*, vol. 13, no. 2, pp. 236–251, 2009.
- [11] R. Nagel, R. Nishikawa, J. Papaioannou, and K. Doi, "Analysis of methods for reducing false positives in the automated detection of clustered microcalcifications in mammograms," *Medical Physics*, vol. 25, p. 1502, 1998.
- [12] S.-N. Yu, K.-Y. Li, and Y.-K. Huang, "Detection of microcalcifications in digital mammograms using wavelet filter and Markov random field model," *Computerized Medical Imaging and Graphics*, vol. 30, no. 3, pp. 163–173, Apr. 2006.
- [13] M. Jirari, "Computer Aided System For Detecting Masses In Mammograms," Ph.D. thesis, Kent State University, 2008.
- [14] S. Yu and L. Guan, "A CAD system for the automatic detection of clustered microcalcifications in digitized mammogram films," *IEEE Trans. Med. Imaging*, vol. 19, no. 2, pp. 115–126, Feb. 2000.
- [15] A. Papadopoulos, D. Fotiadis, and L. Costaridou, "Improvement of microcalcification cluster detection in mammography utilizing image enhancement techniques," *Computers in biology and medicine*, vol. 38, no. 10, pp. 1045–1055, 2008.

- [16] H. Cheng, X. Cai, X. Chen, L. Hu, and X. Lou, "Computer-aided detection and classification of microcalcifications in mammograms: a survey," *Pattern Recognition*, vol. 36, no. 12, pp. 2967–2991, 2003.
- [17] G. te Brake, N. Karssemeijer, and J. Hendriks, "An automatic method to discriminate malignant masses from normal tissue in digital mammograms," *Physics in Medicine and Biology*, vol. 45, pp. 2843–2857, 2000.
- [18] G. Tourassi, R. Vargas-Voracek, D. Catarious Jr, and C. Floyd Jr, "Computer-assisted detection of mammographic masses: A template matching scheme based on mutual information," *Medical Physics*, vol. 30, p. 2123, 2003.
- [19] M. A. Duarte, A. V. Alvarenga, C. M. Azevedo, A. F. C. Infantosi, and W. C. A. Pereira, "Automatic microcalcifications segmentation procedure based on Otsu's method and morphological filters," in *Health Care Exchanges (PAHCE), 2011 Pan American*, 2011, pp. 102–106.
- [20] M. Muštra, M. Grgić, and K. Delac, "Enhancement of microcalcifications in digital mammograms," in *2012 19th International Conference on Systems, Signals and Image Processing (IWSSIP)*, 2012, pp. 248–251.
- [21] B. Thangaraju, I. Vennila, and G. Chinnaamy, "Detection of microcalcification clusters using Hessian matrix and foveal segmentation method on multiscale analysis in digital mammograms," *J Digit Imaging*, vol. 25, no. 5, pp. 607–619, Oct. 2012.
- [22] N. Karssemeijer, "Recognition of clustered microcalcifications using a random field model," in *Proceedings of SPIE*, 1905, vol. 776, p. 1993.
- [23] J. Ren, "ANN vs. SVM: Which one performs better in classification of MCCs in mammogram imaging," *Knowledge-Based Systems*, vol. 26, pp. 144–153, Feb. 2012.
- [24] A. Oliver, A. Torrent, X. Lladó, M. Tortajada, L. Tortajada, M. Sentís, J. Freixenet, and R. Zwigelaar, "Automatic microcalcification and cluster detection for digital and digitised mammograms," *Knowledge-Based Systems*, vol. 28, pp. 68–75, Apr. 2012.
- [25] E. Malar, A. Kandaswamy, D. Chakravarthy, and A. Giri Dharan, "A novel approach for detection and classification of mammographic microcalcifications using wavelet analysis and extreme learning machine," *Computers in Biology and Medicine*, vol. 42, no. 9, pp. 898–905, Sep. 2012.
- [26] J. Dheeba and S. T. Selvi, "A Swarm Optimized Neural Network System for Classification of Microcalcification in Mammograms," *J Med Syst*, vol. 36, no. 5, pp. 3051–3061, Oct. 2012.
- [27] M. Sampat, M. Markey, and A. Bovik, "Computer-Aided Detection and Diagnosis in Mammography," in *Handbook of image and video processing*, vol. 10, Elsevier Academic Press, 2005, pp. 1195–1217.
- [28] R. N. Strickland and Hee Il Hahn, "Wavelet transforms for detecting microcalcifications in mammograms," *IEEE Trans. Med. Imaging*, vol. 15, no. 2, pp. 218–229, Apr. 1996.
- [29] T. Wang and N. Karayiannis, "Detection of microcalcifications in digital mammograms using wavelets," *IEEE Trans. Med. Imaging*, vol. 17, no. 4, pp. 498–509, 1998.
- [30] H. Moradmand, S. Setayeshi, A. R. Karimian, M. Sirous, and M. E. Akbari, "Comparing the Performance of Image Enhancement Methods to Detect Microcalcification Clusters in Digital Mammography," *Iranian Journal of Cancer Prevention*, vol. 5, no. 2, pp. 61–68, Apr. 2012.
- [31] P. Ramírez-Cobo and B. Vidakovic, "A 2D wavelet-based multiscale approach with applications to the analysis of digital mammograms," *Computational Statistics & Data Analysis*, vol. 58, pp. 71–81, Feb. 2013.
- [32] H. Li, K. Liu, and S. Lo, "Fractal modeling and segmentation for the enhancement of microcalcifications in digital mammograms," *IEEE Trans. Med. Imaging*, vol. 16, no. 6, pp. 785–798, 1997.
- [33] A. I. Penn, L. Bolinger, M. D. Schnall, and M. H. Loew, "Discrimination of MR images of breast masses with fractal-interpolation function models," *Academic Radiology*, vol. 6, no. 3, pp. 156–163, Mar. 1999.
- [34] E. Nilsson, "Multifractal-based Image Analysis with applications in Medical Imaging," M.Sc. dissertation, Umeå University, 2007.
- [35] G. Derado, K. Lee, O. Nicolis, F. Bowman, M. Newell, F. Ruggeri, and B. Vidakovic, "Wavelet-based 3-D Multifractal Spectrum with Applications in Breast MRI Images," in *Bioinformatics Research and Applications*, vol. 4983, Springer Berlin / Heidelberg, 2008, pp. 281–292.
- [36] F. Soares, F. Janela, M. Pereira, J. Seabra, and M. Freire, "3D Lacunarity in Multifractal Analysis of Breast Tumor Lesions in Dynamic Contrast-Enhanced Magnetic Resonance Imaging," *IEEE Transactions on Image Processing*, vol. Early Access Online, 2013.
- [37] B. Pesquet-Popescu and J. L. Véhel, "Stochastic fractal models for image processing," *IEEE Signal Processing Magazine*, vol. 19, no. 5, pp. 48–62, 2002.
- [38] P. Kestener, J. M. Lina, P. Saint-Jean, and A. Arneodo, "Wavelet-based multifractal formalism to assist in diagnosis in digitized mammograms," *Image Anal Stereol*, vol. 20, no. 3, pp. 169–174, 2001.
- [39] J. W. Kantelhardt, S. A. Zschiegner, E. Koscielny-Bunde, S. Havlin, A. Bunde, and H. E. Stanley, "Multifractal detrended fluctuation analysis of nonstationary time series," *Physica A: Statistical Mechanics and its Applications*, vol. 316, no. 1–4, pp. 87–114, Dec. 2002.
- [40] P. Oświecimka, J. Kwapien, and S. Drożdż, "Wavelet versus detrended fluctuation analysis of multifractal structures," *Physical Review E*, vol. 74, no. 1, Jul. 2006.
- [41] S. Jaffard, B. Lashermes, and P. Abry, "Wavelet Leaders in Multifractal Analysis," in *Wavelet Analysis and Applications*, T. Qian, M. I. Vai, and Y. Xu, Eds. Basel: Birkhäuser Basel, 2007, pp. 201–246.
- [42] B. Lashermes, S. Jaffard, and P. Abry, "Wavelet leader based multifractal analysis," in *Proceedings of IEEE International Conference on Acoustics, Speech, and Signal Processing*, 2005, vol. 4, pp. iv–161.
- [43] E. Serrano and A. Figliola, "Wavelet Leaders: A new method to estimate the multifractal singularity spectra," *Physica A: Statistical Mechanics and its Applications*, vol. 388, no. 14, pp. 2793–2805, 2009.
- [44] F. Soares, M. M. Freire, M. Pereira, F. Janela, and J. Seabra, "Towards the detection of microcalcifications on mammograms through Multifractal Detrended Fluctuation Analysis," in *Proceedings of the IEEE Pacific Rim Conference on Communications, Computers and Signal Processing*, 2009, pp. 677–681.
- [45] K. Wei, W. Guangzhi, and D. Hui, "Segmentation of the breast region in mammograms using watershed transformation," in *Proceedings of 27th Annual International Conference of the Engineering in Medicine and Biology Society*, 2005, pp. 6500–6503.
- [46] H. Neiber, T. Müller, and R. Stotzka, "Local contrast enhancement for the detection of microcalcifications," in *Proceedings for the 5th International Workshop on Digital Mammography*, 2000, pp. 598–604.
- [47] J. Jan, *Medical image processing, reconstruction, and restoration: concepts and methods*. CRC, 2006.
- [48] A. Méndez, P. Tahoces, M. Lado, M. Souto, J. Correa, and J. Vidal, "Automatic detection of breast border and nipple in digital mammograms," *Computer Methods and Programs in Biomedicine*, vol. 49, no. 3, pp. 253–262, 1996.
- [49] I. Reljin and B. Reljin, "Fractal geometry and multifractals in analyzing and processing medical data and images," *Arch Oncol*, vol. 10, no. 4, pp. 283–293, 2002.
- [50] G.-F. Gu and W.-X. Zhou, "Detrended fluctuation analysis for fractals and multifractals in higher dimensions," *Physical Review E*, vol. 74, no. 6, p. 061104, Dec. 2006.
- [51] H.-O. Peitgen, H. Jürgens, and D. Saupe, *Chaos and Fractals: New Frontiers of Science*. Springer, 1993.
- [52] A. Arneodo, N. Decoster, and S. Roux, "A wavelet-based method for multifractal image analysis. I. Methodology and test applications on isotropic and anisotropic random rough surfaces," *The European Physical Journal B-Condensed Matter and Complex Systems*, vol. 15, no. 3, pp. 567–600, 2000.
- [53] V. Budaev, S. Takamura, N. Ohno, and S. Masuzaki, "Superdiffusion and multifractal statistics of edge plasma turbulence in fusion devices," *Nucl. Fusion*, vol. 46, no. 4, pp. S181–S191, Apr. 2006.
- [54] P. Jock, "Application of the Wavelet Transform Modulus Maxima method to T-wave detection in cardiac signals," M.Sc. dissertation, Maastricht University, 2004.
- [55] R. McAteer, C. Young, J. Ireland, and P. Gallagher, "Bursty X-Ray Flare Emission," *The Astrophysical Journal*, vol. 662, pp. 691–700, 2007.
- [56] E. Sakka, A. Prentza, I. Lamprinos, and D. Koutsouris, "Microcalcification detection using multiresolution analysis based on wavelet transform," in *Proceedings of the International IEEE EMBS Special Topic Conference on Information Technology in Biomedicine*, 2006, p. 126.
- [57] J. L. Véhel, "Introduction to the multifractal analysis of images," *NATO ASI series. Series F: computer and system sciences*, pp. 299–341, 1998.
- [58] J. L. Véhel and J. P. Berroir, "Image analysis through multifractal description," in *Proceedings of the Second IFIP Working Conference on Fractals in the Natural and Applied Sciences*, 1993, pp. 261–274.
- [59] D. Kopans, "Discriminating analysis uncovers breast lesions," *Diagnostic imaging*, vol. 13, no. 9, p. 94, 1991.

- [60] L. Zhang, W. Qian, R. Sankar, D. Song, and R. Clark, "A new false positive reduction method for MCCs detection in digital mammography," in *Proceedings of IEEE International Conference on Acoustics, Speech, and Signal Processing*, 2001, vol. 2.
- [61] S. A. Hojjatoleslami and J. Kittler, "Detection of clusters of microcalcification using a k-nearest neighbour classifier," in *Proceedings of IEE Colloquium on Digital Mammography*, 1996, pp. 10/1–10/6.
- [62] T. Bhangale, U. Desai, and U. Sharma, "An unsupervised scheme for detection of microcalcifications on mammograms," in *Proceedings of the International Conference on Image Processing*, 2000.
- [63] P. R. Mahapatra and V. V. Makkapati, "Ultra high compression for weather radar reflectivity data storage and transmission," in *Proceedings of the 21st International Conference on Interactive Information Processing Systems (IIPS) for Meteorology, Oceanography, and Hydrology*, 2005.
- [64] C.-K. Peng, S. V. Buldyrev, S. Havlin, M. Simons, H. E. Stanley, and A. L. Goldberger, "Mosaic organization of DNA nucleotides," *Physical Review E*, vol. 49, no. 2, p. 1685, Feb. 1994.
- [65] J. Suckling, J. Parker, D. R. Dance, S. Astley, I. Hutt, C. Boggis, I. Ricketts, E. Stamatakis, N. Cerneaz, S. L. Kok, and others, "The mammographic image analysis society digital mammogram database," in *Proceedings of the 2nd International Workshop on Digital Mammography*, 1994, pp. 375–378.
- [66] M. Heath, K. Bowyer, D. Kopans, R. Moore, and P. Kegelmeyer, "The digital database for screening mammography," in *Proceedings of the 5th International Workshop on Digital Mammography*, 2000, pp. 212–218.
- [67] M. Linguraru, "Feature detection in mammographic image analysis," Ph.D. thesis, University of Oxford, 2002.
- [68] A. Dathe, A. M. Tarquis, and E. Perrier, "Multifractal analysis of the pore- and solid-phases in binary two-dimensional images of natural porous structures," *Geoderma*, vol. 134, no. 3–4, pp. 318–326, Oct. 2006.
- [69] J. Roehrig, T. Doi, A. Hasegawa, B. Hunt, J. Marshall, H. Romsdahl, A. Schneider, R. Sharbaugh, and W. Zhang, "Clinical results with R2 imagechecker system," *Computational Imaging and Vision*, vol. 13, pp. 395–400, 1998.
- [70] M. Yaffe, "Screening mammography-detected cancers: sensitivity of a computer-aided detection system applied to full-field digital mammograms," *Breast Diseases: A Year Book Quarterly*, vol. 19, no. 2, pp. 142–143, 2008.
- [71] M. Bazzocchi, F. Mazzarella, C. Del Frate, F. Girometti, and C. Zuiani, "CAD systems for mammography: a real opportunity? A review of the literature," *La Radiologia Medica*, vol. 112, no. 3, pp. 329–353, 2007.
- [72] K. Ganesan, U. R. Acharya, C. K. Chua, L. C. Min, K. T. Abraham, and K. Ng, "Computer-Aided Breast Cancer Detection Using Mammograms: A Review," *Biomedical Engineering, IEEE Reviews in*, vol. 6, pp. 77–98, 2013.
- [73] K. Ganesan, U. R. Acharya, K. C. Chua, L. C. Min, and K. T. Abraham, "Pectoral muscle segmentation: A review," *Computer Methods and Programs in Biomedicine*, vol. 110, no. 1, pp. 48–57, Apr. 2013.
- [74] R. J. Ferrari, R. M. Rangayyan, J. E. L. Desautels, R. A. Borges, and A. F. Frere, "Automatic identification of the pectoral muscle in mammograms," *IEEE Transactions on Medical Imaging*, vol. 23, no. 2, pp. 232–245, 2004.
- [75] K. S. Camilus, V. K. Govindan, and P. S. Sathidevi, "Pectoral muscle identification in mammograms," *Journal of Applied Clinical Medical Physics*, vol. 12, no. 3, Mar. 2011.
- [76] F. H. Souza, E. M. Wendland, M. I. Rosa, and C. A. Polanczyk, "Is full-field digital mammography more accurate than screen-film mammography in overall population screening? A systematic review and meta-analysis," *The Breast*, vol. 22, no. 3, pp. 217–224, Jun. 2013.



## Chapter 4

# Classification of Breast Masses on Contrast-Enhanced Magnetic Resonance Images Through Log Detrended Fluctuation Cumulant-Based Multifractal Analysis

This chapter consists of the following article:

Classification of Breast Masses on Contrast-Enhanced Magnetic Resonance Images Through Log Detrended Fluctuation Cumulant-Based Multifractal Analysis

Filipe Soares, Filipe Janela, Manuela Pereira, João Seabra and Mário M. Freire

*IEEE Systems Journal*, accepted for publication, 2013.

DOI: 10.1109/JSYST.2013.2284101

According to 2012 Journal Citation Reports published by Thomson Reuters in 2013, this journal scored ISI journal performance metrics as follows:

ISI Impact Factor (2012): 1.270

Article Influence Score (2012): 0.445

Journal Ranking (2012): 44/132 (Computer Science, Information Systems), Quartile: Q2

Journal Ranking (2012): 104/243 (Engineering, Electrical & Electronic), Quartile: Q2

Journal Ranking (2012): 32/79 (Operations Research & Management Science), Quartile: Q2

Journal Ranking (2012): 27/78 (Telecommunications), Quartile: Q2



# Classification of Breast Masses on Contrast-Enhanced Magnetic Resonance Images Through Log Detrended Fluctuation Cumulant-Based Multifractal Analysis

Filipe Soares, Filipe Janela, Manuela Pereira, João Seabra and Mário M. Freire, *Member, IEEE*

**Abstract**—This article proposes a multi-scale automated model for the classification of suspicious malignancy of breast masses, through log detrended fluctuation cumulant-based multifractal analysis of images acquired by dynamic contrast enhanced magnetic resonance. Features for classification are extracted by computing the multifractal scaling exponent for each of the 70 clinical cases and, by quantifying the *log-cumulants* reflecting multifractal information related with texture of the enhanced lesions. The output is compared to the radiologist diagnosis that follows the Breast Imaging - Reporting and Data System (BI-RADS). The results suggest that the *log-cumulant*  $c_2$  can be effective to classify typically biopsy-recommended cases. The performance of a supervised classification was evaluated by receiver operating characteristic (ROC) with an area under the curve of 0.985. The proposed multifractal analysis can contribute to novel feature classification techniques to aid radiologists every time there is a change in clinical course, namely when biopsy should be considered.

**Index Terms**—Breast Cancer, Computer-aided diagnosis, Dynamic contrast-enhanced, Feature extraction, Magnetic resonance imaging, Multi-scale, Multifractal analysis.

## I. INTRODUCTION

MAGNETIC Resonance Imaging (MRI) of the breast has been shown to be the most sensitive modality for scanning high-risk women, offering valuable information about breast conditions that cannot be obtained by other imaging modalities, such as mammography or ultrasound [1]. Dynamic Contrast Enhanced - Magnetic Resonance Imaging (DCE-MRI) techniques are based on the injection of a MRI contrast agent and acquisition of

T1-weighted images over time, which provides information on the diffusion of the agent to the tissues.

The diagnosis is generated by visual examination of morphological features and contrast-enhancement kinetics (functional features) using descriptors established in the Breast Imaging - Reporting and Data System (BI-RADS) lexicon [2]. Focus and foci are enhancements measuring less than 5 mm in diameter that are too small to be characterized in MRI. These lesions are typically stable on follow-up, may result from hormonal changes and are considered a part of the normal background enhancement pattern of the breast. Only bigger lesions than foci can be diagnosed and from those, malignant ones tend to present more irregular shape, speculated margins, and heterogeneous inner enhancement [3]. A lesion with contrast-enhancement kinetics of rapid initial rise, followed by a drop-off (washout) in the delayed phase, can have a positive predictive value of 77% for malignancy [4], [5]. Fischer et al. [6] proposed a scoring system (Göttingen score) based on the combination of DCE-MRI morphological and functional features that is coadjutant in the assessment of the BI-RADS grade. Nevertheless, clinical interpretation of breast MRI still remains largely subjective and the reported findings are often qualitative, having therefore an impact on the accuracy of the diagnosis. Computer aided diagnosis (CADx) arises in this context as an approach to reduce the subjectivity in human interpretation by improving specificity and possibly sensitivity, through a quantitative measurement and by offering the possibility of a reduction of the time needed for the breast MRI analysis [7].

The simplest heuristic model used to distinguish between malignant and benign lesions in DCE-MRI is known as the three-time-points (3TP) [8], [9], where points are selected along the time-intensity sequence during contrast uptake to characterize the enhancement slope and the washout rate. The enhancement pattern in the 3TP method varies according to the imaging protocol, but it allows a pixel-by-pixel kinetic analysis from the intensity values. Combining certain physiological parameters with a mathematical model of the temporal kinetics of the signal, parameter maps can be displayed. These depend on the overall shape of the tissue curves, and thus reflect tissue physiology only indirectly. In

Manuscript received July 30, 2012; revised August 16, 2013; accepted August 17, 2013. This work was partially funded by the Fundação para a Ciência e a Tecnologia through grant SFRH/BDE/15624/2006, by Siemens S.A. Healthcare Sector, by Instituto de Telecomunicações and by University of Beira Interior, Portugal. *Asterisk indicates corresponding author.*

\*Filipe Soares is with Siemens S.A. Healthcare Sector, 4456-901 Perafita, Portugal (e-mail: filipecruzsoares@gmail.com).

Filipe Janela and João Seabra are with Siemens S.A. Healthcare Sector, 4456-901 Perafita, Portugal.

Filipe Soares, Manuela Pereira and Mário M. Freire are with Instituto de Telecomunicações, Department of Computer Science, University of Beira Interior, 6201-001 Covilhã, Portugal.

addition, the accuracy of the 3TP method is nearly insensitive to the temporal sampling rate of the acquired data, as shown in [10], which makes it preferable to apply the 3TP on data acquired by standard imaging protocols that suffer from low temporal resolution. Moreover, due to the trade-off between spatial and temporal resolutions, a standard protocol allows the use of morphological and functional analysis in the same data. Albeit providing only an imperfect gold standard which does not necessarily reflect the biological truth, the 3TP represents a clinical routine for visual examination of DCE-MRI data and, hence, may serve as a reference model.

Contrast enhancement of findings, extensively used in mammography [11]–[13], aims to increase the contrast over some threshold levels which often require manual adjustments towards the trade-off between noise suppression and detail preservation. To automate lesion classification in MRI, features extracted by computer-based image analysis have been investigated as diagnostic aids, with mathematical descriptors related with those visually used by radiologists [14]. This approach adds capabilities for the analysis of textural, morphological and kinetic enhancement features. Previous studies [15]–[17] were focused on assessing the margin sharpness of the lesions. However, this is only one of the parameters evaluated by the radiologist. A plethora of other algorithms and classifiers have been proposed. The automated interpretation approach based on enhancement variance dynamics was proposed by Chen et al. [18], using linear discriminant analysis for lesion classification after feature extraction. Later in [19], fuzzy c-means clustering was used to identify enhancement kinetics. Yao et al. proposed in [20] a pixel-by-pixel classification method based on texture analysis and wavelet transform for tumor evaluation in breast DCE-MRI. In [21], Zheng et al. used spatiotemporal enhancement pattern and Fourier transform to analyze breast images. Back-propagation neural network classification of segmented regions was proposed by Meinel et al. [22] using shape and kinetic features combined. Artificial neural networks have been one of the most investigated approaches for the classification of breast lesions in DCE-MRI [23]–[26]. However, it has been shown that support vector machine (SVM) lead to a better performance than a variety of other machine learning techniques in the classification of breast lesions [27]–[30]. Moreover, a CADx system should work as a second-look for the radiologist and therefore it should focus on a comprehensive set of characteristics of the lesions, including features that are indistinguishable to the human eye.

Since images of breast tissue are characterized by a high degree of self-similarity [31], i.e., several parts look as the whole image, if structural deviations from the global regularity of the background occur, then they may be considered breast lesions. Those irregularities can be characterized under the light of fractal or multifractal analysis. The fractal theory has been proposed for breast tumors detection and classification [16], [17]. However, in these studies it was used for margin sharpness characterization only and in [17], Penn et al. have shown that nearly two thirds of the cancers were categorized inconclusive in terms of fractal dimension. A potential

problem is related with the inability of the fractal dimension to uniquely characterize the texture pattern. Different fractal sets may share the same fractal dimension values and yet have different appearances [32]. Nevertheless, from the point of view of multifractal theory, more advanced approaches do exist allowing a deeper exploration of the potential of this theory for medical image analysis. The multifractal analysis provides a spectrum of fractal dimensions, characterizing multiple irregularities. This can potentially give more information about the image than the single fractal dimension, without being exclusively focused on lesion margins.

A preliminary study from our group [31] on the application of the multifractal analysis to mammographic images showed very promising results in the detection of lesions. There are no further conclusive results of multifractal-based analysis in DCE-MR images of the breast. The multifractal study of mammograms has been done with wavelet-based multifractal theory in [33], using the Wavelet Transform Modulus Maxima (WTMM), a promising method with high precision in the scaling analysis in spite of being complex, especially for high-dimensional objects. In our work, the selected method for the multifractal analysis is the Multifractal Detrended Fluctuation Analysis (MF-DFA) [34], a reliable alternative to WTMM being less sensitive to lack of resolution, which is beneficial given the low spatial resolution of the breast DCE-MRI data. The MF-DFA is based on the Detrended Fluctuation Analysis (DFA) [35], a very efficient method in avoiding spurious detection of artifactual correlations. There are evidences that MF-DFA provides similar results to WTMM but the former is simpler and more accurate for low temporal resolution time series. [36], [37]. In fact, WTMM false multifractality can be even more evidenced in medical images, as verified in the study with mammographic images [31].

In this paper, multifractal analysis of breast lesions in DCE-MR images is explored for diagnosis. For the first time, to the best of our knowledge, the MF-DFA is applied in the discrimination of breast lesions in MRI. Our goal is to classify suspicious malignancy of breast masses through a multi-scale automated model that extract self-similarity features by Log Detrended Fluctuation Cumulant-based Multifractal Analysis. These features are studied in order to characterize in detail the morphology and texture of the contrast-enhanced lesions in a supervised classification scheme.

## II. MATERIALS AND METHODS

Existing fractal methods of texture analysis rely on the fractal dimension as a function of scale. We explore the application of multifractal analysis for characterizing multi-scale changes in the textural information related with self-similarity regularity. Multifractal signals are intrinsically more complex than (mono) fractals. Multifractal analysis exploits both local irregularity (roughness) of a given measure and the global distribution of this irregularity, as reported in [31].

A model for multifractal image analysis is proposed as illustrated in Fig. 1. In particular, it comprises a decision-support system in the diagnosis of breast cancer with DCE-MRI. The images and respective clinical reports are the

input of the model. Section II.A and II.B will follow with details on how the images were acquired and characterization of the dataset. Log Detrended Fluctuation Cumulant-Based Multifractal Analysis was implemented in order to evaluate the degree of structural deviation of a tumor from the global regularity of the surrounding breast tissue. The irregularities arise at multiple scales and are characterized through a spectrum of fractal dimensions, the multifractal spectrum, and summarized by *log-cumulants* from the scaling exponent. The core of the multifractal analysis is described in Section II.C and the algorithm for the extraction of features is presented in Section II.D. The 3TP model based on the kinetic curves of enhancement described in Section I was also implemented for comparison with the model proposed herein, using the same acquisition protocol.

A. Image Acquisition

Experimental data was acquired using a Siemens Trio 3T MR Scanner at the health institution Clínica João Carlos Costa, Viana do Castelo, Portugal. This study was approved by the research ethics committee of the health institution. Dynamic imaging was performed using a T1-weighted FLASH 3D (FL3D) pulse sequence with fat saturation following subtraction. The patients were scanned in prone position using a standard double breast coil. The acquisition protocol parameters were 3.76 ms of repetition time, 1.38 ms of echo time with flip angle = 12°, the in-plane spatial resolution was 0.65 × 0.65 mm<sup>2</sup> and the slice thickness 0.6 mm for the generated 3D volumes. Each slice of the volumes contains 448 × 448 pixels for a typical field of view of 30 × 30 cm<sup>2</sup>. Imaging is performed before and after a bolus intravenous injection of 0.1 mmol/kg of Gadopentetate dimeglumine (Gd-DTPA). Five bilateral axial acquisition series were taken per patient at intervals of 1 min and 51 s. The first post-contrast images acquired after contrast arrival were used for the multifractal analysis of the enhanced lesions since it was found that the information from the initial portion of the time was the most predictive of malignancy as reported in [25]. The time points 0, 111 s and 444 s were used for 3TP.

B. Dataset Characterization and Tumor Selection

A dataset of 70 clinical cases were sequentially selected retrospectively by a radiologist not including vascular structures, architectural distortions and other nonmasses. A diagnosis report was processed with a BI-RADS grade assigned to each case, according to the morphology (see Fig. 2) and dynamic enhancement of the findings. In addition to the BI-RADS grade, the dataset also included the information of biopsy recommendation, which was considered an indication of suspicious malignancy in the present study. The dataset was therefore divided in two main categories of cases: 39 (PM) probably malignant and biopsied – all BI-RADS 4 or 5 plus some BI-RADS 3; 31 (PB) probably benign and nonbiopsied all BI-RADS 2 or 3. Simple cases graded with BI-RADS 1 with weak enhancement or nothing to comment on, were not included in the dataset.

After the central slice from the acquired image was defined

in the clinical case report, a region of interest (ROI) was selected according to the tumor location to be evaluated, including the background. The sizes of the lesions are evenly distributed among the categories (see Fig. 3). The longest diameter was estimated by the radiologist using an electronic ruler, on the central slice where the lesion was best visualized. Focus and foci findings less than 5 mm were not included since they cannot be specified according to BI-RADS [2].

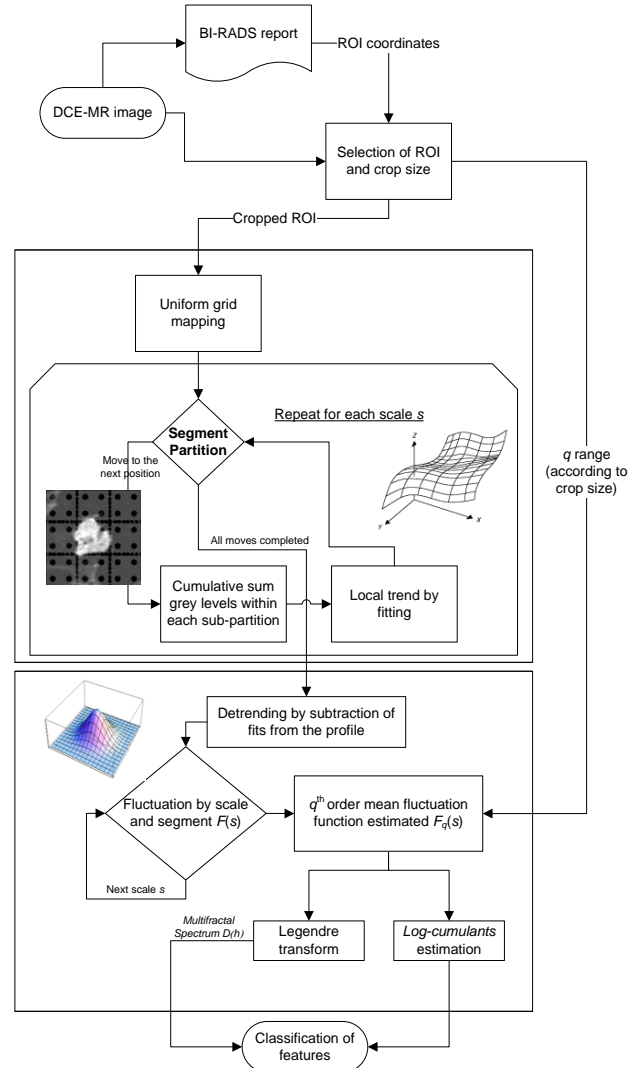


Fig. 1. Flowchart of the model for Log Detrended Fluctuation Cumulant-Based Multifractal Analysis.

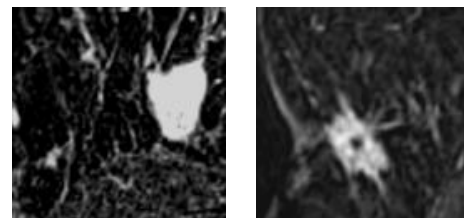


Fig. 2. Morphology features. (Left) Typical benign case on the left, with oval shaped mass smooth, margin and homogeneous enhancement. (Right) Typical malignant case on the right with irregular shaped mass, spiculated margin and heterogeneous enhancement.

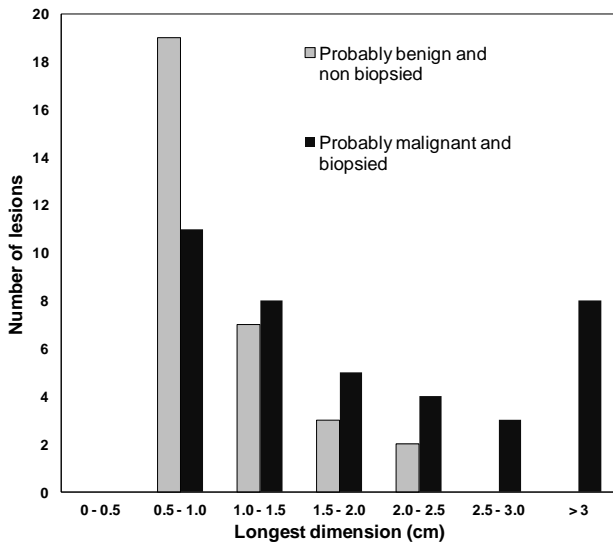


Fig. 3. Histogram of the longest diameter of the lesions in the data set. The longest diameter was measured where the lesion was best visualized as determined by radiologist.

### C. Multifractal Analysis

The multifractal spectrum summarizes various degrees of scaling. The dynamics of the scaling can be used as discriminatory descriptors, providing an additional perspective of the data. In this sense, it was attempted to confirm that selected ROIs of the breast MR images have multiple degrees of scaling, by the prevalence of a multifractal spectrum and a non linear multifractal scaling exponent  $\tau(q)$ . This  $\tau(q)$  can be seen as a collection of scaling exponents replacing a single self-similarity parameter and, hence, conveying versatility in actual data analysis.

To interpret breast MR images as multifractals we assume that they are composed of several superimposed sets of fractals. A multifractal object can be characterized by assessing number and size of the fractal sets associated to a certain influence on the scale. These measures are provided by the Hölder exponent  $h$  and the Hausdorff dimension  $D(h)$ , for impact and size, respectively [38]. The relationship between the  $D(h)$  and the corresponding  $h$  results in the multifractal spectrum. This spectrum describes the quality and quantity of irregularities in the data and its characteristic shape is sensitively dependent on periodic patterns. Therefore, in this study  $\tau(q)$  and  $D(h)$  were estimated for each tumor images selected.

According to the explanation in the Section I, the selected method for the multifractal study was the Multifractal Detrended Fluctuation Analysis (MF-DFA) [34], due to the limitations in the acquisition of breast MRI data, namely the low spatial resolution. The DFA presented in [35], comprises an integration of the original data followed by a division into segments of equal length. For each segment, a fitting to the data represents the trend in that segment. A subtraction of a local trend point from a local original point, so-called detrending step, is required to obtain local fluctuations at different timescales. Such procedure enables investigating the

scaling properties (self-similarity) and the power-law long-range correlations.

The multifractal generalization of this procedure (MF-DFA) is based on the identification of scaling of the  $q$ th-order moments, which have a power-law dependence on the signal length. In this sense, the methodological challenge is how to detect and quantify the scaling and correlation properties with MR images. This method was generalized to be capable of analyzing multifractal properties of objects with higher dimensions by Gu and Zhou in [39]. The MF-DFA two-dimensional method was preliminary applied by Soares et al. in [31] to detect lesions in mammographic studies based on multifractal theory. Following that research work, the MF-DFA adapted here to detect scaling in two-dimensional MR images consists of five stages, where a more detailed description of stage 1 and stage 2 can be found in [39].

Stage 1: Consider a self-similar surface denoted by a two-dimensional array of grey levels  $f(i, j)$ , where  $i = 1, 2, \dots, M$  and  $j = 1, 2, \dots, N$ . The surface is partitioned into  $M_s \times N_s$  disjoint segments of lateral size  $2^s$ , as applying a uniform grid map. The scale  $s$  is then related with the grid elements size.

Stage 2: In each segment  $f_{v,w}$  identified by  $v$  and  $w$ , the cumulative sum of the grey levels is named  $u_{v,w}(i, j)$  where  $i, j$  are pixel coordinates and  $1 \leq i, j \leq s$ .

Stage 3: The local trend  $\tilde{u}$  of the constructed surface  $u_{v,w}$  can be determined by fitting it with a polynomial function and the detrended fluctuation function  $F(v,w, s)$  are evaluated for each segment as

$$F(v, w, s) = \sqrt{\frac{1}{s^2} \sum_{i=1}^s \sum_{j=1}^s [u_{v,w}(i, j) - \tilde{u}_{v,w}(i, j)]^2}, \quad (1)$$

where many fitting procedures ( $m$ -order 2D polynomials)  $\tilde{u}$  can be used. Since the detrending is done by the subtraction of the fits from the profile, the order of the polynomials differs in their capability of eliminating trends in the data. Second-order was confirmed to be adequate for spurious free fitting with MRI data detrending, this way eliminating the influence of possible first-order trends in the original two-dimensional array, for scales larger than the segment size. Therefore, the following polynomial is adopted,

$$\tilde{u}_{v,w}(i, j) = ai^2 + bj^2 + cij + di + ej + f, \quad (2)$$

where  $1 \leq i, j \leq s$ , and  $a, b, c, d, e$ , and  $f$  are free parameters that can be estimated through matrix operations, derived from the least-squares method.

Stage 4: The  $q$ th-order mean fluctuation function is obtained by averaging over all segments lengths  $s$ , that is, by [39]:

$$F_q(s) = \left\{ \frac{1}{M_s N_s} \sum_{v=1}^{M_s} \sum_{w=1}^{N_s} [F(v, w, s)]^q \right\}^{\frac{1}{q}}, \quad (3)$$

where  $q$  can take any real value except zero. The parameter  $q$  can be seen as a focus control of a “microscope lens” for exploring different regions of irregularity. Several ranges of  $q$  were tested leading to an optimal  $-18 < q < 18$  range for the

problem in study. The key property of  $F_q(s)$  is that for an image with self-similarity properties, a presence of a power-law scaling is revealed with a linear relationship on a double log plot within a significant range of  $s$ . We are interested in how the fluctuation functions depend on  $q$  and how this dependence is related to multifractal features of the surface, determining how it depends on scale.

Stage 5: The scaling behavior of the fluctuation function may be determined by varying  $s$  in the range from 4 to 8 with the scaling relation between the detrended fluctuation function  $F_q$  and the size scale  $s$ , given by [34]:

$$F_q(s) \sim s^{h(q)}, \quad (4)$$

where the  $h(q)$  is called generalized Hurst exponent, a family of scaling exponents. This is the final outcome of the MF-DFA, which is a decreasing function of  $q$  for multifractal surfaces. For monofractals, it remains constant with identical scaling behavior for all values of  $q$ . The range of the scales aforementioned was chosen following the recommendations in [34] for statistically reliability and in agreement to the procedure of fitting our MR images in stage 3.

In the multifractal analysis  $D(h)$ ,  $h(q)$  and  $\tau(q)$  may be related resorting to the Legendre transform [40], being  $d$  the dimension of space (for an image,  $d = 2$ ), as

$$D(h) = \inf_{q \neq 0} (d + qh(q) - \tau(q)). \quad (5)$$

#### D. Self-Similarity Extraction

The previous method of multifractal analysis is applied to each clinical case, to obtain a possible non linear scaling exponent  $\tau(q)$  and a spectrum  $D(h)$  to confirm the presence of multifractality.

Instead of measuring the multifractal scaling exponent  $\tau(q)$  theoretically for all  $q$ , an empirical scaling analysis of  $\tau(q)$  has been suggested to be regarded as a polynomial expansion of order  $p$  [41]:

$$\tau(q) = \sum_{p \geq 1} c_p \frac{q^p}{p!}. \quad (6)$$

The *log-cumulants*  $c_p$  that do not depend on scale can be obtained from the scale dependence of  $C(j, p)$ , the cumulant of order  $p \geq 1$  and scale  $j$ , of a random variable  $X$ , by [42]:

$$C(j, p) = c_p^0 + c_p \ln 2^j. \quad (7)$$

A process is said to be multifractal when  $\tau(q)$  departs from linear behavior with  $c_2 \neq 0$ . The most commonly used *Log-normal* multifractal in practice can be characterized only by  $c_1$  and  $c_2 \neq 0$ , but more complex multifractal models may involve polynomials of order higher than 2. Consequently, the study of  $\tau(q)$  can be rephrased in terms of the *log-cumulants* estimated by linear regression in (6).

We want to evaluate if the ROIs from the DCE-MRI of the breast could be represented or not by  $p \geq 2$ ,  $c_p \neq 0$  and thus reveal a simple or more complex multifractal behavior. We retain this *log-cumulant* triplet  $(c_1, c_2, c_3)$  as features that allow

differentiating tumors with the aid of supervised classification.

Our self-similarity extraction, presented in Algorithm 1, calculates (when possible) *log-cumulants* from the estimated scaling exponent, but also descriptors of a spectrum  $D(h)$ . Different spectral characteristics are quantified (Fig. 4). This quantification of features values should not be confused with the quantification of MR signal intensity. This article does not describe any conversion between MR signal intensity and contrast agent concentration, because values used in the analysis are not meant to be quantitatively comparable between scans. In this study, only the relative intensity between pixels in a ROI (including the background of a lesion) is used to characterize anatomical detail of the contrast-enhanced lesions.

---

#### Algorithm 1 Self-similarity extraction

---

- 1) For each image  $k$  in the dataset
    - a) Set  $q$  step according to  $k$  size
    - b) Set  $q$  range  $qr$  as  $-2 < qr < 2$  in steps of  $qstep$
    - c) For each moment  $q$  between  $qr$ 
      - i) Compute mean fluctuation function  $F_q(s)$  between scales  $s$
      - ii) Estimate multifractal scaling exponent  $\tau(q)$
      - iii) Estimate multifractal spectrum  $D(h)$  from  $F_q(s)$
    - d) Compute *log-cumulant*  $c_1, c_2, c_3$  from  $\tau(q)$
    - e) Compute descriptors  $LS, H, Dh, W, RS$ , from  $D(h)$
    - f) Store the multifractal descriptors and *log-cumulants* on a feature matrix  $(f(qr), k)$
    - g) Expand  $q$  range and repeat Step b) to Step e) while all members of  $f \in \mathfrak{R}$ , otherwise jump to next image  $k$
  - 2) For each feature  $f(qr)$ , vary gamma  $\gamma$  and regularization parameter  $C$ 
    - a) Classify image  $k$  into two main categories (PB or PM) with SVM in LOO cross-validation scheme.
    - b) Obtain the performance metrics  $A_z$ , Sensitivity, Specificity, Accuracy, according to the actual clinical diagnosis of  $k$
    - c) Store a matrix of performance metrics for each combination of SVM parameters per feature
  - 3) Select the profile of SVM parameters that maximize  $A_z$  as well as Accuracy, for each feature  $f$  among all  $qr$
- 

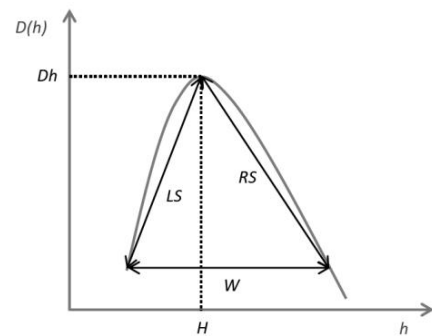


Fig. 4. Scheme of the descriptors used for the multifractal spectrum characterization.

One important descriptor is the  $h$  where the spectrum is maximum. It shows at which Hölder exponents is positioned the most statistically significant part of the image, i.e. the subsets with maximum fractal dimension. *Hurst* parameter ( $H$ ) is often associated with this exponent reminding the

monofractal theory where there is only one fractal dimension. The corresponding maximum fractal dimension is given by  $Dh$ . This is directly related with the irregularity of the analysed object. Other important descriptors are the left slope of the curve ( $LS$ ), right slope of the curve ( $RS$ ) and the curve width ( $W$ ). These can be related to how far from monofractal a ROI is.

Supervised classification of tumors was performed by applying SVMs with the extracted multifractal-based features, using the SVM<sup>light</sup> [43] package for its efficient optimization algorithm, which allows choosing multiple kernel functions to obtain a different classification hyperplane. Radial Basis Function that requires the parameter gamma  $\gamma$  was the kernel used in this work, tested in numerous applications and introduced in a previews study with breast DCE-MRI by Levman et al. [44]. The condition for optimal hyperplane also includes a regularization parameter  $C$  that controls the trade-off between maximization of the margin and minimization of the training error. Small  $C$  tends to emphasize the margin while ignoring the outliers in the training data, while large  $C$  may tend to over fit the training data, which is not recommended.

The role of multifractal descriptors and *log-cumulants* is still an open problem for the characterization of tumors. In Algorithm 1, a single feature independent classification was adopted to better understand differences among these features of distinct theoretical meaning. However, for comparison purposes and to evaluate whether joint features may yield better classification, optimized feature sets were also selected among the extracted features based on a ranking criterion using the recursive feature elimination (RFE) [45] combined with SVM. This algorithm determines the feature ranking based on sequential backward elimination that removes one feature at a time, and searches for a nonlinear separating margin to obtain the optimal hyperplane in the feature space.

To select the potentially optimal model for our classification problem (type of kernel function to use, its associated parameters, and  $C$ ), we applied Leave-one-out (LOO) cross-validation to the working dataset [43]. This LOO technique involves training the machine learning algorithm for estimating the likelihood of malignancy from all cases but one, testing classification on that single case. This procedure is repeated until each case has been tested individually. The cross-validation ensures that all elements of the dataset may be used for both training and testing. Our approach to achieve the best classification based on each feature was to choose the parameters of SVM that produce the model with smaller errors in the cross-validation and use it for testing in order to maximize the accuracy.

The performance of the features in the classification between PM and PB lesions was evaluated by the receiver operating characteristics (ROC) area under the curve ( $A_z$ ), Sensitivity, Specificity and Accuracy. In order to more accurately place the proposed Log Detrended Fluctuation Cumulant-Based Multifractal Analysis in the landscape of lesion classification in DCE-MRI, the 3TP model was compared by ROC within the same experimental setup.

### III. RESULTS

For the images in the dataset, the scaling exponent  $\pi(q)$  in Fig. 6 has a concave shape that hence departs from the linear behavior  $qH$ , known as the signature of self-similarity. Even though, monofractal behaviors occur at some scales (see Fig. 5), particularly for negative moments  $q$ . In addition, through the estimation of *log-cumulants* it is confirmed in Fig. 7 that  $c_1$  and  $c_2 \neq 0$ , i.e, we are in the presence of a multifractal process. The concavity of  $\pi(q)$  implies  $c_2 < 0$ . Also, the multifractal spectra  $D(h)$  of the analyzed images points to multifractality as they are not limited to a single Hölder exponent  $h$ .

Solely based on  $D(h)$  or  $\pi(q)$  (Fig. 6), the distinction between benign and malignant tumors remains unclear. Neither isolated spectral descriptors nor *log-cumulants* were able to properly differentiate the cases. False negatives arise as represented by the outliers in Fig. 7. The outliers from the top report to masses with strong enhancement and all morphological characteristics of malignant findings, as opposed to the relatively slow enhancement of the bottom outliers. In addition, between box-plots from PB and PM there are no statistically significant differences (confidence interval of 95%) and supervised learning classification was conducted.

Fig. 8 and Table I present the performance of the proposed method evaluated by the area under the ROC curve for a SVM classification using each feature derived from multifractal theory, and the top feature set of *RFE-3* features ( $LS$ ,  $c_2$ ,  $c_3$ ) identified with the highest accuracy among the features sets.

The *log-cumulant*  $c_2$  appears as the best feature with 0.985 of  $A_z$ . This is more effective in classifying typically biopsy-recommended cases, compared with the 3TP model. ROC curves were compared using the Mann–Whitney U-statistics (DeLong et al. [46]). Statistically significant differences were found (p-value  $< 0.05$ ) between:  $c_2$  vs. all the others, *3TP* vs. all the others except  $c_3$  and *RFE-3*,  $c_1$  vs.  $c_3$ ,  $c_1$  vs.  $Dh$ .

As it was pointed in Algorithm 1-3), a profile of SVM parameters was optimized (final parameters in Table I) to reach the best  $A_z$  and Accuracy. Concurrently, it was evaluated the impact of the  $q$  range chosen into the computational efficiency by CPU time in seconds (s). The performance of the best feature *log-cumulant*  $c_2$  is presented in Fig. 9. The optimal classification power was achieved with  $-18 < q < 18$  for the problem in study. For larger expansions of  $q$  the CPU time starts increasing rapidly. The average execution time per case of the entire Log Detrended Fluctuation Cumulant-Based Multifractal Analysis is 1.65s, on a 2.53GHz Intel® Core™ i5 M540 workstation.

### IV. DISCUSSION

In DCE-MRI of the breast, the evaluation of time course kinetics introduces a completely independent parameter that can help to distinguish benign lesions from apparently circumscribed malignant lesions. If a lesion looks benign in terms of morphology, a different diagnosis may be done if signal intensity time courses are evaluated [47]. However, the false-positive rate in MRI is still high and further features that characterize in more detail the morphology and texture of the

contrast-enhanced lesions might be beneficial in the diagnosis of a breast cancer.

Multifractal analysis focuses on understanding and exploring the nature of the irregularities in the image and, not on a single most prevalent irregularity or global trend. The ROI of the enhanced lesions revealed multiple degrees of scaling, i.e., the prevalence of a multifractal spectrum.

Self-similarity features were automatically generated for each early post-contrast images acquired. For each clinical case, the association of extracted multifractal descriptors from  $D(h)$  and  $\log$ -cumulants from  $\tau(q)$  with BI-RADS visual descriptors was explored. For these computer-extracted features to be accepted, the correlation with morphological descriptors defined in BI-RADS lexicon needs to be established.

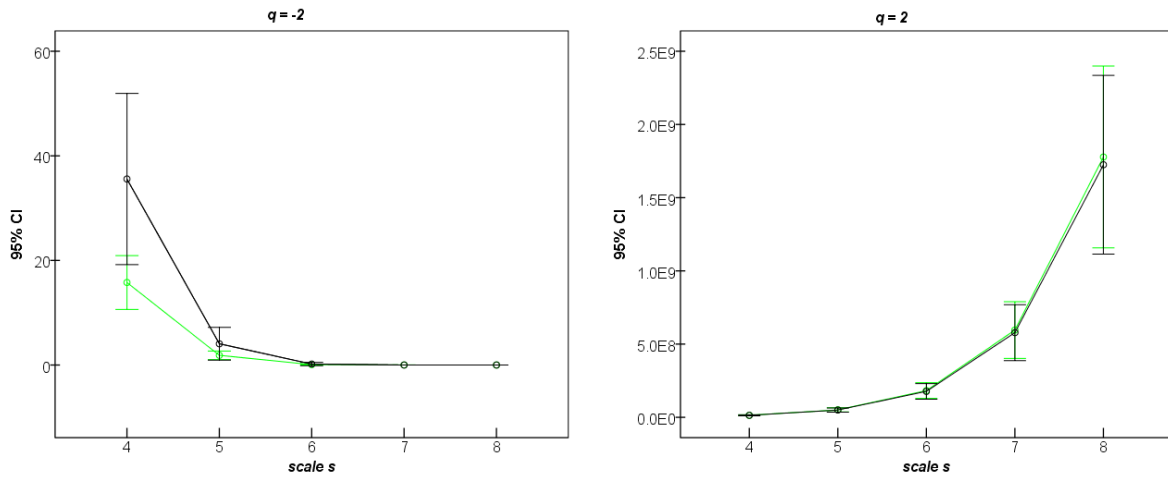


Fig. 5. Detrended fluctuation function  $Fq(s)$  at different scales for  $q = -2$  (left) and  $q = 2$  (right). (Black) PM cases. (Green) PB cases. It is shown the presence of scaling range in particular for negative moment  $q$ , with the extreme scales showing more deviation from the power law scaling (smaller scales in  $q = -2$  and larger scales in  $q = 2$ ). Bars from the group of cases represent 95% confidence interval for mean.

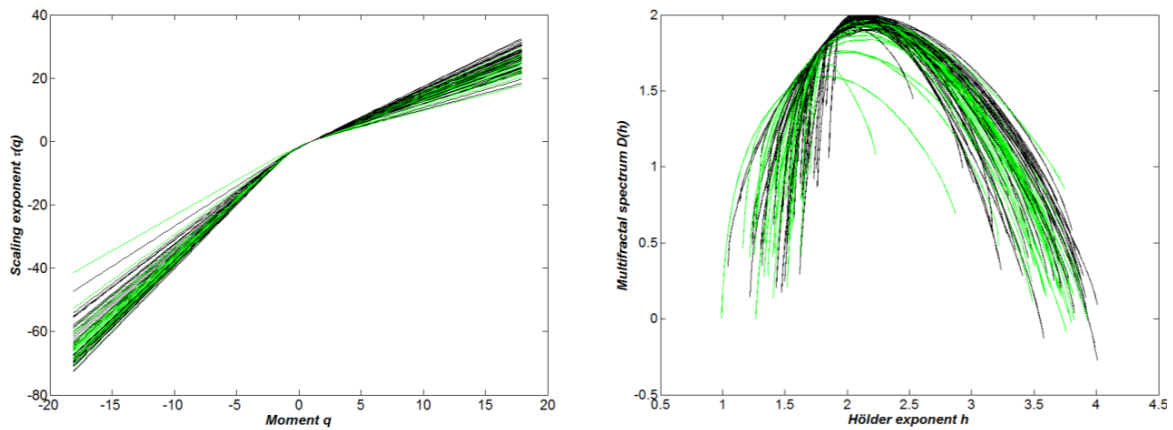


Fig. 6. Estimated scaling exponent  $\tau(q)$  (left) and multifractal spectrum  $D(h)$  (right) for the lesions in the dataset. PM cases: in black. PB cases: in green.

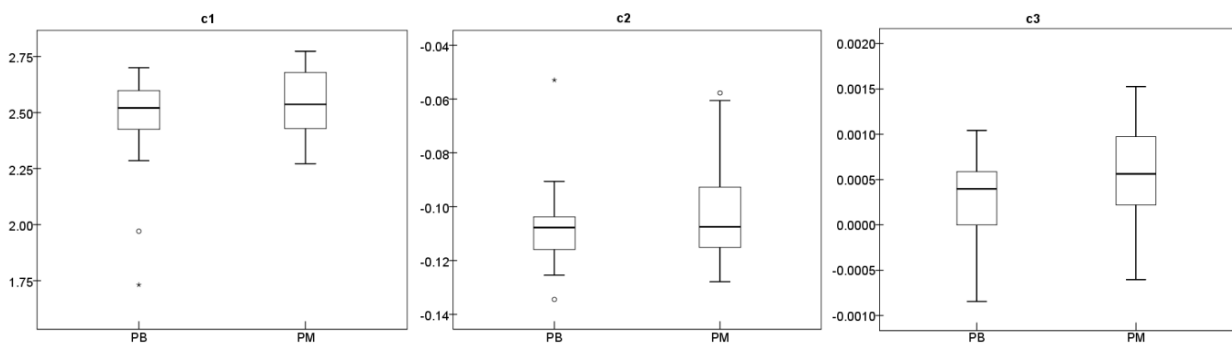


Fig. 7. Comparison of the three  $\log$ -cumulants estimated from  $\tau(q)$  before SVM analysis for PB (left bar) and PM (right bar) cases. The box-plots show the lower and upper quartile and median.

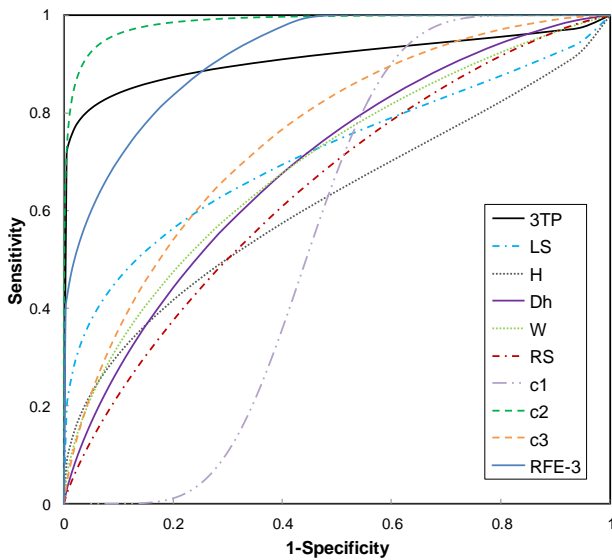


Fig. 8. Comparison of the ROC curves using SVM with the self-similarity extracted features, *RFE-3* feature set and the 3TP.

TABLE I  
COMPARISON OF THE AREA UNDER THE ROC CURVE  $A_z$  AND CORRESPONDING STANDARD DEVIATION (STD) USING SVM

Feature	$A_z$	( $\pm$ std)	Sensitivity	Specificity	Accuracy	$\gamma$	$C$
3TP	0.912	0.05	80%	96%	88%		
LS	0.714	0.06	52%	85%	68%	6	10
H	0.617	0.07	42%	80%	61%	6	1
Dh	0.692	0.06	68%	60%	64%	6	100
W	0.695	0.06	59%	70%	64%	6	10
RS	0.646	0.06	61%	60%	60%	3	100
$c_1$	0.555	0.07	94%	37%	65%	2	10
$c_2$	0.985	0.02	94%	94%	94%	3	100
$c_3$	0.753	0.06	67%	70%	68%	6	1000
<i>RFE-3</i>	0.917	0.05	82%	82%	82%	6	100

$\Gamma$  and regularization parameter ( $C$ ) as SVM associated kernel parameters.

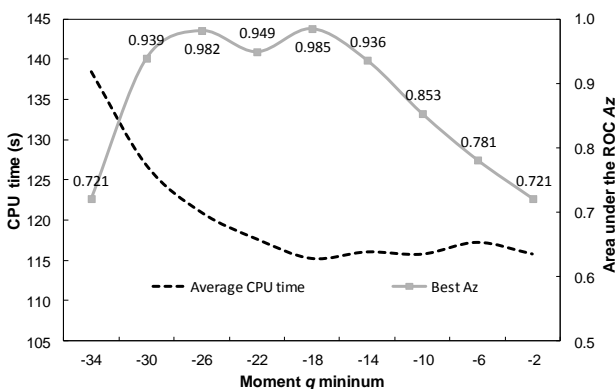


Fig. 9. Comparison of computational efficiency by CPU time in seconds (s) with achieved area under the ROC curve  $A_z$  with *log-cumulant*  $c_2$ , for multiple expansions of moment  $q$  range. The CPU time presented is an average of the total time for running the complete dataset of 70 cases.

It was found that  $H$  was related with the most prevalent irregularity of the mass in the ROI, namely shape and margins.  $LS$  was found to be related with the inner enhancement of the lesion, and how diverged from the monofractal the  $D(h)$  was, at positive moments  $q$ . The *log-cumulants* are known to be related with the aforementioned descriptors of  $D(h)$ , with  $c_1$  being related with the location of the  $H$ , while  $c_2$  with its width  $W$ , and  $c_3$  possibly characterizing the asymmetry of  $D(h)$ . The best result was obtained with *log-cumulant*  $c_2$  that clearly leads us to describe the data as a multifractal rather than monofractal process. This *log-cumulant* represents a compound of the global nature of the multifractal spectrum. In a general interpretation, the malignant cases are more globally inhomogeneous, show higher contrast-enhanced changes that are anti-persistent, and lower contrast-enhanced changes with persistence.

A feature selection algorithm was used as pre-processing for optimization of the hyperdimensional feature space. The rationale of the ranking is that the inputs which are more weighted have the greatest influence on the classification decision. The procedure identified an optimized feature set of three features *RFE-3* ( $LS$ ,  $c_2$ ,  $c_3$ ), but with lower area under the ROC than  $c_2$ .

It was empirically found that adjusting  $qstep$  according to the sizes of the crops would improve the results, because bigger lesions that required larger crop sizes will have more steps in the scaling behavior and, therefore, the steps in  $qr$  should also be adjusted in the same ratio.

From the observed  $Fq(s)$  at different scales, positive moments  $q$  have similar deviations among PM and PB. Compared with what happens at negative  $q$ , with PB deviating less from monofractal than PM at smaller scales,  $RS$  gave unexpected poor results. Therefore, it should be interesting to deepen the research of  $RS$  probably with volumetric lesion analysis, since the performance is likely to improve when one takes full advantage of the 3D nature of the data onto the multifractal analysis.

In this paper, there were no temporal features associated with the proposed multifractal method, since that would require good temporal sampling rate and standard protocols in DCE-MRI of the breast are limited with respect to temporal resolution (usually 5 time points are found as herein) because it depends on contrast agent circulation time and on MR sequence repetition time. Also for this reason, the results were compared with 3TP instead of more advanced pharmacokinetic models. The latter would require acquisition protocols of higher temporal resolution in order to surpass the diagnosis accuracy of 3TP [10].

Future work would include optimization of different acquisition protocols, with sufficient temporal resolution to extend the multifractal methods in the temporal dimension, and would be compared with the application of more advanced pharmacokinetic models. However, it is worth noticing that the multifractal temporal features derived should not have a correspondence to the pharmacokinetic parameters, which more directly reflect the physiology.

## V. CONCLUSION

In this paper, a model for multifractal image analysis, relying on Log Detrended Fluctuation Cumulants, is proposed to assist the radiologist in the diagnosis of breast cancer. According to the results on experimental data from clinical cases of DCE-MRI, the decision-support system presents high accuracy (94%) distinguishing biopsy-recommended lesions from probably benign lesions, with one of the eight features studied. The performance of a supervised classification was evaluated by ROC analysis yielding a maximum area under the curve of 0.985. Even without using all of the consecutive acquired images to build a kinetic curve of enhancement, the best outcome of the proposed model confirms the biopsy recommendations, and overcomes the performance of 3TP, which is a clinical standard protocol for the examination of DCE-MRI data.

## REFERENCES

- [1] L. Moy, K. Elias, V. Patel, J. Lee, J. Babb, H. Toth, and C. Mercado, "Is breast MRI helpful in the evaluation of inconclusive mammographic findings?," *American Journal of Roentgenology*, vol. 193, no. 4, p. 986, Oct. 2009.
- [2] E. A. Morris, "Illustrated breast MR lexicon," *Semin Roentgenol*, vol. 36, no. 3, pp. 238–249, Jul. 2001.
- [3] E. Rosen, S. Smith-Foley, W. DeMartini, P. Eby, S. Peacock, and C. Lehman, "BI-RADS MRI enhancement characteristics of ductal carcinoma in situ," *Breast Journal*, vol. 13, no. 6, p. 545, Nov. 2007.
- [4] B. Erguvan-Dogan, G. Whitman, A. Kushwaha, M. Phelps, and P. Dempsey, "BI-RADS-MRI: A Primer," *American Journal of Roentgenology*, vol. 187, no. 2, p. W152, Aug. 2006.
- [5] S. A. Jansen, X. Fan, G. S. Karczmar, H. Abe, R. A. Schmidt, M. Giger, and G. M. Newstead, "DCEMRI of breast lesions: Is kinetic analysis equally effective for both mass and nonmass-like enhancement?," *Medical Physics*, vol. 35, no. 7, pp. 3102–3109, Jul. 2008.
- [6] U. Fischer, L. Kopka, and E. Grabbe, "Breast Carcinoma: Effect of Preoperative Contrast-enhanced MR Imaging on the Therapeutic Approach," *Radiology*, vol. 213, no. 3, pp. 881–888, Dec. 1999.
- [7] Y. Gal, A. Mehnert, A. Bradley, D. Kennedy, and S. Crozier, "Feature and Classifier Selection for Automatic Classification of Lesions in Dynamic Contrast-Enhanced MRI of the breast," in *Proceedings of the Digital Image Computing: Techniques and Applications*, 2009, pp. 132–139.
- [8] C. Kuhl, P. Mielcareck, S. Klaschik, C. Leutner, E. Wardelmann, J. Gieseke, and H. H. Schild, "Dynamic Breast MR Imaging: Are Signal Intensity Time Course Data Useful for Differential Diagnosis of Enhancing Lesions?," *Radiology*, vol. 211, no. 1, pp. 101–110, Apr. 1999.
- [9] E. Furman-Haran, D. Grobeld, R. Margalit, and H. Degani, "Response of MCF7 human breast cancer to tamoxifen: evaluation by the three-time-point, contrast-enhanced magnetic resonance imaging method," *Clinical Cancer Research*, vol. 4, no. 10, pp. 2299–2304, Oct. 1998.
- [10] J. U. Fluckiger, M. C. Schabel, and E. V. R. DiBella, "The effect of temporal sampling on quantitative pharmacokinetic and three-time-point analysis of breast DCE-MRI," *Magnetic Resonance Imaging*, vol. 30, no. 7, pp. 934–943, Sep. 2012.
- [11] Y. Zhou, K. Panetta, and S. Agaian, "Mammogram enhancement using alpha weighted quadratic filter," in *Proceedings of the 31st Annual International Conference of the IEEE Engineering in Medicine and Biology Society*, 2009, pp. 3681–3684.
- [12] Y. Zhou, K. Panetta, and S. Agaian, "Human visual system based mammogram enhancement and analysis," in *Proceedings of the International Conference on Image Processing Theory Tools and Applications*, 2010, pp. 229–234.
- [13] K. Panetta, Y. Zhou, S. Agaian, and H. Jia, "Nonlinear unsharp masking for mammogram enhancement," *Information Technology in Biomedicine, IEEE Transactions on*, vol. 15, no. 6, pp. 918–928, 2011.
- [14] M. Giger, "Computerized analysis of images in the detection and diagnosis of breast cancer," *Seminars in Ultrasound CT and MRI*, vol. 25, no. 5, pp. 411–418, Oct. 2004.
- [15] K. G. Gilhuijs, M. L. Giger, and U. Bick, "Computerized analysis of breast lesions in three dimensions using dynamic magnetic-resonance imaging," *Medical Physics*, vol. 25, no. 9, pp. 1647–1654, Sep. 1998.
- [16] A. I. Penn, L. Bolinger, M. D. Schnall, and M. H. Loew, "Discrimination of MR images of breast masses with fractal-interpolation function models," *Academic Radiology*, vol. 6, no. 3, pp. 156–163, Mar. 1999.
- [17] A. Penn, S. Thompson, M. Schnall, M. Loew, and L. Bolinger, "Fractal discrimination of MRI breast masses using multiple segmentations," in *Proceedings of SPIE*, 2000, vol. 3979, pp. 959–966.
- [18] W. Chen, M. Giger, L. Lan, and U. Bick, "Computerized interpretation of breast MRI: Investigation of enhancement-variance dynamics," *Medical Physics*, vol. 31, no. 5, p. 1076, Apr. 2004.
- [19] W. Chen, M. L. Giger, U. Bick, and G. M. Newstead, "Automatic identification and classification of characteristic kinetic curves of breast lesions on DCE-MRI," *Medical Physics*, vol. 33, no. 8, pp. 2878–2887, Aug. 2006.
- [20] J. Yao, J. Chen, and C. Chow, "Breast Tumor Analysis in Dynamic Contrast Enhanced MRI Using Texture Features and Wavelet Transform," *IEEE Journal of Selected Topics in Signal Processing*, vol. 3, no. 1, pp. 94–100, Feb. 2009.
- [21] Y. Zheng, S. Englander, S. Baloch, E. Zacharaki, Y. Fan, M. Schnall, and D. Shen, "STEP: Spatiotemporal enhancement pattern for MR-based breast tumor diagnosis," *Medical physics*, vol. 36, no. 7, pp. 3192–3204, Jul. 2009.
- [22] L. A. Meinel, A. H. Stolpen, K. S. Berbaum, L. L. Fajardo, and J. M. Reinhardt, "Breast MRI lesion classification: improved performance of human readers with a backpropagation neural network computer-aided diagnosis (CAD) system," *J Magn Reson Imaging*, vol. 25, no. 1, pp. 89–95, Jan. 2007.
- [23] R. Lucht, M. Knopp, and G. Brix, "Classification of signal-time curves from dynamic MR mammography by neural networks," *Magnetic Resonance Imaging*, vol. 19, no. 1, pp. 51–57, Jan. 2001.
- [24] T. Twellmann, O. Lichte, and T. W. Nattkemper, "An adaptive tissue characterization network for model-free visualization of dynamic contrast-enhanced magnetic resonance image data," *IEEE Transactions on Medical Imaging*, vol. 24, no. 10, pp. 1256–1266, Oct. 2005.
- [25] K. Nie, J.-H. Chen, H. J. Yu, Y. Chu, O. Nalcioglu, and M.-Y. Su, "Quantitative Analysis of Lesion Morphology and Texture Features for Diagnostic Prediction in Breast MRI," *Acad Radiol*, vol. 15, no. 12, pp. 1513–1525, Dec. 2008.
- [26] C. McLaren, W. Chen, K. Nie, and M. Su, "Prediction of Malignant Breast Lesions from MRI Features: A Comparison of Artificial Neural Network and Logistic Regression Techniques," *Academic radiology*, vol. 16, no. 7, pp. 842–851, Jul. 2009.
- [27] T. W. Nattkemper, B. Arnrich, O. Lichte, W. Timm, A. Degenhard, L. Pointon, C. Hayes, and M. O. Leach, "Evaluation of radiological features for breast tumour classification in clinical screening with machine learning methods," *Artif Intell Med*, vol. 34, no. 2, pp. 129–139, Jun. 2005.
- [28] J. Levman, T. Leung, P. Causer, D. Plewes, and A. L. Martel, "Classification of Dynamic Contrast-Enhanced Magnetic Resonance Breast Lesions by Support Vector Machines," *IEEE Trans. Med. Imaging*, vol. 27, no. 5, pp. 688–696, May 2008.
- [29] A. Basavanthally, S. Doyle, and A. Madabhushi, "Predicting classifier performance with a small training set: Applications to computer-aided diagnosis and prognosis," in *Proceedings of the IEEE International Symposium on Biomedical Imaging: From Nano to Macro*, 2010, pp. 229–232.
- [30] S. H. Lee, J. H. Kim, N. Cho, J. S. Park, Z. Yang, Y. S. Jung, and W. K. Moon, "Multilevel analysis of spatiotemporal association features for differentiation of tumor enhancement patterns in breast DCE-MRI," *Med Phys*, vol. 37, no. 8, pp. 3940–3956, Aug. 2010.
- [31] F. Soares, M. M. Freire, M. Pereira, F. Janela, and J. Seabra, "Towards the detection of microcalcifications on mammograms through Multifractal Detrended Fluctuation Analysis," in *Proceedings of the IEEE Pacific Rim Conference on Communications, Computers and Signal Processing*, 2009, pp. 677–681.
- [32] Q. Guo, J. Shao, and V. Ruiz, "Characterization and classification of tumor lesions using computerized fractal-based texture analysis and support vector machines in digital mammograms," *International Journal*

- of *Computer Assisted Radiology and Surgery*, vol. 4, no. 1, pp. 11–25, 2009.
- [33] P. Kestener, J. M. Lina, P. Saint-Jean, and A. Arneodo, “Wavelet-based multifractal formalism to assist in diagnosis in digitized mammograms,” *Image Anal Stereol*, vol. 20, no. 3, pp. 169–174, 2001.
- [34] J. W. Kantelhardt, S. A. Zschiegner, E. Koscielny-Bunde, S. Havlin, A. Bunde, and H. E. Stanley, “Multifractal detrended fluctuation analysis of nonstationary time series,” *Physica A: Statistical Mechanics and its Applications*, vol. 316, no. 1–4, pp. 87–114, Dec. 2002.
- [35] C.-K. Peng, S. V. Buldyrev, S. Havlin, M. Simons, H. E. Stanley, and A. L. Goldberger, “Mosaic organization of DNA nucleotides,” *Physical Review E*, vol. 49, no. 2, p. 1685, Feb. 1994.
- [36] P. Oświecimka, J. Kwapień, and S. Drożdż, “Wavelet versus detrended fluctuation analysis of multifractal structures,” *Physical Review E*, vol. 74, no. 1, Jul. 2006.
- [37] F. Soares, I. Sousa, F. Janela, J. Seabra, M. Pereira, and M. M. Freire, “Multifractal analysis of Arterial Spin Labeling functional Magnetic Resonance Imaging of the brain,” in *Proceedings of the IEEE International Workshop on Medical Measurements and Applications*, 2010, pp. 161–164.
- [38] R. Lopes and N. Betrouni, “Fractal and multifractal analysis: A review,” *Medical Image Analysis*, vol. 13, no. 4, pp. 634–649, Aug. 2009.
- [39] G.-F. Gu and W.-X. Zhou, “Detrended fluctuation analysis for fractals and multifractals in higher dimensions,” *Physical Review E*, vol. 74, no. 6, p. 061104, Dec. 2006.
- [40] H.-O. Peitgen, H. Jürgens, and D. Saupe, *Chaos and Fractals: New Frontiers of Science*. Springer, 1993.
- [41] J. Delour, J. F. Muzy, and A. Arnéodo, “Intermittency of 1D velocity spatial profiles in turbulence: a magnitude cumulant analysis,” *Eur. Phys. J. B*, vol. 23, no. 2, pp. 243–248, Sep. 2001.
- [42] H. Wendt, P. Abry, and S. Jaffard, “Bootstrap for empirical multifractal analysis,” *IEEE Signal Processing Magazine*, vol. 24, no. 4, pp. 38–48, 2007.
- [43] T. Joachims, *Making large-scale SVM learning practical*. MIT press, 1999.
- [44] J. Levman and A. Martel, “Computer-aided diagnosis of breast cancer from magnetic resonance imaging examinations by custom radial basis function vector machine,” in *Proceedings of the 32nd Annual International Conference of the IEEE Engineering in Medicine and Biology Society*, 2010, pp. 5577–5580.
- [45] I. Guyon, J. Weston, S. Barnhill, and V. Vapnik, “Gene Selection for Cancer Classification using Support Vector Machines,” *Machine Learning*, vol. 46, no. 1–3, pp. 389–422, Jan. 2002.
- [46] E. R. DeLong, D. M. DeLong, and D. L. Clarke-Pearson, “Comparing the areas under two or more correlated receiver operating characteristic curves: a nonparametric approach,” *Biometrics*, pp. 837–845, 1988.
- [47] C. Kuhl and H. Schild, “Dynamic image interpretation of MRI of the breast,” *Journal of Magnetic Resonance Imaging*, vol. 12, no. 6, pp. 965–974, Dec. 2000.

## Chapter 5

### 3D Lacunarity in Multifractal Analysis of Breast Tumor Lesions in Dynamic Contrast-Enhanced Magnetic Resonance Imaging

This chapter consists of the following article:

3D Lacunarity in Multifractal Analysis of Breast Tumor Lesions in Dynamic Contrast-Enhanced Magnetic Resonance Imaging

Filipe Soares, Filipe Janela, Manuela Pereira, João Seabra and Mário M. Freire

*IEEE Transactions on Image Processing*, accepted for publication, 2013.

DOI: 10.1109/TIP.2013.2273669

According to 2012 Journal Citation Reports published by Thomson Reuters in 2013, this journal scored ISI journal performance metrics as follows:

ISI Impact Factor (2012): 3.199

Article Influence Score (2012): 1.642

Journal Ranking (2012): 13/115 (Computer Science, Artificial Intelligence), Quartile: Q1

Journal Ranking (2012): 17/243 (Engineering, Electrical & Electronic), Quartile: Q1



# 3D Lacunarity in Multifractal Analysis of Breast Tumor Lesions in Dynamic Contrast-Enhanced Magnetic Resonance Imaging

Filipe Soares, Filipe Janela, Manuela Pereira, João Seabra, and Mário M. Freire, *Member, IEEE*

**Abstract**—Dynamic contrast-enhanced magnetic resonance (DCE-MR) of the breast is especially robust for the diagnosis of cancer in high-risk women due to its high sensitivity. Its specificity may be, however, compromised since several benign masses take up contrast agent as malignant lesions do. In this paper, we propose a novel method of 3D multifractal analysis to characterize the spatial complexity (spatial arrangement of texture) of breast tumors at multiple scales. Self-similar properties are extracted from the estimation of the multifractal scaling exponent for each clinical case, using lacunarity as the multifractal measure. These properties include several descriptors of the multifractal spectra reflecting the morphology and internal spatial structure of the enhanced lesions relatively to normal tissue. The results suggest that the combined multifractal characteristics can be effective to distinguish benign and malignant findings, judged by the performance of the support vector machine classification method evaluated by receiver operating characteristics with an area under the curve of 0.96. In addition, this paper confirms the presence of multifractality in DCE-MR volumes of the breast, whereby multiple degrees of self-similarity prevail at multiple scales. The proposed feature extraction and classification method have the potential to complement the interpretation of the radiologists and supply a computer-aided diagnosis system.

**Index Terms**—Breast cancer, classification, computer-aided diagnosis, dynamic contrast-enhanced, feature extraction, magnetic resonance, multifractal analysis, texture analysis.

## I. INTRODUCTION

MAGNETIC Resonance Imaging (MRI) of the breast has been shown to be the most sensitive modality for imaging high-risk women, offering valuable information about breast conditions that cannot be obtained by other imaging modalities, such as mammography or ultrasound [1], [2].

Manuscript received August 28, 2012; revised January 28, 2013 and June 2, 2013; accepted June 20, 2013. Date of publication July 17, 2013; date of current version September 17, 2013. This work was supported in part by the Fundação para a Ciência e a Tecnologia under grant SFRH/BDE/15624/2006, the Siemens S.A. Healthcare Sector, the Instituto de Telecomunicações, and the University of Beira Interior, Portugal. The associate editor coordinating the review of this manuscript and approving it for publication was Prof. Ali Bilgin.

F. Soares is with Siemens S.A. Healthcare Sector, Perafita 4456-901, Portugal, and also with the Instituto de Telecomunicações, Department of Computer Science, University of Beira Interior, Covilhã 6201-001, Portugal (e-mail: filipecruzsoares@gmail.com).

F. Janela and J. Seabra are with Siemens S.A. Healthcare Sector, Perafita 4456-901, Portugal (e-mail: filipe.janela@siemens.com; joao.seabra@siemens.com).

M. Pereira and M. M. Freire are with the Instituto de Telecomunicações, Department of Computer Science, University of Beira Interior, Covilhã 6201-001, Portugal (e-mail: mpereira@di.ubi.pt; mario@di.ubi.pt).

Color versions of one or more of the figures in this paper are available online at <http://ieeexplore.ieee.org>.

Digital Object Identifier 10.1109/TIP.2013.2273669

Dynamic contrast-enhanced magnetic resonance imaging (DCE-MRI) techniques are based on the injection of an MR contrast agent and acquisition of T1-weighted images over time, which provides information on the rate of passage of the agent between the blood and tissues. Tumor lesions are more vascularized due to angiogenesis than the surrounding normal tissue, and therefore these areas are distinguished from the background [3].

The diagnosis is generated by visual examination of morphology features and contrast-enhancement kinetics (functional features) using descriptors established in the Breast Imaging - Reporting and Data System (BI-RADS) lexicon [4]. Malignant lesions tend to have more irregular shape, spiculated margins, and heterogeneous inner enhancement [5]. A lesion with kinetics of rapid initial rise, followed by a drop-off with time (washout) in the delayed phase, can have a positive predictive value of 77% for malignancy [6], [7]. Although BI-RADS provides useful criteria, the priority and weights on different morphological features are not standardized. In addition, the analysis of functional features by radiologists is a time consuming task and a bottleneck in diagnostic workflow [8]. Fischer et al. [9] proposed the combination of DCE-MRI morphological and functional features for a scoring system (Göttingen score) that is nowadays useful to assess the BI-RADS grade. The reported values of sensitivity are frequently higher in DCE-MRI than any other breast imaging modality, whereas the specificity has been reported to fluctuate [10]. Indeed, clinical evaluation of breast MRI still remains largely subjective and the reported findings are often qualitative, having therefore an impact on the consistency and reproducibility of the interpretation [11]. Computer assisted interpretation arises in this context as an approach to reduce the subjectivity in human interpretation by improving specificity and possibly sensitivity, through an objective measurement, and offering the possibility of a reduction of the time needed for the breast MRI analysis [12].

To automate lesion classification, features extracted by computer-based image analysis have been investigated as diagnostic aids, with mathematical descriptors related with the ones visually used by radiologists [13]. This approach can be developed towards the quantitative analysis of textural, morphological and kinetic enhancement features.

Considerable efforts have been put on the development of computer-aided diagnosis (CADx) systems that give an impression about the suspicion level of the lesion. The general approach is based on tumor characterization and

the application of automatic or semi-automatic classification. The simplest heuristic model used to distinguish between malignant and benign lesions in DCE-MRI is known as the three-time-points (3TP), [3], [14], where points are selected along the time-intensity sequence during contrast uptake to characterize the enhancement slope and the washout rate. The enhancement patterns in the 3TP method varies depending on imaging protocol, but all of the first post contrast series of malignant tumors with wash-out behavior in late phase do not show the peak contrast enhancement. Nevertheless, a plethora of other algorithms and classifiers have been proposed. The automated interpretation approach based on enhancement variance dynamics proposed by Chen *et al.* [15] used linear discriminant analysis for lesion classification after feature extraction. Later in [16], Chen *et al.* used the fuzzy c-means clustering technique to identify kinetics. For quantitative morphology analysis, Gilhuijs *et al.* [17] employed radial gradient histogram and other shape measures. Yao *et al.* proposed in [18] a pixel-by-pixel classification method based on texture analysis and wavelet transform for tumor evaluation in breast DCE-MRI. In [19], Zheng *et al.* used spatiotemporal enhancement pattern and Fourier transform to analyze two-dimensional images of breast tumors. Back-propagation neural network classification of segmented tumor regions was proposed by Meinel *et al.* [20] using a combined set of shape and kinetic features. The method for classification proposed by Nattkemper *et al.* [21] also includes both kinetic and morphological features and compares several classifiers of both unsupervised and supervised learning. Artificial neural networks have been one of the most investigated approaches for the classification of breast lesions in DCE-MRI [22]–[25]. However, it has been shown that support vector machine (SVM) lead to a better performance than a variety of other machine learning techniques when applied in discrimination of breast lesions [21], [26], [27].

Diagnostic findings in MR images of the breast may be disguised with respect to the surrounding features [28], since, for instance, non-mass vascular structures can dynamically enhance as malignant masses. In addition, some of the aforementioned studies that use classifiers of breast lesions in DCE-MRI apply a region analysis based on thresholding the enhancement signal [29], [30]. Once the signal intensity depends on the particular MRI instrumentation and contrast agent used in data acquisition, even fitting a pharmacokinetic model to the rise of intensities after contrast injection, there is no general approach for selecting threshold values. These methods require careful user interaction [31], hence other model-free approaches may be more suitable for classification of lesions with therapeutic changes of tissue perfusion and microvascular permeability.

Currently, the only fully-automated classification with reported use in the clinical practice is the one available in the first MRI CADx system DynaCAD® which solely relies on morphological analysis. The research behind this system is based on fractal theory as described by Penn *et al.* in [32], and focused on assessing the margin sharpness of the breast lesions, which is only one of the possible ways to analyze tissues in the breast [15], [17], [30], [33]. Moreover, a CADx

system should also work as a second-look for the radiologist and therefore focus on a comprehensive set of characteristics of the lesions, including features that are indistinguishable to the human eye.

The fractal theory and the human tissue are related since both can be characterized by a high degree of self-similarity. In this context, self-similarity refers to images that have several parts looking like the whole image. When self-similar objects are evaluated, the irregularities are then considered as structural deviations from the global regularity of the background [34], [35]. In [36], Penn *et al.* have shown that nearly two thirds of the cancers were categorized inconclusive in terms of fractal dimension. A potential problem with the fractal dimension approach is that distinct fractal sets may share the same fractal dimension values with different appearances or texture patterns [37]. Therefore, the concept of lacunarity was introduced as a scale-dependent measure that describes the texture of a spatial pattern as a counterpart measurement of fractal dimension. Lacunarity explicitly characterizes the spatial organization of an image, and its composing sub-units, which are potentially useful in representing the tumor inner structure. From the anatomical point of view, the lacunarity helps to estimate the spatial heterogeneity of the lesions when the object complexity given by fractal dimension is not enough. Guo *et al.* [38] explored the use of fractal and lacunarity analysis independently for the characterization of the spatial distribution of the pixel intensities and classification of mammographic images. Lacunarity was an effective counterpart measure of texture analysis. Both fractal and lacunarity studies rely on a measure as a function of scale. However, multifractal theory introduces a more advanced approach that allows a deeper exploration of the potential of the theory for medical image analysis. The multifractal analysis provides a spectrum of fractal dimensions, characterizing multiple irregularities. This can potentially provide more information about the image compared to the single fractal dimension [39], without being exclusively focused on lesion margins as in [36]. To the best of our knowledge, there are no further conclusive results of multifractal-based analysis in DCE-MR images of the breast. The closest work uses the Multifractal Detrended Fluctuation Analysis (MF-DFA) method [34] applied only in 2D Mammography, based on the structure of fluctuations and detrending steps without employing the lacunarity dimension. In this paper, we show how multifractal analysis may depend on the concept of lacunarity, when used for the description of the spatial distribution of the pixel intensities in image volumes with multiscaling behaviors.

Some studies have also been designed with the extraction of features in tri-dimensional (3D) volumes of interest (VOI). The performance is likely to improve when taking full advantage of the 3D nature of the MR data. In [17], a 3D analysis was compared to two-dimensional (2D) analysis using a representative slice through the middle of the lesion. 3D was found to result in higher performance for the majority of the shape-based features. However, the manual lesion segmentation employed there would limit the inclusion of this technique in an automated CAD. Automatic segmentation has been shown to be useful when evaluating state-of-art features

in 2D or 3D [40]. This is mainly due to the fact that these features rely on lesion morphology, and segmentation reduces the influence of normal tissue of the breast surrounding a tumor on that features. On the other side, usually the surroundings (background) of the lesions are not included in the analysis of texture complexity. The possible inner inhomogeneity of a mass and its relation to normal background is frequently ignored. Besides, most of 3D segmentation algorithms demand the use of connected-component labeling post-processing to remove scattered voxels not connecting to the main lesion [41]. This can lead to the modification of the original shape of the segmented tumor and classification errors. Moreover, sharp changes of the patterns of enhancement on border slices of a segmented tumor are known to occur with most of the techniques based on slice by slice assessment of the morphology. This results in lower specificity, probably caused by partial volume or the recently studied morphological blooming effect [32]. Blooming evaluates the transition of the margin to the surroundings by a progradient unsharpness of lesion borders, however, the spatial volumetric dependency was not investigated and multifractal approach has been also neglected as in [8]. Multifractal methods have the advantage of exploiting the differences in self-similarity properties between lesion and surrounding background. We therefore hypothesized that, in the task of distinguishing between malignant and benign breast lesions on DCE-MRI, multifractal texture analysis with lacunarity, as the multifractal measure, based on 3D isotropic volumes would yield improved performance than single or multi-slice 2D methods, whereas avoiding 3D segmentation and other post-processing.

In this article, we investigate the use of multifractal theory conditioned by the 3D lacunarity measure, for classification of breast lesions in DCE-MR volumes. We aim to evaluate new features for classification which characterize in more detail the morphology and texture of the contrast-enhanced breast lesions. This aim is accomplished by automated extraction of features from the multifractal scaling exponent and SVM-based classification of malignant and benign lesions. In order to study the irregularity patterns within a tumor relatively to its surroundings, the volumes selected include the normal background around the main lesion. The results obtained with the proposed method are compared within the same experimental setup with the MF-DFA 2D method, also based on multifractal characteristics, and with the 3TP, which represents a clinical standard for analysis of tumor kinetics.

## II. BACKGROUND AND THEORY

This section describes the theoretical background required to comprehend the proposed method specified in section III.

### A. Multifractal Analysis

Fractal dimensions are estimates of object complexity. They were originally developed to characterize geometrical patterns resulting from abstract recursive procedures called fractal processes [37]. Although fractal dimensions were developed for application to abstract mathematical objects, they can be

applied to objects that do not arise from fractal processes, such as MR images [42], [43].

Fractals are self-similar in the sense that they have the same scaling properties, characterized by only one singularity exponent throughout the entire process. This means that when a part of a structure is removed and compared with the whole, they match. Self-similarity is a demanding model with respect to empirical data as it requires that scaling property holds for all scales and that a single Hurst ( $H$ ) parameter controls all the statistical properties of the data. This is often a too severe limitation for practical purposes and multifractal models are preferred instead, which are considered as further extension to scale invariance since they enable to account for a declination of scaling properties often observed on empirical data. Moreover, in the same process we may notice similarity at different scales, located in different areas. This means that multiple fractal sets lie interwoven, each one with their own scaling behavior. Therefore, multifractals require a larger, and theoretically infinite, number of indices to characterize their scaling properties. Scaling refers to the propagation of energy or intensity when for example image data is inspected at various resolutions.

A multifractal object or process can be characterized through its spectrum by assessing which and how many fractal sets are associated to a certain influence (self-similarity trend) on time or space scale. These measures are provided with the dependence of the Hausdorff dimension  $D(h)$  from the Hölder exponent  $h$ , where  $D(h)$  represents the size of a certain trend with impact described by  $h$ . This multifractal spectrum describes the quality and quantity of irregularities in the data and its characteristic shape depends on periodic patterns [44].

A detailed description of the multifractal theory is beyond the scope of this article, but the reader is referred to e.g., [42], [44]. We only restate here a few key points. Multifractal analysis is based on the definition of a finite measure  $\mu$  that can be considered as a mass distribution on a bounded subset of real numbers  $\mathbb{R}^E$ , where  $E$  stands for the Euclidean dimension of the space ( $E = 1, 2$  or  $3$ ). For example, the distribution of a handful of sand on a box in a given point corresponds to the  $\mu$ , a way to assign a numerical size to sets, such that if a set is decomposed into a countable pieces, then the size of the whole is the sum of the pieces sizes. This measure related with scale can estimate the local irregularity within that subset intersecting each cell of a linear grid map of size  $\varepsilon$ , i.e., for a multifractal measure  $\mu$ , the partition function  $X$  has a power law relation with scale  $r\varepsilon$  for variable range of moment order  $q$ , given by [45]:

$$X_q(r\varepsilon) \propto r\varepsilon^{\tau(q)}. \quad (1)$$

For simplicity, the parameter  $q$  can be seen as the focus control of a photographic lens for exploring different regions of irregularity. For  $q > 1$ ,  $\tau(q)$  represents the more singular regions, for  $q < 1$ , it accentuates the less singular regions and for  $q = 1$ , it represents the information dimension. The scaling exponent  $\tau(q)$  has a concave shape that hence departs from the linear behavior  $qH$ , known as the signature of self-similarity.  $\tau(q)$  can be seen as a collection of scaling exponents replacing the single self-similarity parameter  $H$  and, hence, conveying

versatility in actual data analysis [46]. Multifractal analysis is often theoretically phrased in terms of multifractal spectrum  $D(h)$  rather than  $\tau(q)$ , even though both function are related by a Legendre transform [37]. It also requires the measurement of  $q$ , a range that should be carefully chosen according to the data in study to avoid unstable power laws.

### B. Lacunarity Estimation

Lacunarity measures the deviation of a geometric object, such as a fractal, from translational invariance. It is a scale-dependent measure of heterogeneity that allows to distinguish between two fractals with the same fractal dimension. Lacunarity complements the fractal dimension that measures how much space is filled, by measuring how the data fills the space [45], [47], [48].

Lacunarity can be defined in terms of the local first and second moments (i.e., local mean and variance) measured for different neighbourhood sizes about every pixel within the image. Lacunarity as a function of neighbourhood size is generally presented as a double log plot, which illustrates the scale dependency of spatial nonstationarity in the image. Higher lacunarity values indicate more translational invariance, i.e., a wider range of sizes of structures within an image. The decay pattern of the lacunarity plot contains significant information about the spatial structure of the image. For example, a linear decay represents a self-similar fractal with no change in spatial pattern or texture with window size [49].

Based on the analysis of the mass distribution in a deterministic or a random set, Allain and Cloitre [50] proposed a gliding box algorithm for lacunarity estimation. This method involves the assessment of the variance of the box mass  $M$  at each step, where the mass is the sum of white pixels in a gliding box along the coordinates in the Euclidean space. This procedure is repeated as the box moves pixel by pixel through the whole region. The probability distribution,  $Q(M, r)$ , is then calculated as the ratio of the number of gliding boxes with the lateral size  $r$  and mass  $M$  over the total number of boxes. The lacunarity at scale  $r$  is then defined by the mean-square deviation of the fluctuations of mass distribution probability  $Q(M, r)$ , divided by its square mean [50], as follows:

$$\Lambda(r) = \frac{\sum_M M^2 Q(M, r)}{\left[ \sum_M M Q(M, r) \right]^2}, \quad (2)$$

where  $M$  can be calculated according to the purpose of application and problem requirements, since lacunarity estimation is not confined to binary configurations but can also be used with grayscale images [51], [52].

### III. 3D MULTIFRACTAL SCALING EXPONENT LACUNARITY ANALYSIS (MF-SELA)

In this section, the method proposed to characterize the tri-dimensional complexity, or spatial arrangement of texture roughness of breast tumors, is described.

Through the theory it is stated that the dynamics of scaling can be used as discriminatory descriptors, providing an

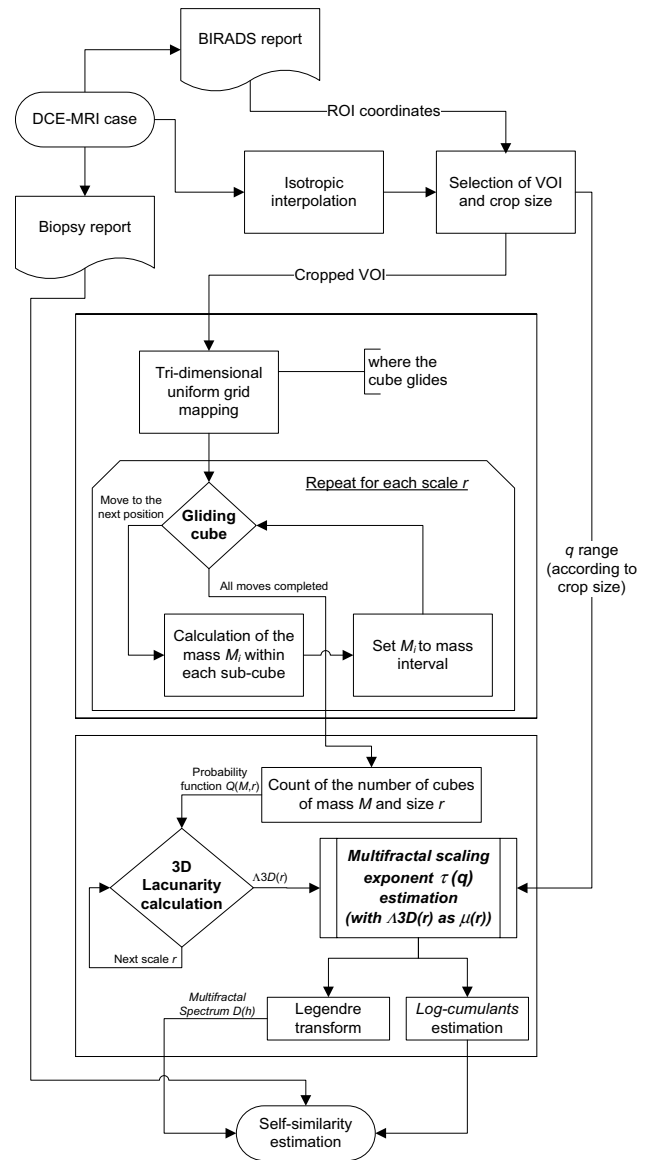


Fig. 1. Flowchart of the model for Multifractal Scaling Exponent Lacunarity Analysis (MF-SELA).

additional perspective of the data when inspected at various resolutions. Furthermore, in this study it was attempted to confirm that selected VOIs from breast MRI have multiple degrees of scaling by the prevalence of a multifractal spectrum  $D(h)$  or a non-linear multifractal scaling exponent  $\tau(q)$ .

Fig. 1 illustrates the flowchart of the model for the decision-support in the diagnosis of breast cancer with DCE-MRI. The cases and respective clinical reports are the input of the model. The analysis scheme proceeds to the pre-processing and selection of a grayscale VOI in which the multiscale extraction of features related with self-similarity, the core of the model, takes place. Herein the framework of the implementation is a gliding cube, which is an extension from the efficient estimation of the gliding box lacunarity presented in [47]. The features are extracted from the estimation of the scaling exponent, taking advantage of using 3D lacunarity as

the measure to feed the multifractal characterization of the VOI, which includes the lesion and surroundings, at multiple scales.

In addition, it is worth notice that in the present work the pixel intensity is not considered as extra dimension, as in [53] and [54]. Dong et al. [48] shown that spatial patterns of 3D points, not images, with different degrees of heterogeneity can be separated using lacunarity, and those that cannot be discriminated from each other at one scale can be separated at some other scales. Also distinct is the work in [55], since a multifractal modeling used to validate an experimental method of lacunarity estimation should not be confused with the multifractal analysis of images proposed here. Our estimation of a scale-dependent degree of heterogeneity given by the lacunarity emerges as the multifractal measure of complexity that will allow the multiscale extraction of features, namely texture and its distribution in each DCE-MRI case.

The entire procedure of the 3D Multifractal Scaling Exponent Lacunarity Analysis (MF-SELA) includes four major steps: (A) Pre-processing and VOI selection, (B) 3D lacunarity estimation with gliding cube, (C) Multifractal analysis with 3D lacunarity, (D) Self-similarity and scaling dynamics as descriptors.

#### A. Pre-Processing and VOI Selection

Voxels are usually anisotropic in breast DCE-MRI, i.e., the spatial resolution in the cross-slice direction is poorer than in plane. Thus, a bi-linear interpolation was used to yield isotropic voxels in the volume image. This pre-processing step is a requirement for the multifractal method proposed, as described below.

A cubic VOI of lateral size between 32 and 64 pixels was cropped from each 3D MRI, according to the location and size of the lesion defined in the BIRADS report by the radiologists. This was performed in a subtraction image, of the first post-contrast acquisition after contrast arrival subtracted from the pre-contrast image. In order to study the inherent properties of the lesions relatively to its surroundings, the VOI includes not only the lesion but also the normal tissue. The effect of the amount of non-lesion background on multifractal analysis was assessed by selecting variable VOI sizes centered in the same lesion point. This coordinates are inputted manually and the remaining stages are fully automated.

#### B. 3D lacunarity Estimation With Gliding Cube

As a base level, we start by mapping a 3D uniform grid where the cube glides. Based on (2) and using accumulated statistical moments as the cube glides through the VOI [47], the gliding cube estimation of lacunarity is proposed herein by

$$\Lambda_{3D}(r) = \frac{N(r) \sum_{i=1}^{N(r)} M_i^2 n(M_i, r)}{\left[ \sum_{i=1}^{N(r)} M_i n(M_i, r) \right]^2}, \quad (3)$$

where for each gliding along every grid position, the mass  $M$  within the  $i$ th cube is carried as well as the running

sums needed to calculate  $n(M, r)$ , here extended to number of cubes with mass  $M$  and lateral size  $r$ , being  $N(r)$  the total number of cubes of size  $r$ . This required a partition of mass intervals for counting purposes and, therefore, an extra parameter of interval precision in our proposed method of lacunarity analysis.  $M$  was calculated for each cube by adding the grayscale intensity values of the voxels contained in the cube divided by the cube volume. This approach revealed better discrimination power in the last steps of the MF-SELA, with our validation experiments, when compared with other alternatives like the relative intensities used in [54] and [55]. The reason why isotropic voxels were required and the images were interpolated is due to the usage of a cubic neighborhood, that constrains the expression of the spatial heterogeneity to translational invariance, in a similar way to [56], [57] for self-similarity estimation.

As  $r$  increases with respect to the base level grid, the procedure raises its efficiency while the number of gliding cubes tends to one and the  $\Lambda_{3D}(r)$  measure tends to zero. Since we are not working with exactly pure self-similar fractals, it is important to calibrate the range of scales according to the empirical data. This problem was already raised in Section II.A concerning multifractal analysis. Too small or too large limits of  $r$  can cause disturbance of linearity in the lacunarity function, as it is common with fractals [58]. Therefore, after calibration with DCE-MRI data, the MF-SELA was parameterized with  $r$  ranged from 6 to VOI size/4. Finally, the complexity of the fundamental operation of 3D lacunarity estimation is  $O(n^3)$ , where  $n$  is the dimension of the interpolated VOI.

#### C. Multifractal Analysis With 3D Lacunarity

Multifractal analysis exploits both the local irregularity (often seen as texture roughness or complexity) of a given object and the global distribution of this irregularity, as reported in [34]. The next step of MF-SELA is the core multifractal analysis of the VOI, to obtain the scaling exponent and multifractal spectrum.

Fractal and multifractal analysis often involves partitioning the space of study into subsets to build samples with multiple scales. The number of the samples at a given scale is limited by the size of the partitioning space and data resolution (sampling resolution), which is usually the main factor influencing statistical estimation. Several techniques have been developed for estimating multifractal  $D(h)$  by means of the box-counting algorithm [39]. Gliding box methods can be integrated into the existing multifractal techniques such as the moment method. Here the multifractal analysis begins with the estimation of  $\tau(q)$  that controls how the moments of measure  $\mu$  scale with  $r$ . Cheng et al. [59] proposed a gliding box alternative for implementing the moment method in multifractal analysis as follows:

$$\langle \tau(q) \rangle + E = \lim_{r \rightarrow 0} \frac{\log \left( \frac{1}{N(r)} \sum_{i=1}^{N(r)} \mu_i^q(r) \right)}{\log r}, \quad (4)$$

where  $\langle \rangle$  stands for statistical moment with measure  $\mu \neq 0$ . This method was generalized for 3D in our implementation.

Consequently, it is possible to obtain larger sampling resolution, precisely one of the common drawbacks of DCE-MR volumes, leading to better statistical results [59].

The measure  $\mu$  in the scope of MF-SELA is defined as the mass distribution given by  $\Lambda 3D(r)$  as

$$\sum_{i=1}^{N(r)} \mu_i^q(r) \equiv \Lambda 3D^q(r). \quad (5)$$

Accordingly, by using (4) and (5) it is possible to obtain the scaling exponent  $\tau(q)$  that can later be used for estimating the multifractal spectrum  $D(h)$  as explained in Section II.A. This approach of a scaling exponent with a gliding box estimation of 3D lacunarity end-up being the key point for multifractal characterization of a VOI, by

$$\langle \tau(q) \rangle + E = \lim_{r \rightarrow 0} \frac{\log \left( \frac{1}{N(r)} \right) \Lambda 3D^q(r)}{\log r}. \quad (6)$$

#### D. Self-Similarity and Scaling Dynamics as Descriptors

The existence of a distribution or spectrum  $D(h)$  may confirm the presence of multifractality, as multiple degrees of self-similarity can be estimated at multiple scales. Given  $\tau(q)$  and  $D(h)$  outcome of multifractal analysis of a VOI, the last step of MF-SELA is the extraction of features related with the spatial arrangement of voxel intensities (texture) in the images of breast tumors. This can be achieved by studying the dynamics of the scaling as multifractal descriptors that may be linked with morphology and internal spatial structure of the enhanced lesions to discriminate.

Different spectral characteristics are quantified from  $D(h)$ , that is directly related with the irregularity of the analyzed object. The higher  $D(h)$ , the more frequently we can find intensity changes of a specific type  $h$ . One important descriptor studied is precisely the  $h$  where the spectrum is maximum. It shows at which Hölder exponents is positioned the most statistically significant part of the VOI, i.e. the subsets with maximum fractal dimension. Hurst parameter ( $H$ ) is often associated with this exponent reminding the monofractal theory where there is only one fractal dimension. Curve width ( $W$ ) can be a descriptor related to how far from monofractal a ROI is. Multifractal analysis focuses on exploring and understanding the nature of the irregularities in the image, and not on a single, most prevalent irregularity, or global trend. Other important descriptors can be right slope ( $RS$ ) of the curve, from the rightmost Hölder point ( $R\alpha$ ) to the maximum  $D(h)$ . On the other side,  $LS$  represents the slope of the distribution of the collection of Hölder exponents below  $H$ , where large fluctuations from the global irregularity (most prevalent) are exploited.

A unique parameter that combines the previous ones has been introduced to better differentiate the MR cases. This suggestion of a single parameter was introduced by [60], with a distinct use of descriptors and with application in brain imaging. The combined spectral parameter ( $CP$ ) proposed in this work for multifractal analysis of DCE-MRI of the breast, is determined as a ratio between  $H$  and  $LS$ . This specific combination leads to low values for simple random

noise intensities of the VOI, and result in high  $CP$  for VOIs containing more complex properties due to tumor presence in self-similar background. Hence, we raise the hypothesis that  $CP$  can be a reasonable measure for distinguishing likelihood of malignancy of breast cancers.

Moreover, an empirical scaling analysis of the multifractal scaling exponent  $\tau(q)$  has been suggested to be studied as a polynomial expansion of order  $p$ [61]

$$\tau(q) = \sum_{p \geq 1} c_p \frac{q^p}{p!}, \quad (7)$$

instead of measuring  $\tau(q)$  by estimation for all  $q$ . The *log-cumulants*  $c_p$  can be obtained from the scale dependence of  $C(j, p)$ , the cumulant of order  $p \geq 1$  and scale  $j$ , of a random variable  $X$ . Equation (7) implies that  $C(j, p)$  must satisfy [62]

$$C(j, p) = c_p^0 + c_p \ln 2^j. \quad (8)$$

Therefore, the study of  $\tau(q)$  and hence  $D(h)$  can be rephrased in terms of the log-cumulants. This is interesting since a process is said to be multifractal when  $\tau(q)$  departs from linear behavior with  $c_2 \neq 0$ . The most practically used *Log-normal* multifractal can be characterized only by  $c_1$  and  $c_2 \neq 0$ , but more complex multifractal models may involve polynomials of higher order than 2. The log-cumulants can be estimated by linear regression, with  $c_1$  being related with the location of the  $H$ , while  $c_2$  with its width, and  $c_3$  possibly characterizing the asymmetry of  $D(h)$ .

This article aims to evaluate if the VOIs from the DCE-MRI of the breast can be represented or not by  $p \geq 2$ ,  $c_p \neq 0$  and thus reveal a simple or more complex multifractal behavior, by rephrasing  $\tau(q)$  in terms of the log-cumulants estimated by linear regression as

$$\tau(q) = c_1 q + c_2 \frac{q^2}{2!} + c_3 \frac{q^3}{3!}. \quad (9)$$

We retain the characteristics that allow differentiating tumoral tissues from healthy tissues. The ranges of multifractal descriptors and log-cumulants which correspond to malignant areas will be set, and classifiers will be obtained.

## IV. EXPERIMENTAL SETUP AND PERFORMANCE ASSESSMENT

The validation of the MF-SELA proposed was carried out using the following experimental setup. Here we provide details about how the images were acquired, what type of lesions were diagnosed by the radiologists and followed by a biopsy intervention resulting in a histological proof, as illustrated in the beginning of the flowchart in Fig. 1. The section ends with the description of a SVM-based supervised learning technique for classification of malignant and benign lesions.

### A. Image Acquisition

Experimental data was acquired using a Siemens Trio 3T MR Scanner at the health institution Clínica João Carlos Costa, Viana do Castelo, Portugal. Written informed consents

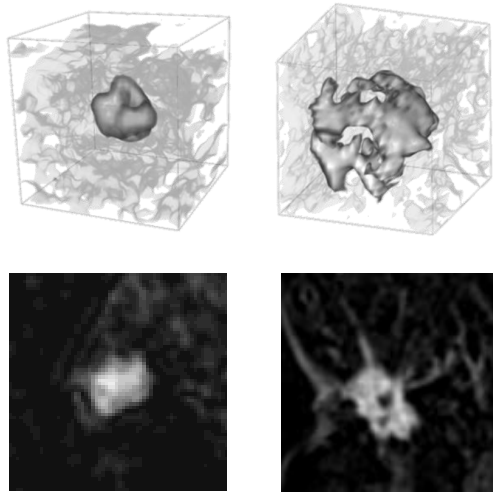


Fig. 2. Morphology features of lesions in the dataset. Representation of tumor VOIs (top). A sliced region of interest of a typical: benign case (bottom left), with oval shaped mass smooth, margin and homogeneous enhancement; malignant case (bottom right), with irregular shaped mass, spiculated margin and heterogeneous enhancement.

were obtained from the patients as well as the approval from the institution’s research ethics committee for this study. Dynamic imaging was performed using a T1-weighted FLASH 3D (FL3D) pulse sequence with fat saturation. The patients were scanned in prone position using a standard double breast coil. The acquisition protocol parameters were 3.76 ms of repetition time, 1.38 ms of echo time with flip angle = 12°. Each slice contains 448 × 448 pixels and has a typical field of view of 30 × 30 cm<sup>2</sup>, yielding an in-plane spatial resolution of 0.65 × 0.65 mm<sup>2</sup> and a slice thickness of 0.6 mm for the generated 3D volumes. Imaging is performed before and after a bolus intravenous injection of 0.1 mmol/kg of Gadopentetate dimeglumine (Gd-DTPA). Five bilateral axial acquisition series were taken per patient at intervals of 1 min and 51 seconds. The first post-contrast images acquired after contrast arrival were used for the analysis of the enhanced lesions since it was found that the information from the initial portion of the time was the most predictive of malignancy as reported in [41] and [63].

**B. Tumor Collection and Diagnosis**

The initial database of 130 consecutive clinical cases was collected from August 2009 to May 2011 and retrospectively analyzed, not including vascular structures, architectural distortions and other non-masses. It is important to note that in this work “case” refers to a physical lesion, not a patient. Patients were previously checked for renal function as part of clinical routine for MR contrast administration. No pregnant women were included and patients with breast implants posed additional difficulties and they were excluded from the present analysis in breast DCE-MR. There was no exclusion criterion concerning the type of benign or malignant tumor.

A diagnosis report was processed by radiologists with a BI-RADS grade assigned for each case, depending on the

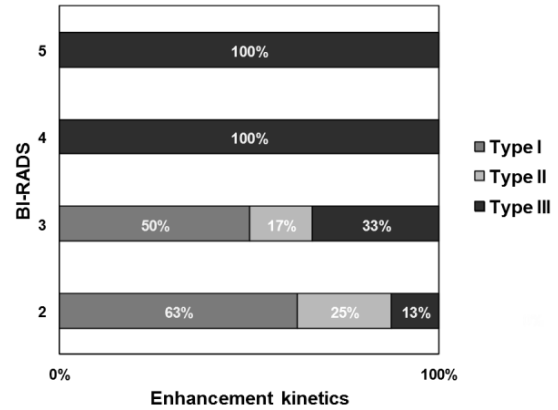


Fig. 3. BI-RADS grade of the lesions in the dataset plotted against the kinetic curve types of contrast enhancement as determined by radiologist.

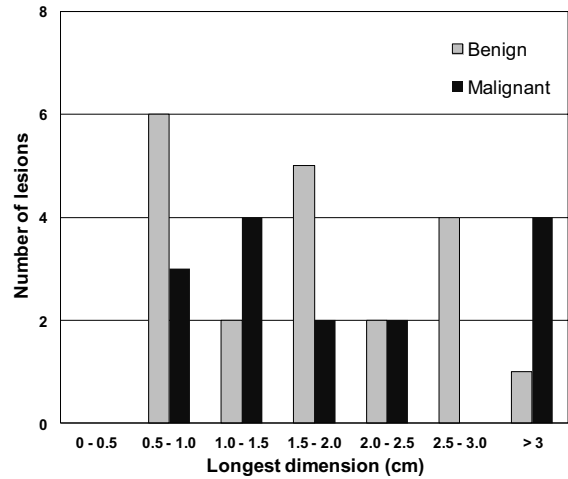


Fig. 4. Histogram of the longest diameter of the lesions in the dataset. The longest diameter was measured where the lesion was best visualized as determined by radiologist.

morphology (see Fig. 2) and dynamic enhancement (Fig. 3) of each finding. A total of 35 lesions had biopsy recommendation and underwent to histological examinations. According to these pathology-proven cases, the clinical positive predictive value for biopsy was only 62% and, for that reason, these cases were included in our analysis. Consequently, the working dataset is composed of 15 malignant and 20 benign lesions. Table I shows the histopathology and disease state of the clinical cases analyzed. The most prevalent type of benign lesion was the fibroadenoma, being the invasive ductal carcinoma the most prevalent among the malignant histological proofs. The sizes of the lesions are evenly distributed among the malignancy (see Fig. 4). The longest diameter was estimated by radiologists using an electronic ruler, where the lesion was best visualized. Focus and foci are enhancements measuring less than 5 mm in diameter that are too small to be characterized in MR data and cannot be otherwise specified. These lesions are typically stable on follow-up, may result from hormonal changes and are considered to be a part of the normal background enhancement pattern in the breast [4] and [6].

TABLE I  
CLINICAL CASES IN THE DATASET

Case ID	Patient ID	Longest dimension (cm)	BIRADS	Histopathology	Disease state
01	P01	2.5	5	IDC	Malignant
02	P02	2.8	3	Fibroadenoma	Benign
03	P03	1.9	4	Sclerosing Adenoma	Benign
04	P04	1.6	4	DCIS	Malignant
05	P05	1.8	3	Fibrocystic changes	Benign
06	P06	1.4	6	DCIS	Malignant
07	P07	2.8	2	Fibroadenoma	Benign
08	P08	1.7	3	PASH	Benign
09	P09	0.8	4	Myoepithelial cells	Benign
10	P10	6.8	6	IDC	Malignant
11	P11	4.2	4	PASH	Benign
12	P12	2.9	2	Fibrocystic changes	Benign
13	P13	0.5	4	IDC	Malignant
14	P14	3.8	6	IDC	Malignant
15	P15	1.4	6	DCIS	Malignant
16	P16	1	4	Fibroadenoma	Benign
17	P17	0.9	3	DCIS	Malignant
18	P18	2	4	Stromal fibrosis	Benign
19	P19	2.9	2	Fibroadenoma	Benign
20	P19	1.5	3	Lymph node	Malignant
21	P20	4.1	5	IDC	Malignant
22	P20	7.8	5	DCIS	Malignant
23	P21	1.3	4	LCIS	Malignant
24	P21	0.8	4	IDC	Malignant
25	P22	1	4	Fibroadenoma	Benign
26	P23	2.5	2	Fibroadenoma	Benign
27	P23	1.5	2	Fibroadenoma	Benign
28	P23	1.8	2	Fibroadenoma	Benign
29	P24	2.4	6	IDC	Malignant
30	P25	0.7	2	Fibroadenoma	Benign
31	P26	2.3	2	Fibrocystic changes	Benign
32	P26	1.3	4	Fibroadenoma	Benign
33	P26	1.8	4	DCIS	Malignant
34	P27	0.7	3	Fibrocystic changes	Benign
35	P27	0.6	4	Fibrocystic changes	Benign

Ductal Carcinoma In Situ (DCIS), Invasive Ductal Carcinoma (IDC), Lobular Carcinoma In Situ (LCIS), Pseudo-angiomatous Stromal Hyperplasia (PASH).

The final cohort of patients had an average age of  $47 \pm 9$  years and an average weight of  $66 \pm 6$  kg.

### C. SVM-Based Classification

Classification of tumors as malignant or benign was performed by applying SVMs with the extracted multifractal-based features, each SVM using just a single feature. The role of multifractal descriptors and log-cumulants are still and

open problem for the characterization of tumors. The single feature independent classification was adopted instead of using all features jointly to better understand ROC curve differences, among all of these features with distinct theoretical meaning. SVM-based classification was performed using the SVM<sup>light</sup> [64] open source package for its efficient optimization algorithm, which allows choosing multiple kernel functions and its parameters to obtain a different classification hyperplane. Radial Basis Function (RBF) that requires the parameter  $\gamma$  was the kernel used in this work. The condition for optimal hyperplane also includes a regularization parameter  $C$  that controls the trade-off between maximization of the margin and minimization of the training error. Small  $C$  tends to emphasize the margin while ignoring the outliers in the training data, while large  $C$  may tend to over fit the training data.

In order to determine which type of kernel function to use, its associated parameters, and  $C$  in the structural risk function, i.e. to select the possibly optimal model for our classification problem, we applied Leave-one-out (LOO) cross-validation to the working dataset [64]. This LOO technique involves training the machine learning algorithm for estimating the likelihood of malignancy from all cases but one, testing classification on that single case. This procedure is repeated until each case has been tested individually. The cross-validation ensures that all elements of the dataset are may be used for both training and testing. Misclassification errors were averaged to obtain an estimate of the generalization error of the SVM classifier. Our approach to yield the best classification based on each feature was to choose the parameters of SVM that produce the model with smaller errors in the cross-validation and use it for testing in order to maximize the accuracy.

### D. ROC Analysis

The capability of the features in distinguishing between malignant and benign lesions are further examined and evaluated by receiver operating characteristics (ROC). The area under the ROC curve ( $A_z$ ) was used as a performance measure of the discrimination power of the individual features and of the SVM classification in a LOO scheme.

In order to more accurately place our method in the landscape of breast lesions classification, we applied a clinical standard protocol, the 3TP technique, to our dataset. On the other hand, we sought to evaluate the effect of skipping the lacunarity measure in the multifractal analysis to better understand the source of our performance. As lacunarity is intrinsically associated to the 3D analysis in the method proposed, we used a previously implemented 2D multifractal analysis (MF-DFA 2D) for comparison in the same setup, also evaluated with ROC analysis.

## V. RESULTS

The first major validation of the applicability of the methodology was achieved by verifying that the data possess multiple scaling properties. Fig. 5 shows the multifractal spectra of the analyzed VOIs where several degrees of scaling prevail for all

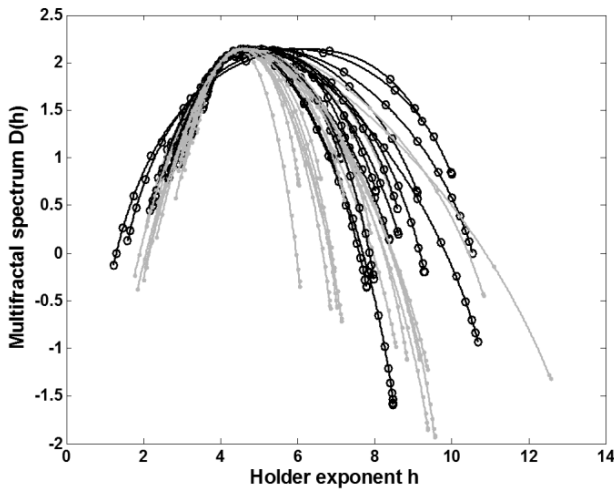


Fig. 5. Multifractal spectra  $D(h)$  of the VOIs of the cases in the dataset. Benign cases in gray. Malignant cases in black.

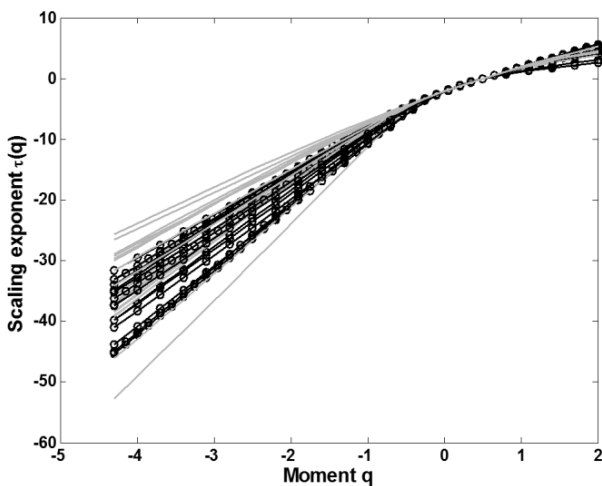


Fig. 6. Multifractal scaling exponent  $\tau(q)$  of the VOIs of the cases in the dataset. Benign cases in gray. Malignant cases in black.

the cases, as they are not limited to a single Hölder exponent. We can see that the  $D(h)$  curves are quite similar in shape and span. However, looking solely at the spectra the distinction between benign and malignant tumors remains unclear. In order to characterize the multifractal spectra of the VOIs from the clinical cases studied, the aforementioned (see Section III-D) spectral descriptors were quantified. Another verification of the multifractality resulted from studying scaling exponent  $\tau(q)$  (see Fig. 6) through the estimation of log-cumulants, as it may be confirmed in Fig. 7 that  $c_1$  and  $c_2 \neq 0$ . The concavity of  $\tau(q)$  in Fig. 6 implies non-normalized values of  $c_2 \neq 0$ .

All features investigated in this study show moderate potential for distinguishing between benign and malignant lesions, relating the measurements in Fig. 7 (top) directly with likelihood of malignancy. However, false negatives arise as represented by the outliers from the top in the benign boxes. Those report cases with a strong enhancement and

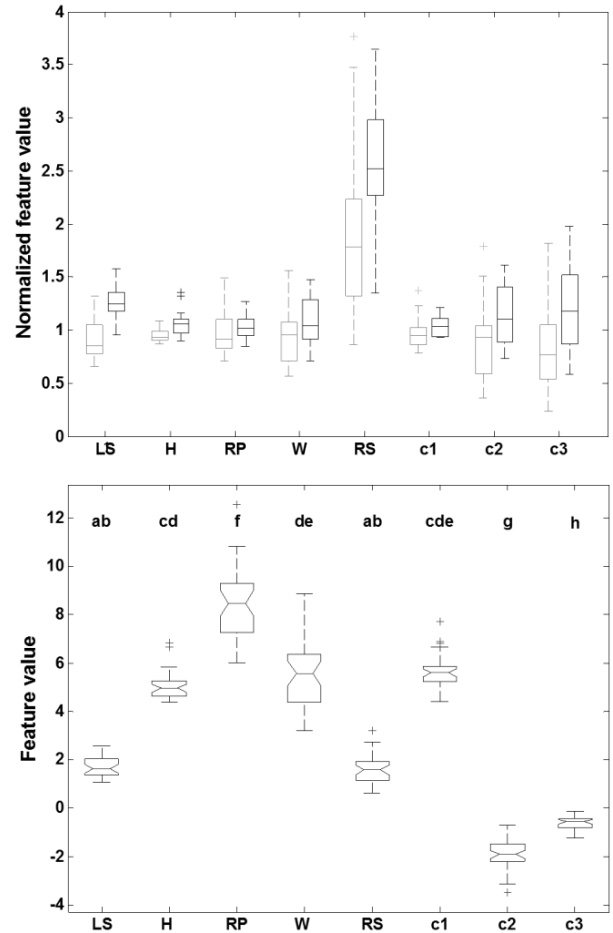


Fig. 7. Comparison of multifractal descriptors and log-cumulants as features. Top: For each feature normalized by its mean value, benign cases in gray and malignant cases in black. Bottom: Pooled features values tested for statistically significant differences with One-way ANOVA resulting in  $F$ -statistic = 588.32 and  $p$ -value < 0.05. Statistically significant differences among descriptors are identified by letters according to Post-Hoc Tukey test.

all morphological characteristics of malignancy. In addition, false positives occur in-between zone of the box-plots from benign and malignant groups. This had reinforced the need for a better multifractal descriptor. A statistical analysis was further conducted by One-way analysis of variance (ANOVA) followed by a Post-Hoc Tukey test corrected for multiple comparisons (see Fig. 7, bottom).  $CP$  was proposed as several descriptors (with statistically significant differences) were combined and  $H$  (strongest irregularity) against  $LS$  (inner enhancement) resulted better than the others.

Fig. 8 and Table II present the performance of the proposed method evaluated by the area under the ROC curve for the SVM classifiers using each feature. Smoothed ROC curves were generated according to the binormal model [66]. The  $A_z$  of the discrimination was calculated varying a threshold level on each feature to separate benign and malignant groups. For all features analyzed, it is observed that SVM classification produced higher  $A_z$  values than the discrimination alone. The combined parameter  $CP$  and the individual  $LS$  and  $RS$  stand

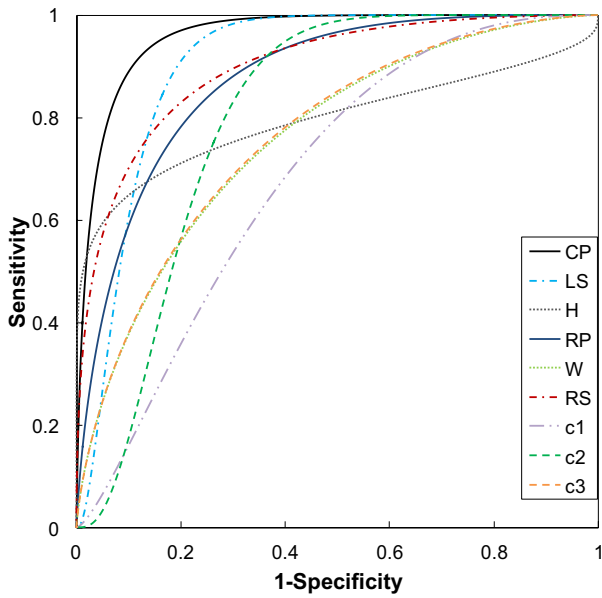


Fig. 8. ROC curves comparing the classification performance of the multifractal features and the combined parameter (*CP*) using SVM with a leave-one-out testing.

out as better features with higher  $A_z$  and lower testing error (TE) with SVM. The complementary shape of the ROC curves from *H* and *LS* justifies the maximum  $A_z$  obtained with *CP*. Statistically significant differences ( $p$ -value  $< 0.05$ ) were found between  $A_z$  corrected for multiple pairwise comparisons (using MEDCALC): *CP* vs. *H*, *W*, *c1* and *c3*.

It is also worth noting that for the estimation of  $\tau(q)$  several ranges of  $q$  were tested (results not shown), leading to an optimal discrimination power of lesions with  $-4.3 < q < 2.1$  for the problem in study. The chosen  $q$  range includes interval steps adapted for the multiple sizes of VOI tested according to our DCE-MRI data to avoid unstable power laws and statistical errors leading to better ROC performance, without compromising the computational performance. The average execution time per case of the entire MF-SELA is 7.89 s, on a 2.53-GHz Intel@Core™i5 M540 workstation.

Table III presents the  $A_z$  obtained when applying three different methods to our dataset: 3TP, another multifractal approach MF-DFA 2D and MF-SELA 3D. The  $A_z$  obtained with the multifractal methods is well above the 3TP performance.

## VI. DISCUSSION

DCE-MRI is useful in evaluating lesions that appear morphologically benign on conventional imaging studies. Diverging results were published concerning the diagnostic value of the lesion enhancement rate in the time course data [3]. Radiologists identify cancers with benign-like kinetics and normal tissues that exhibit cancer-like morphology. Therefore, we suggest that further features might be beneficial for the diagnosis of a breast cancer. In the early post-contrast period, it is established that the enhancement serves as a differential diagnostic criterion, with malignant lesions exhibiting stronger

TABLE II  
AREA UNDER THE ROC CURVE  $A_z$  IN DISCRIMINATING MALIGNANT FROM BENIGN LESIONS WITH MULTIFRACTAL-BASED FEATURES.  $A_z$  OF THE SVM CLASSIFIER USING EACH FEATURE (LEAVE-ONE-OUT CROSS-VALIDATION)

Feature	Discrimination		SVM classification				
	$A_z$	( $\pm$ STD)	$A_z$	( $\pm$ STD)	$\gamma$	$C$	TE
<i>CP</i>	0.868	0.050	0.960	0.027	6	10	0.1429
<i>LS</i>	0.896	0.050	0.901	0.055	6	10	0.2286
<i>H</i>	0.786	0.076	0.795	0.076	6	10	0.2286
<i>RP</i>	0.617	0.097	0.873	0.062	8	10	0.1714
<i>W</i>	0.643	0.091	0.760	0.081	6	100	0.2571
<i>RS</i>	0.726	0.091	0.898	0.063	6	1000	0.1714
<i>c1</i>	0.672	0.079	0.685	0.086	0.6	10	0.3143
<i>c2</i>	0.695	0.087	0.800	0.061	6	100	0.2286
<i>c3</i>	0.736	0.087	0.763	0.076	2	1000	0.2571

*Gamma*  $\gamma$  and regularization parameter ( $C$ ) as associated kernel parameters and corresponding expected testing error (TE).

and faster enhancement than benign changes do [4]. In fact, this was verified in our preliminary experiments in [35] and confirmed in this work. We found that the information from the initial portion of the time was the most predictive of malignancy and, consequently, the first post-contrast images acquired after contrast arrival were used for the analysis of the enhanced lesions.

The proposed MF-SELA (see Fig. 1) establishes a multifractal analysis with a tri-dimensional lacunarity  $\Lambda 3D(r)$  as measure to obtain the scaling exponent and multifractal spectrum.  $\Lambda 3D(r)$  is estimated using the gliding cube method, with the advantage of large sample size that usually leads to better statistical results. Self-similarity features of the  $\tau(q)$  and  $D(h)$ , automatically generated for each early post-contrast volume image acquired after contrast arrival, were analyzed quantitatively. This quantification of features values should not be confused with the quantification of signal intensity values of voxels.

For our working dataset, the radiologists from the medical institution where the images were acquired reported 60% of specificity at 87% of sensitivity as diagnostic performance. Experimental results shown here by ROC curves reveal higher specificity at the same level of sensitivity with five features (*CP*, *LS*, *RS*, *RP* and log-cumulant  $c_2$ ) derived from multifractal theory. SVM-based classification of the likelihood of malignancy of breast tumors showed good performance with VOIs containing mass lesions and their surroundings. Results suggest that *CP* and *LS* are the most appropriate feature for characterizing the inner texture heterogeneity of a VOI at different scales, with higher values for malignant cases. ROC analysis demonstrated that approximations of the  $\tau(q)$  by the log-cumulants does not provide a complete characterization of the texture with sufficient discrimination power. However,

TABLE III  
ROC  $A_z$  OF 3TP AND TWO MULTIFRACTAL METHODS ON OUR DATASET OF 35 CASES

Method	3TP	MF-DFA 2D	MF-SELA 3D
$A_z$	0.71	0.87	0.96

the SVM classifier using the feature  $c_2$  produced the best performance among the log-cumulants, with higher  $A_z$  than its theoretically related  $W$ . The main benefit of the log-cumulant triplet  $(c_1, c_2, c_3)$  was to emphasize the difference between  $\tau(q)$  that departed from linear in  $q$ . This was confirmed in practice by approximating the function  $\tau(q)$  with limited number of  $c_p$  that could simplify the classification task based on multifractal analysis.

For the computer-extracted features to be accepted, the link with morphology descriptors defined in BI-RADS lexicon needs to be established. Concerning lacunarity nothing should be discussed as its value was not directly used as a feature, but as a multifractal measure to compute the spectra  $D(h)$ . However, regarding self-similarity, it was found that  $H$  was related with the most prevalent irregularity in the VOI, namely shape and margins.

The descriptor  $W$  and log-cumulant  $c_2$  are related to inhomogeneous degree of enhancement regularity (texture) and theoretically how far from monofractal a ROI is.  $W$  is generally bigger in malignant cases that represents richer scaling behavior compared to benign lesions. In addition, the more negative unnormalized value of  $c_2$  the stronger the experimental evidence in favor of multifractality. Negative findings (no enhancement, results not shown) wherein there is nothing to comment on,  $W$  and  $c_2$  tend to zero. False negative detection of findings can be depicted based on this criterion.

The descriptor Hurst parameter ( $H$ ) shows at which Hölder exponents ( $h$ ) is positioned the most statistically significant subsets of VOI voxels with maximum fractal dimension. This is directly related with the irregularity of the analyzed VOI, and it was slightly lower for the benign cases. Besides this prevalent scaling behavior, a multitude of other scalings might be present although occurring much less frequently.

Smaller slopes of  $LS$  reveal further scaling of large fluctuations from the  $H$ . Benign lesions with lower slopes show more sharp transitions of intensities that are different from the global irregularity. The  $RS$  descriptor represents the slope of the distribution of the collection of Holder exponents above  $H$ , where small fluctuations from the global irregularity could be analyzed. Thus, the higher  $RS$  of malignant cases can be seen as a weaker scaling pattern of the smooth variability relative to the most prevalent characteristic irregular  $H$ . On the other hand, for the associated scale parameters ( $q$  and  $r$ ) chosen, the role of  $RP$  translates into the limit where it is possible to define a smooth variation from the global regularity. The bigger the limit for a case, the larger multi-scale heterogeneity is present.

In a general interpretation, the malignant cases are more globally inhomogeneous, show higher contrast-enhanced

TABLE IV  
ROC  $A_z$  AMONG STATE-OF-ART STUDIES ON THEIR DATASETS

Reference	[8]	[15]	[17]	[20]	[26]	[40]	[41]
Dataset size	111	121	28	80	94	121	71
Classifier	SVM	LDA	RR	BNN	SVM	LRA	ANN
$A_z$	0.88	0.80	0.96	0.97	0.74	0.86	0.86

Support vector machines (SVM), linear discriminant analysis (LDA), Round-robin (RR), backpropagation neural network (BNN), linear regression analysis (LRA), artificial neural network (ANN).

changes that are anti-persistent, and lower contrast-enhanced changes with persistence. However, the false-positives in each individual descriptor had lead to a new proposed descriptor ( $CP$ ), which combines previous ones intending to improve the differentiation of the tumor cases.

In computer-aided diagnostics, it is very important to obtain a machine learning model with good generalization, i.e., with good results of predicting the unseen samples. The results obtained in this work suggest that the SVM is an effective method with great potential for classification in DCE-MRI of the breast. SVM improved the classification by producing higher  $A_z$  using each of the nine features than the discrimination power of the features alone.

LOO cross-validation has been shown to give an almost unbiased estimator of the generalization properties of statistical models, and therefore provides a sensible criterion for model selection and comparison [65]. The purpose of using model complexity controlled by the regularization parameter  $C$  in SVM, to constrain the optimization of empirical risk, is to avoid *overfitting*, a situation in which the decision boundary too precisely corresponds to the training data, and thereby fails on data outside the training set.

After comparing 3TP, MF-DFA 2D and MF-SELA 3D in Table III, we attribute the good performance of the proposed working scheme to the employment of the 3D and multifractal analysis in DCE-MRI of the breast. This is the main difference to the closest works with fractal theory that obtained lower classification performance (see [32], [33], [36]).

Table IV presents a comparison of the performance results from previous breast MRI CAD studies [8], [15], [17], [20], [26], [40], [41] in which  $A_z$  ranged from 0.74 to 0.97, on their private datasets. In comparison with those studies, the performance of MF-SELA with SVM feature classification appears to be in high level (0.96 with  $CP$ ). However, the patient population differs in each study among the literature, due to the lack of a public DCE-MRI breast lesions database. Since the  $A_z$  is presumably expected to vary depending on the lesion characteristics, the  $A_z$  comparison can be regarded as less convincing. Moreover, the effects contributing to  $A_z$  variation across populations are diluted in very large databases. Despite the fact that our sample size is small, it is composed solely of cases that underwent biopsy, which usually raise doubts in diagnosis. Therefore, we believe that it represents

a good sample and the comparison of MF-SELA with the studies in Table IV is meaningful.

The developed framework raises the possibility of using measures other than lacunarity in 3D. The discriminatory potential of different 3D measures is yet to be assessed leaving an open topic to explore in the future. Moreover, it would be interesting to study the relation between multifractal parameters and tracer kinetic parameters, as kinetic texture features without having to lose the 3D information of lesions.

The proposed method could be applied to roughly any kind of tumor. A correspondence between the general anatomical structure and the possible feature-based classification of VOI is natural, by the multifractality that may prevail in medical images. The main limitation of it is to assess if the data possess multiple scaling properties or not. It is also predictable that imaging modalities with lower spatial resolution than MRI would lead to inferior discrimination power using similar scaling descriptors. In this case, the method should be calibrated with respect to the lateral size  $r$  of cubic VOI to maintain linearity in the lacunarity function. Moreover, several ranges of  $q$  should be tested for multifractal analysis to avoid unstable power laws and statistical errors.

## VII. CONCLUSION

In this study, we contribute by investigating the feasibility of applying multifractal analysis using 3D lacunarity as a measure to the characterization of image texture. The VOI of the enhanced lesions revealed multiple degrees of scaling, i.e., the prevalence of a multifractal spectrum and a non linear multifractal scaling exponent. After testing the hypothesis that multifractal spectral characteristics could be related with likelihood of malignancy, our results are in line with histological ground-truth. This work suggests that the quantitative assessment of multifractal features, as proposed here, can be translated into a new and more efficient method for classification that could potentially be integrated in a computer-aided diagnosis (CADx).

## REFERENCES

- [1] L. Moy, K. Elias, V. Patel, J. Lee, J. S. Babb, H. K. Toth, and C. L. Mercado, "Is breast MRI helpful in the evaluation of inconclusive mammographic findings?" *Amer. J. Roentgenol.*, vol. 193, no. 4, pp. 986–993, Oct. 2009.
- [2] E. Warner, D. B. Plewes, K. A. Hill, P. A. Causer, J. T. Zubovits, R. A. Jong, M. R. Cutrara, G. DeBoer, M. J. Yaffe, S. J. Messner, W. S. Meschino, C. A. Piron, and S. A. Narod, "Surveillance of BRCA1 and BRCA2 mutation carriers with magnetic resonance imaging, ultrasound, mammography, and clinical breast examination," *J. Amer. Med. Assoc.*, vol. 292, no. 11, pp. 1317–1325, Sep. 2004.
- [3] C. K. Kuhl, P. Mielcarek, S. Klaschik, C. Leutner, E. Wardelmann, J. Gieseke, and H. H. Schild, "Dynamic breast MR imaging: Are signal intensity time course data useful for differential diagnosis of enhancing lesions?," *Radiology*, vol. 211, no. 1, pp. 101–110, Apr. 1999.
- [4] E. A. Morris, "Illustrated breast MR lexicon," *Seminars Roentgenol.*, vol. 36, no. 3, pp. 238–249, Jul. 2001.
- [5] M. D. Schnall, J. Blume, D. A. Bluemke, G. A. DeAngelis, N. DeBruhl, S. Harms, S. H. Heywang-Köbrunner, N. Hylton, C. K. Kuhl, E. D. Pisano, P. Causer, S. J. Schnitt, D. Thickman, C. B. Stelling, P. T. Weatherall, C. Lehman, and C. A. Gatsonis, "Diagnostic architectural and dynamic features at breast MR imaging: Multicenter study," *Radiology*, vol. 238, no. 1, pp. 42–53, Jan. 2006.
- [6] B. Erguvan-Dogan, G. Whitman, A. Kushwaha, M. Phelps, and P. Dempsey, "BI-RADS-MRI: A primer," *Amer. J. Roentgenol.*, vol. 187, no. 2, p. W152, Aug. 2006.
- [7] S. A. Jansen, X. Fan, G. S. Karczmar, H. Abe, R. A. Schmidt, M. Giger, and G. M. Newstead, "DCE-MRI of breast lesions: Is kinetic analysis equally effective for both mass and nonmass-like enhancement?" *Med. Phys.*, vol. 35, no. 7, pp. 3102–3109, Jul. 2008.
- [8] S. H. Lee, J. H. Kim, N. Cho, J. S. Park, Z. Yang, Y. S. Jung, and W. K. Moon, "Multilevel analysis of spatiotemporal association features for differentiation of tumor enhancement patterns in breast DCE-MRI," *Med. Phys.*, vol. 37, no. 8, pp. 3940–3956, Aug. 2010.
- [9] U. Fischer, L. Kopka, and E. Grabbe, "Breast carcinoma: Effect of pre-operative contrast-enhanced MR imaging on the therapeutic approach," *Radiology*, vol. 213, no. 3, pp. 881–888, Dec. 1999.
- [10] D. R. Fischer, P. Baltzer, A. Malich, S. Wurdinger, M. G. Freesmeyer, C. Marx, and W. A. Kaiser, "Is the 'blooming sign' a promising additional tool to determine malignancy in MR mammography?" *Eur. Radiol.*, vol. 14, no. 3, pp. 394–401, Mar. 2004.
- [11] K. Kinkel and N. Hylton, "Challenges to interpretation of breast MRI," *J. Magn. Resonance Imaging*, vol. 13, no. 6, pp. 821–829, Jun. 2001.
- [12] Y. Gal, A. Mehnert, A. Bradley, D. Kennedy, and S. Crozier, "Feature and classifier selection for automatic classification of lesions in dynamic contrast-enhanced MRI of the breast," in *Proc. DICTA*, Dec. 2009, pp. 132–139.
- [13] M. Giger, "Computerized analysis of images in the detection and diagnosis of breast cancer," *Seminars Ultrasound CT MRI*, vol. 25, no. 5, pp. 411–418, Oct. 2004.
- [14] E. Furman-Haran, D. Grobgeld, R. Margalit, and H. Degani, "Response of MCF7 human breast cancer to tamoxifen: Evaluation by the three-time-point, contrast-enhanced magnetic resonance imaging method," *Clinical Cancer Res.*, vol. 4, no. 10, pp. 2299–2304, Oct. 1998.
- [15] W. Chen, M. Giger, L. Lan, and U. Bick, "Computerized interpretation of breast MRI: Investigation of enhancement-variance dynamics," *Med. Phys.*, vol. 31, no. 5, pp. 1076–1–1076-7, Apr. 2004.
- [16] W. Chen, M. L. Giger, U. Bick, and G. M. Newstead, "Automatic identification and classification of characteristic kinetic curves of breast lesions on DCE-MRI," *Med. Phys.*, vol. 33, no. 8, pp. 2878–2887, Aug. 2006.
- [17] K. G. Gilhuijs, M. L. Giger, and U. Bick, "Computerized analysis of breast lesions in three dimensions using dynamic magnetic-resonance imaging," *Med. Phys.*, vol. 25, no. 9, pp. 1647–1654, Sep. 1998.
- [18] J. Yao, J. Chen, and C. Chow, "Breast tumor analysis in dynamic contrast enhanced MRI using texture features and wavelet transform," *IEEE J. Sel. Topics Signal Process.*, vol. 3, no. 1, pp. 94–100, Feb. 2009.
- [19] Y. Zheng, S. Englander, M. D. Schnall, and D. Shen, "STEP: Spatiotemporal enhancement pattern for MR-based breast tumor diagnosis," *Med. Phys.*, vol. 36, no. 7, pp. 3192–3204, Jul. 2009.
- [20] L. A. Meinel, A. H. Stolpen, K. S. Berbaum, L. L. Fajardo, and J. M. Reinhardt, "Breast MRI lesion classification: Improved performance of human readers with a backpropagation neural network computer-aided diagnosis (CAD) system," *J. Magn. Resonance Imaging*, vol. 25, no. 1, pp. 89–95, Jan. 2007.
- [21] T. W. Nattkemper, B. Arnrich, O. Lichte, W. Timm, A. Degenhard, L. Pointon, C. Hayes, and M. O. Leach, "Evaluation of radiological features for breast tumour classification in clinical screening with machine learning methods," *Artif. Intell. Med.*, vol. 34, no. 2, pp. 129–139, Jun. 2005.
- [22] J. Baker, P. Kornguth, J. Lo, M. Williford, and C. Floyd, "Breast cancer: Prediction with artificial neural network based on BI-RADS standardized lexicon," *Radiology*, vol. 196, no. 3, pp. 817–822, Sep. 1995.
- [23] C. McLaren, W. Chen, K. Nie, and M. Su, "Prediction of malignant breast lesions from MRI features: A comparison of artificial neural network and logistic regression techniques," *Acad. Radiol.*, vol. 16, no. 7, pp. 842–851, Jul. 2009.
- [24] R. Lucht, M. Knopp, and G. Brix, "Classification of signal-time curves from dynamic MR mammography by neural networks," *Magn. Resonance Imaging*, vol. 19, no. 1, pp. 51–57, Jan. 2001.
- [25] T. Twellmann, O. Lichte, and T. W. Nattkemper, "An adaptive tissue characterization network for model-free visualization of dynamic contrast-enhanced magnetic resonance image data," *IEEE Trans. Med. Imaging*, vol. 24, no. 10, pp. 1256–1266, Oct. 2005.
- [26] J. Levman, T. Leung, P. Causer, D. Plewes, and A. L. Martel, "Classification of dynamic contrast-enhanced magnetic resonance breast lesions by support vector machines," *IEEE Trans. Med. Imaging*, vol. 27, no. 5, pp. 688–696, May 2008.

[27] A. Basavanthally, S. Doyle, and A. Madabhushi, "Predicting classifier performance with a small training set: Applications to computer-aided diagnosis and prognosis," in *Proc. IEEE Int. Symp. Biomed. Imaging: From Nano to Macro*, Apr. 2010, pp. 229–232.

[28] D. Newell, K. Nie, J.-H. Chen, C.-C. Hsu, H. J. Yu, O. Nalcioglu, and M.-Y. Su, "Selection of diagnostic features on breast MRI to differentiate between malignant and benign lesions using computer-aided diagnosis: Differences in lesions presenting as mass and non-mass-like enhancement," *Eur. Radiol.*, vol. 20, no. 4, pp. 771–781, Apr. 2010.

[29] P. Hayton, M. Brady, L. Tarassenko, and N. Moore, "Analysis of dynamic MR breast images using a model of contrast enhancement," *Med. Image Anal.*, vol. 1, no. 3, pp. 207–224, Apr. 1997.

[30] L. Arbach, A. Stolpen, and J. Reinhardt, "Classification of breast MRI lesions using a backpropagation neural network (BNN)," in *Proc. IEEE Int. Symp. Biomed. Imaging, Nano Macro*, Apr. 2004, pp. 253–256.

[31] Q. Wu and M. Markey, "Computer-aided diagnosis of breast cancer on MR imaging," *Proc. SPIE*, vol. 155, pp. 743–766, Oct. 2006.

[32] A. Penn, S. Thompson, R. Brem, C. Lehman, P. Weatherall, M. Schnall, G. Newstead, E. Conant, S. Ascher, E. Morris, and E. Pisano, "Morphologic blooming in breast MRI as a characterization of margin for discriminating benign from malignant lesions," *Acad. Radiol.*, vol. 13, no. 11, pp. 1344–1354, Nov. 2006.

[33] A. I. Penn, L. Bolinger, M. D. Schnall, and M. H. Loew, "Discrimination of MR images of breast masses with fractal-interpolation function models," *Acad. Radiol.*, vol. 6, no. 3, pp. 156–163, Mar. 1999.

[34] F. Soares, M. M. Freire, M. Pereira, F. Janela, and J. Seabra, "Towards the detection of microcalcifications on mammograms through multifractal detrended fluctuation analysis," in *Proc. IEEE Pacific Rim Conf. Commun., Comput. Signal Process.*, Aug. 2009, pp. 677–681.

[35] F. Soares, F. Janela, J. Seabra, M. Pereira, and M. M. Freire, "Self-similarity classification of breast tumour lesions on dynamic contrast-enhanced magnetic resonance images—Special session on breast CAD," *Int. J. Comput. Assist. Radiol. Surgery*, vol. 5, no. 1, pp. S203–S205, Jun. 2010.

[36] A. Penn, S. Thompson, M. Schnall, M. Loew, and L. Bolinger, "Fractal discrimination of MRI breast masses using multiple segmentations," *Proc. SPIE*, vol. 3979, pp. 959–966, Jun. 2000.

[37] H. O. Peitgen, H. Jürgens, and D. Saupe, *Chaos and Fractals: New Frontiers of Sciences*. New York, NY, USA: Springer-Verlag, 1993.

[38] Q. Guo, J. Shao, and V. Ruiz, "Characterization and classification of tumor lesions using computerized fractal-based texture analysis and support vector machines in digital mammograms," *Int. J. Comput. Assist. Radiol. Surgery*, vol. 4, no. 1, pp. 11–25, 2009.

[39] R. Lopes, P. Dubois, I. Bhouiri, M. Bedoui, S. Maouche, and N. Betrouni, "Local fractal and multifractal features for volumic texture characterization," *Pattern Recognit.*, vol. 44, no. 8, pp. 1690–1697, 2011.

[40] W. Chen, M. L. Giger, H. Li, U. Bick, and G. M. Newstead, "Volumetric texture analysis of breast lesions on contrast-enhanced magnetic resonance images," *Magn. Resonance Med.*, vol. 58, no. 3, pp. 562–571, 2007.

[41] K. Nie, J.-H. Chen, H. J. Yu, Y. Chu, O. Nalcioglu, and M.-Y. Su, "Quantitative analysis of lesion morphology and texture features for diagnostic prediction in breast MRI," *Acad. Radiol.*, vol. 15, no. 12, pp. 1513–1525, Dec. 2008.

[42] R. Lopes and N. Betrouni, "Fractal and multifractal analysis: A review," *Med. Image Anal.*, vol. 13, no. 4, pp. 634–649, Aug. 2009.

[43] C. J. Rose, S. J. Mills, J. P. B. O'Connor, G. A. Buonaccorsi, C. Roberts, Y. Watson, S. Cheung, S. Zhao, B. Whitcher, A. Jackson, and G. J. M. Parker, "Quantifying spatial heterogeneity in dynamic contrast-enhanced MRI parameter maps," *Magn. Resonance Med.*, vol. 62, no. 2, pp. 488–499, Aug. 2009.

[44] R. Riedi, "Multifractal processes," in *Theory and Applications of Long Range Dependence*, P. Doukhan, G. Oppenheim, and M. S. Taqqu, Eds. Boston, MA, USA: Birkhäuser, 2003, pp. 625–716.

[45] Q. Cheng, "Multifractal modeling and lacunarity analysis," *Math. Geol.*, vol. 29, no. 7, pp. 919–932, Oct. 1997.

[46] P. Ciuciu, P. Abry, C. Rabrait, and H. Wendt, "Log wavelet leaders cumulant based multifractal analysis of EVI fMRI time series: Evidence of scaling in ongoing and evoked brain activity," *IEEE J. Sel. Topics Signal Process.*, vol. 2, no. 6, pp. 929–943, Jun. 2008.

[47] C. Tolle, T. Mcjunkin, and D. Gorsich, "An efficient implementation of the gliding box lacunarity algorithm," *Phys. D, Nonlinear Phenomena*, vol. 237, no. 3, pp. 306–315, 2008.

[48] P. Dong, "Lacunarity analysis of raster datasets and 1D, 2D, and 3D point patterns," *Comput. Geosci.*, vol. 35, no. 10, pp. 2100–2110, 2009.

[49] G. Dougherty and G. M. Henebry, "Lacunarity analysis of spatial pattern in CT images of vertebral trabecular bone for assessing osteoporosis," *Med. Eng. Phys.*, vol. 24, no. 2, pp. 129–138, Mar. 2002.

[50] C. Allain and M. Cloitre, "Characterizing the lacunarity of random and deterministic fractal sets," *Phys. Rev. A*, vol. 44, no. 6, pp. 3552–3558, Sep. 1991.

[51] R. E. Plotnick, R. H. Gardner, W. W. Hargrove, K. Prestegard, and M. Perlmutter, "Lacunarity analysis: A general technique for the analysis of spatial patterns," *Phys. Rev. E*, vol. 53, no. 5, pp. 5461–5468, May 1996.

[52] S. W. Myint and N. Lam, "A study of lacunarity-based texture analysis approaches to improve urban image classification," *Comput., Environ. Urban Syst.*, vol. 29, no. 5, pp. 501–523, Sep. 2005.

[53] S. Stach, J. Cybo, J. Cwajna, and S. Roskosz, "Multifractal description of fracture morphology. Full 3D analysis of a fracture surface," *Mater. Sci. Poland*, vol. 23, no. 2, pp. 577–584, 2005.

[54] P. Dong, "Test of a new lacunarity estimation method for image texture analysis," *Int. J. Remote Sens.*, vol. 21, no. 17, pp. 3369–3373, 2000.

[55] A. Hanen, B. Imen, B. A. Asma, D. Patrick, and B. M. Hédi, "Multifractal modelling and 3D lacunarity analysis," *Phys. Lett. A*, vol. 373, no. 40, pp. 3604–3609, 2009.

[56] D. Fabio, A. Reis, and R. Riera, "Lacunarity calculation in the true fractal limit," *J. Phys. A, Math. General*, vol. 27, no. 6, pp. 1827–1835, Mar. 1994.

[57] M. Doman and E. Honda, "Correlation of measured fractal dimensions with lacunarity in computer-generated three-dimensional images of Cantor sets and those of fractional Brownian motion," *FORMA TOKYO*, vol. 14, no. 3, pp. 249–263, 1999.

[58] L. Zhang, J. Z. Liu, D. Dean, V. Sahgal, and G. H. Yue, "A three-dimensional fractal analysis method for quantifying white matter structure in human brain," *J. Neurosci. Methods*, vol. 150, no. 2, pp. 242–253, Jan. 2006.

[59] Q. Cheng, "The gliding box method for multifractal modeling," *Comput. Geosci.*, vol. 25, no. 9, pp. 1073–1079, Nov. 1999.

[60] Y. Shimizu, M. Barth, C. Windischberger, E. Moser, and S. Thurner, "Wavelet-based multifractal analysis of fMRI time series," *Neuroimage*, vol. 22, no. 3, pp. 1195–1202, Jul. 2004.

[61] J. Delour, J. F. Muzy, and A. Arnéodo, "Intermittency of 1D velocity spatial profiles in turbulence: A magnitude cumulant analysis," *Eur. Phys. J. B*, vol. 23, no. 2, pp. 243–248, Sep. 2001.

[62] H. Wendt, P. Abry, and S. Jaffard, "Bootstrap for empirical multifractal analysis," *IEEE Signal Process. Mag.*, vol. 24, no. 4, pp. 38–48, Jul. 2007.

[63] B. Szabo, P. Aspelin, M. Kristoffersen Wiberg, and B. Bone, "Dynamic MR imaging of the breast: Analysis of kinetic and morphologic diagnostic criteria," *Acta Radiol.*, vol. 44, no. 4, pp. 379–386, Jul. 2003.

[64] T. Joachims, *Making Large-Scale SVM Learning Practical*. Cambridge, MA, USA: MIT Press, 1999.

[65] J. Ramana and D. Gupta, "LipocalinPred: A SVM-based method for prediction of lipocalins," *BMC Bioinf.*, vol. 10, no. 1, p. 445, 2009.

[66] K. H. Brodersen, C. S. Ong, K. E. Stephan, and J. M. Buhmann, "The binomial assumption on precision-recall curves," in *Proc. 20th ICPR*, Aug. 2010, pp. 4263–4266.



**Filipe Soares** is a computer scientist specializing in the field of medical image processing and decision support systems. He received the five-year B.Sc. degree in computer science and engineering from the University of Beira Interior (UBI), Covilhã, Portugal, in 2006. He is a Researcher with Siemens S.A. Healthcare Sector, Portugal. He is currently pursuing the Ph.D. degree in computer science and engineering from UBI, with a focus on computer-aided diagnosis in breast cancer. His work led to the development of prototype software with innovative detection of microcalcifications in mammography and breast masses in magnetic resonance imaging, for which he received the Siemens Innovation Award in 2012. He is the author or co-author of eight papers in refereed international journals and conferences, and the author of a chapter in a book. His current research interests include software engineering, image processing, breast cancer, multifractal and wavelet analysis, computer-aided diagnosis, pattern recognition, artificial intelligence, computer networks, and bioinformatics.



**Filipe Janela** received the five-year B.Sc. degree in chemical engineering and the post-graduate degree in engineering and technology management from Instituto Superior Técnico of the Technical University of Lisbon, Lisbon, Portugal, in 2004 and 2007, respectively. In 2012, he received the master's degree in business administration from IESE/AESE School of Management. He was a Process Engineer with the Oil & Energy Sector, Norsk Hydro, Norway, in 2004. He engaged the business consulting, integrating Siemens S.A. Healthcare Sector in 2006. He is currently the Head of the Innovation and Collaboration and owner of Innovation Program of Siemens Healthcare Sector, Portugal. He is the co-author of several papers in refereed international journals and conferences. He has developed competence in strategic consulting, business development management, technology and innovation management, and research and development.



**João Seabra** received the five-year B.Sc. degree in electrical and computer engineering from the Faculty of Engineering, University of Porto, Porto, Portugal, in 1997. He started his professional activity at Siemens, in the operating group Medical Solutions. He is currently the General Manager of Siemens Healthcare Sector, Portugal, and the Division Cluster Lead for the region of Southwest Europe. He has developed competences in the fields of imaging systems and healthcare IT, playing roles in the areas of project management, and product and business management. He is a member of the Siemens Corporate Executive Committee in Portugal, where he is responsible for the corporate areas of Innovation and Globalization. He has played administration roles in Amb3E (Electrical and Electronic Waste Management Company) and AEP (Portuguese Enterprise Association). From 2010 to 2012, he was a member of the General Counsel with the University of Beira Interior, Covilhã, Portugal.



**Manuela Pereira** received the five-year B.Sc. degree in mathematics and computer science and the M.Sc. degree in computational mathematics from the University of Minho, Braga, Portugal, in 1994 and 1999, respectively, and the Ph.D. degree in signal and image processing from the University of Nice Sophia Antipolis, Nice, France, in 2004. She is an Assistant Professor of computer science with the University of Beira Interior, Covilhã, Portugal. Her current research interests include multiple description coding, joint source/channel coding, image and video coding, holographic 3-D video coding, wavelet analysis, information theory, image segmentation and real-time video streaming, quality of experience (QoE) assessment, and QoE modeling. She is the co-editor of six books and has authored or co-authored over 50 papers in international refereed journals and conferences. She served as a Technical and Program Committee Member for several IEEE journals and conferences. She is a member of the editorial review board of several international journals.



**Mário M. Freire** (M'96) received the five-year B.Sc. degree in electrical engineering and the two-year M.Sc. degree in systems and automation from the University of Coimbra, Coimbra, Portugal, in 1992 and 1994, respectively, and the Ph.D. degree in electrical engineering and the Habilitation degree in computer science from the University of Beira Interior, Covilhã, Portugal, in 2000 and 2007, respectively. He is a Full Professor of computer science with the University of Beira Interior, which he joined in 1994. He was a Trainee Researcher with the Research Centre, Alcatel-SEL (now Alcatel-Lucent), Stuttgart, Germany, in 1993. His current research interests include multimedia networking and peer-to-peer systems, multimedia traffic analysis and synthesis, network forensics and security, and data centers and cloud computing. He is the co-author of seven international patents, co-editor of eight books published in the *Springer Lecture Notes in Computer Science* book series, and the author or co-author of over 120 papers in refereed international journals and conferences. He serves as an Editorial Board Member of the *ACM SIGAPP Applied Computing Review* and the *Wiley Journal on Security and Communication Networks*, and served as an Editor of the *IEEE Communications Surveys and Tutorials*. He served as a Guest Editor of two feature topics in *IEEE Communications Magazine* and of a special issue of *Wiley International Journal of Communication Systems*. He served as a Technical Program Committee Member for several IEEE international conferences and is the Co-Chair of the Track on Networking of the ACM SAC 2014. He is a Chartered Engineer by the Portuguese Order of Engineers and he is a member of the IEEE Computer Society and the IEEE Communications Society, and the Association for Computing Machinery.

# Chapter 6

## Conclusions and Future Work

The early detection and accurate diagnosis of breast cancer is of utmost importance in providing effective and efficient treatment in order to increase survival rates. The tendency of increasing the incidence of breast cancer, due to higher life expectancy, and the positive prognostic when detected in early stages, motivated the implementation of screening programs based on mammographic imaging. Data from screening mammography is usually interpreted by trained radiologists that look for suspicious lesions. However, the accuracy of breast cancer detection is highly dependent on the experience of the radiologist and may be hampered by the fatigue when evaluating large amounts of data. In mammography, volumetric anatomical information is projected into a two-dimensional (2D) projection, which may hide early signs of breast cancer, such as microcalcifications, especially in the case of dense breasts. Computer-aided detection (CADe) systems are therefore important, especially in the search for microcalcifications in screening mammography. Breast MRI, on the other hand, is a very sensitive technique, more used to image high risk patients, to which it would be helpful to add capabilities for differentiating among groups of lesions. Computer-aided diagnosis (CADx) systems may be used to improve the specificity of breast MRI or even to provide an indication of the tumor staging and therapy follow-up. Equally important is its potential role in avoiding unnecessary invasive procedures as biopsies or therapies, which have consequences in health costs and patient burden. In this Thesis, improvements of breast cancer early detection and diagnosis are described by the development of computer-aided systems based on the multifractal properties of breast tissues. Computer-aided detection (CADe) systems are investigated for detection of early signs of abnormality, namely to distinguish microcalcifications in mammographic images. Computer-aided diagnosis (CADx) systems are implemented for malignancy classification of 2D and 3D images obtained with breast MRI.

Firstly, a comprehensive review is provided on computer-aided detection (CADe) and diagnosis (CADx) schemes are developed for two complementary imaging modalities, mammography and breast MRI. Radiological imaging is one of the most effective means of early detection of breast cancer. However, the differentiation between benign and malignant findings is still difficult. Computer-aided medical imaging analysis (CAD) arises in this sense. Computerized software models known as CADe have been proposed to assist radiologists in locating and identifying possible abnormalities. CADx are decision aids to radiologists in characterizing findings from radiologic images identified either by a radiologist or CADe. In mammography the results of CADx, though encouraging, are not yet conclusive enough to warrant a credible clinical usage.

The state-of-art methods show that the accuracy of cancer detection has indeed improved with introduction of CADx. There is still a long way to go for implementation of the same in a clinical setting as it already happen in mammography on CADe. Almost all of the existing CADx schemes are trained and tested on retrospectively collected cases that may not represent the real clinical practice. Large prospective studies are required to evaluate the performance of CADx systems in real life before employing them in a clinical setting.

Most of the commercial CAD systems in breast MRI are advertized as CADx, but not based on learning. On the other side, what can be found on Chapter 2 of this Thesis is that almost no scientific research on CADe exists nowadays. Dynamic contrast-enhanced MRI (DCE-MRI) is without doubt a valuable technique with room for improvement in false positive reduction and sensitivity increasing. In this sense, researchers had been investing lot of effort in first, to characterize breast lesions as radiologists usually do, and more recently to investigate differentiation between lesions through unconventional approaches as multifractal, textural-kinetics and spatio-temporal analysis on region or volumes of interest. In the future, well-designed and executed studies which specifically evaluate the addition of CADx to MRI clinical cycle are needed to determine whether or not the use of CAD provides a positive clinical benefit to the patients; similarly to what have been shown through the role of CADe in mammography. With the aim to incorporate all possible information from different sources when making recommendations to radiologists, more CAD multimodal approaches should be investigated.

A review and comparison of 2D multifractal methods is proposed for the first time in the image field to address the problem of texture characterization. The work aimed the detection of microcalcification clusters in mammography. In addition, it was also proposed a technique to reduce the false positives by using clustering and self-similarity analysis to identify and create a likelihood map of potential structures to remove. Good performance of detection was obtained with this method. The results from the study suggest that the multifractal characterization of features as proposed can be useful for a computer-aided breast cancer detection system. The procedure of inspecting singularities and their fluctuations at multiple resolutions revealed that multifractal information is of very importance. The inclusion of a classifier should play a role for disambiguation of results and stronger false positive reduction. The high sensitivity of the multifractal-based detection of clustered microcalcifications can lead to a gain in confidence by the radiologist to rely on CADe to find these abnormalities. This would allow in the future that radiologists just have to check the computer-detected clusters of microcalcifications and then to look for mass lesions when reading the mammograms, reducing the fatigue and increasing the productivity of the experts.

A multi-scale automated model for the classification of suspicious malignancy of breast masses, through log detrended fluctuation cumulant-based multifractal, is also proposed. Features for classification are extracted by computing the multifractal scaling exponent. The performance

of a supervised classification was evaluated by receiver operating characteristic (ROC) with an area under the curve of 0.985, by validation against the radiologist diagnosis that follows the Breast Imaging - Reporting and Data System (BI-RADS). The proposed multifractal analysis can contribute to novel feature classification techniques to aid radiologists every time there is a change in clinical course, namely when biopsy should be considered. Even without using all of the consecutive acquired images to build a kinetic curve of enhancement, the best outcome of the proposed model confirms the biopsy recommendations, and overcomes the performance of Three-Time-Points (3TP) technique, which is a clinical standard protocol for the examination of DCE-MRI data. Future work would include optimization of different acquisition protocols, with sufficient temporal resolution to extend the multifractal methods in the temporal dimension, and would be compared with the application of more advanced pharmacokinetic models. However, it is worth noticing that the multifractal temporal features derived should not have a correspondence to the pharmacokinetic parameters, which more directly reflect the physiology.

A novel method of 3D multifractal analysis is proposed to characterize the spatial complexity of breast tumors at multiple scales. Self-similar properties are found from the estimation of the multifractal scaling exponent for each clinical case, using lacunarity as the multifractal measure. These properties include several descriptors of the multifractal spectra reflecting the morphology and internal spatial structure of the enhanced lesions relatively to normal tissue. The results suggest that the combined multifractal characteristics can be effective to distinguish benign and malignant findings, judged by the performance of the support vector machine (SVM) classification method evaluated by receiver operating characteristics (ROC). It was shown how multifractal analysis may depend on the concept of lacunarity, when used for the description of the spatial distribution of the pixel intensities in image volumes with multiscaling behaviors. After testing the hypothesis that multifractal spectral characteristics could be related with likelihood of malignancy, our results are in line with histological ground-truth with an area under the curve of 0.96. This work suggests that the quantitative assessment of multifractal features, as proposed here, can be translated into a new and more efficient method for classification that could potentially be integrated in a computer-aided diagnosis (CADx).

In the future, the developed framework raises the possibility of using measures other than lacunarity in 3D. The discriminatory potential of different 3D measures is yet to be assessed leaving an open topic to explore in the future. Moreover, it would be interesting to study the relation between multifractal parameters and tracer kinetic parameters, as kinetic texture features without having to lose the 3D information of lesions. The proposed method could be applied to roughly any kind of tumor. A correspondence between the general anatomical structure and the possible feature-based classification of regions is natural, by the multifractality that may prevail in medical images. The main limitation of it is to assess if the data possess multiple scaling properties or not. Both MRI studies in this Thesis confirm the presence of multiple degrees of

*Computer-Aided Detection and Diagnosis of Breast Cancer in 2D and 3D Medical Imaging Through Multifractal Analysis*

scaling on multifractal analysis in DCE-MR of the breast, in 2D and 3D. It is also predictable that imaging modalities with lower spatial resolution than MRI would lead to inferior discrimination power using similar scaling descriptors.

In conclusion, multifractal analysis provides useful information for computer-aided detection in mammography and for computer-aided diagnosis in 2D and 3D breast MR images and have the potential to complement the interpretation of the radiologists. Multifractal analysis focuses on understanding and exploring the nature of the irregularities in the image and, not on a single most prevalent irregularity or global trend. Multifractal features are well correlated with tumor staging and provide an indication of the likelihood of malignancy.